Scalable Room-Temperature Synthesis of Glass-like MOF Thin Films on Arbitrary Substrates with Versatile Functionality

Wei Zhang [a,b,e]*, Sijia Cao,[b] Yanchen Liu,[e] Qingping Wu,[b] Zibo Zhang,[b,g] Martin A. Karlsen[f], Liqiang Lu[b], Nicola Pinna[e] and Yan Lu [b,c,d]*

a. Key Laboratory of Organic Compound Pollution Control Engineering (MOE), School of Environmental and Chemical Engineering, Shanghai University, Shanghai 200444, China.
b. Institute of Electrochemical Energy Storage, Helmholtz-Zentrum Berlin für Materialien und Energie, Berlin 14109, Germany.
c. Institute for Technical and Environmental Chemistry, Friedrich-Schiller-Universität Jena, Jena 07743, Germany.
d. Helmholtz Institute for Polymers in Energy Applications Jena (HIPOLE Jena), 07743 Jena, Germany.
e. Department of Chemistry and The Center for the Science of Materials Berlin, Humboldt-Universität zu Berlin, Berlin 12489, Germany.
f. Deutsches Elektronen-Synchrotron DESY, Notkestr. 85, 22607 Hamburg, Germany
g. School of Chemical Engineering, University of Science and Technology Liaoning, Anshan 114051, China

Email: weizhang88@shu.edu.cn; yan.lu@helmholtz-berlin.de

General information

All chemical reagents in this work were bought from commercial sources and used without further purification. 4,6-dihydroxy-1,3-benzenedicarboxylic acid, 4,4'-dihydroxy-3,3'-biphenyldicarboxylic acid, 1,5-dihydroxy-2,6-naphthalenedicarboxylic acid, 4,4"-dihydroxy-(1,1':4',1"-terphenyl)-3,3"-dicarboxylic acid, 4,4'-(anthracene-9,10-diyl)bis(2-hydroxybenzoic acid), 2,3,6,7,10,11-Hexahydroxytriphenylene (H_6HHTP) were purchased from BLDpharm. Iron(III) chloride, Cobalt(II) nitrate hexahydrate, Zinc nitrate hexahydrate, Copper(II) nitrate, Iron(II) chloride tetrahydrate, Potassium ferricyanide, Potassium cobalt cyanide, Potassium nickel cyanide, Potassium silver cyanide, Vinylimidazole, 2,5-dihydroxyterephthalate, Trimesic acid, 2-Methylimidazole, Aminoterephthalic acid, Terephthalic acid, Methanol, Ethanol, and N,N-Dimethylformamide (DMF) were all purchased from Sigma-Aldrich.

Experimental Section

Glass-like MOF thin film synthesis

Synthesis of gFe-DOBDC film: 480 mg of $FeCl_2 \cdot 4H_2O$ was dissolved in 50 mL of methanol to prepare solution A. 180 mg of 2,5-dihydroxyterephthalate (H_4dobdc) was dissolved in 50 mL of a methanol/DMF mixture with a volume ratio of 4.1:0.9 to form solution B, followed by the addition of 0.12 mL of vinylimidazole. Solution B was then slowly poured into solution A to obtain the final reaction mother solution. The substrate was vertically placed into the mother solution and kept stationary at room temperature for 0.5-5 h. After the reaction, the substrate was taken out, rinsed with ethanol, and dried for subsequent characterization.

Synthesis of gFe-mDOBDC film: 480 mg of $FeCl_2 \cdot 4H_2O$ was dissolved in 50 mL of methanol to prepare solution A. 180 mg of 4,6-dihydroxy-1,3-benzenedicarboxylic acid (H_4m-dobdc) was dissolved in 50 mL of a methanol/DMF mixture with a volume ratio of 4.1:0.9 to form solution B, followed by the addition of 0.12 mL of vinylimidazole. Solution B was then slowly poured into solution A to obtain the final reaction mother solution. The substrate was vertically placed into the mother solution and kept stationary at room temperature for 0.5-5 h. After the reaction, the substrate was taken out, rinsed with ethanol, and dried for subsequent characterization.

Synthesis of gFe-DOBPDC film: 240 mg of $FeCl_2 \cdot 4H_2O$ was dissolved in 50 mL of methanol to prepare solution A. 90 mg of 4,4'-dihydroxy-3,3'-biphenyldicarboxylic acid (H4dobpdc) was dissolved in 50 mL of a methanol/DMF mixture with a volume ratio of 4.1:0.9 to form solution B, followed by the addition of 0.05 mL of vinylimidazole. Solution B was then slowly poured into solution A to obtain the final reaction mother solution. The substrate was vertically placed into the mother solution and kept stationary at room temperature for 0.5-5 h. After the reaction, the substrate was taken out, rinsed with ethanol, and dried for subsequent characterization.

Synthesis of gFe-DONDC film: 240 mg of $FeCl_2 \cdot 4H_2O$ was dissolved in 50 mL of methanol to prepare solution A. 90 mg of 1,5-dihydroxy-2,6-naphthalenedicarboxylic acid (H_4dondc) was dissolved in 50 mL of a methanol/DMF mixture with

a volume ratio of 4.1:0.9 to form solution B, followed by the addition of 0.05 mL of vinylimidazole. Solution B was then slowly poured into solution A to obtain the final reaction mother solution. The substrate was vertically placed into the mother solution and kept stationary at room temperature for 0.5-5 h. After the reaction, the substrate was taken out, rinsed with ethanol, and dried for subsequent characterization.

Synthesis of gFe-DOTPDC film: 120 mg of $FeCl_2 \cdot 4H_2O$ was dissolved in 50 mL of methanol to prepare solution A. 50 mg of 1,5-dihydroxy-2,6-naphthalenedicarboxylic acid (H_4dotpdc) was dissolved in 50 mL of a methanol/DMF mixture with a volume ratio of 4.1:0.9 to form solution B, followed by the addition of 0.02 mL of vinylimidazole. Solution B was then slowly poured into solution A to obtain the final reaction mother solution. The substrate was vertically placed into the mother solution and kept stationary at room temperature for 0.5-5 h. After the reaction, the substrate was taken out, rinsed with ethanol, and dried for subsequent characterization.

Synthesis of gFe-anDOBDC film: 120 mg of $FeCl_2 \cdot 4H_2O$ was dissolved in 50 mL of methanol to prepare solution A. 60 mg of 4,4'-(anthracene-9,10-diyl)bis(2-hydroxybenzoic acid) (H_4an-dobdc) was dissolved in 50 mL of a methanol/DMF mixture with a volume ratio of 4.1:0.9 to form solution B, followed by the addition of 0.02 mL of vinylimidazole. Solution B was then slowly poured into solution A to obtain the final reaction mother solution. The substrate was vertically placed into the mother solution and kept stationary at room temperature for 0.5-5 h. After the reaction, the substrate was taken out, rinsed with ethanol, and dried for subsequent characterization.

Crystalline MOF thin film synthesis

Synthesis of $Co_3[Fe(CN)_6]_2$ thin film: 30 mg of $CoCl_2 \cdot 6H_2O$ and 60 mg of sodium citrate were dissolved in 5 mL of water to form Solution A. 30 mg of $K_3[Fe(CN)_6]$ was dissolved in another 5 mL of water to form Solution B. Solution B was poured into Solution A and mixed uniformly. The various substrates with pre-deposited gFe-DOBDC was immersed into the mixture solution for 5 min at room temperature (RT) and then taken out. The obtained $Co_3[Fe(CN)_6]_2$ film was washed alternately with water and ethanol, and dried at 60 °C for 24 h.

Synthesis of Cu-HHTP thin film: 10 mg of $CuCl_2 \cdot 2H_2O$ was dissolved in 5 mL of water to form Solution A. 4 mg of 2,3,6,7,10,11-Hexahydroxytriphenylene (H_6HHTP) was dissolved in 5 ml of a mixed solution consisting of 3.8 ml H_2O, 1 ml ethanol, and 0.2 ml DMF. to form Solution B. Solution B was poured into Solution A and mixed uniformly. The glass substrate with pre-deposited gFe-DOBDC was immersed into the mixture solution for 1h at RT and then taken out. The obtained Cu-HHTP film was washed alternately with water and ethanol, and dried at 60 °C for 24 h.

Synthesis of ZIF-8 thin film: 37 mg of $Zn(NO_3)_2 \cdot 6H_2O$ was dissolved in 5 mL of methanol to form Solution A. 20 mg of 2-Methylimidazole was dissolved in another 5 mL of methanol to form Solution B. Solution B was poured into Solution

A and mixed uniformly. The glass substrate with pre-deposited gFe-DOBDC was immersed into the mixture for 2h at RT and then taken out. The obtained ZIF-8 film was washed three times with ethanol, and dried at 60 °C for 24 h.

Synthesis of ZIF-67 thin film: 30 mg of $Co(NO_3)_2 \cdot 6H_2O$ was dissolved in 5 mL of methanol to form Solution A. 100 mg of 2-methylimidazole was dissolved in another 5 mL of methanol to form Solution B. Solution B was poured into Solution A and mixed uniformly. The glass substrate with pre-deposited gFe-DOBDC was immersed into the mixture for 2h at RT and then taken out. The obtained ZIF-67 film was washed three times with ethanol, and dried at 60 °C for 24 h.

Synthesis of MIL-88B(Fe) thin film: 40 mg of $FeCl_3$ was dissolved in 8 mL of ethanol to form Solution A. 5 mg of 2-terephthalic acid and 1 μl of triethylamine were dissolved in another 2 mL of ethanol to form Solution B. Solution B was poured into Solution A and mixed uniformly. The glass substrate with pre-deposited gFe-DOBDC was immersed into the mixture for 3h at RT and then taken out. The obtained MIL-88B(Fe) film was washed three times with ethanol, and dried at 60 °C for 24 h.

Synthesis of MIL-88C(Fe) thin film: 40 mg of $FeCl_3$ was dissolved in 8 mL of ethanol to form Solution A. 7 mg of 2-2,6-naphthalenedicarboxylic acid and 1 μl of triethylamine was dissolved in another 2 mL of ethanol to form Solution B. Solution B was poured into Solution A and mixed uniformly. The glass substrate with pre-deposited gFe-DOBDC was immersed into the mixture for 10h at RT and then taken out. The obtained MIL-88C(Fe) film was washed three times with ethanol, and dried at 60 °C for 24 h.

Synthesis of ZIF-L(Zn) thin film: 121 mg of $Zn(NO_3)_2 \cdot 6H_2O$ was dissolved in 5 mL of H_2O to form Solution A. 247 mg of 2-Methylimidazole was dissolved in another 5 mL of H_2O to form Solution B. Solution B was poured into Solution A and mixed uniformly. The glass substrate with pre-deposited gFe-DOBDC was immersed into the mixture for 2h at RT and then taken out. The obtained ZIF-L(Zn) film was washed three times with ethanol, and dried at 60 °C for 24 h.

Synthesis of ZIF-L(Co) thin film: 72 mg of $Co(NO_3)_2 \cdot 6H_2O$ was dissolved in 5 mL of H_2O to form Solution A. 164 mg of 2-Methylimidazole was dissolved in another 5 mL of H_2O to form Solution B. Solution B was poured into Solution A and mixed uniformly. The glass substrate with pre-deposited gFe-DOBDC was immersed into the mixture for 2h at RT and then taken out. The obtained ZIF-L(Co) film was washed three times with ethanol, and dried at 60 °C for 24 h.

Synthesis of $Mn_3[Co(CN)_6]_2$ thin film: 30 mg of $MnCl_2 \cdot 4H_2O$ and 60 mg of sodium citrate were dissolved in 5 mL of water to form Solution A. 30 mg of $K_3[Co(CN)_6]$ was dissolved in another 5 mL of water to form Solution B. Solution B was poured into Solution A and mixed uniformly. The glass substrate with pre-deposited gFe-DOBDC was immersed into the mixture for 5 min at RT and then taken out. The obtained film was washed alternately with water and ethanol, and dried at 60 °C for 24 h.

Synthesis of Cu-BDC-NH_2 thin film: 7 mg of $Cu(NO_3)_2 \cdot 2H_2O$ was dissolved in 5 mL of ethanol to form Solution A. 9 mg of aminoterephthalic acid ($H_2BDC\text{-}NH_2$) was dissolved in another 5 mL of ethanol to form Solution B. Solution B was poured into Solution A and mixed uniformly. The glass substrate with pre-deposited gFe-DOBDC was immersed into the

mixture solution. Meanwhile, prepare an ethanolic solution of triethylamine by adding 3 mL of triethylamine to 9 mL of ethanol. Place both this triethylamine solution and the reaction solution in a large beaker and seal the beaker to allow triethylamine vapor to diffuse slowly into the reaction mixture. Stir the reaction solution gently for 3 hours. The obtained Cu-BDC-NH_2 film was washed three times with ethanol, and dried at 60 °C for 24 h.

Synthesis of Ni[Ni(CN)$_4$] thin film: 24 mg of $NiCl_2 \cdot 6H_2O$ and 23 mg of sodium citrate were dissolved in 5 mL of water to form Solution A. 24 mg of $K_2[Ni(CN)_4]$ was dissolved in another 5 mL of water to form Solution B. Solution B was poured into Solution A and mixed uniformly. The glass substrate with pre-deposited gFe-DOBDC was immersed into the mixture for 2h at RT and then taken out. The obtained $Ni[Ni(CN)_4]$ film was washed alternately with water and ethanol, and dried at 60 °C for 24 h.

Synthesis of MOF-74(Co) thin film: 8 mg of $Cu(NO_3)_2 \cdot 2H_2O$ was dissolved in 5 mL of ethanol to form Solution A. 2 mg of 2,5-dihydroxyterephthalate was dissolved in another 5 mL of ethanol to form Solution B. Solution B was poured into Solution A and mixed uniformly. The glass substrate with pre-deposited gFe-DOBDC was immersed into the mixture solution. Meanwhile, prepare an ethanolic solution of triethylamine by adding 3 mL of triethylamine to 9 mL of ethanol. Place both this triethylamine solution and the reaction solution in a large beaker and seal the beaker to allow triethylamine vapor to diffuse slowly into the reaction mixture. Stir the reaction solution gently for 3 hours. The obtained MOF-74(Co) film was washed three times with ethanol, and dried at 60 °C for 24 h.

Synthesis of $Ni_3[Fe(CN)_6]_2$ thin film: 36 mg of $NiCl_2 \cdot 6H_2O$ and 63 mg of sodium citrate were dissolved in 5 mL of water to form Solution A. 33 mg of $K_3[Fe(CN)_6]$ was dissolved in another 5 mL of water to form Solution B. Solution B was poured into Solution A and mixed uniformly. The glass substrates with pre-deposited gFe-DOBDC was immersed into the mixture solution for 1h at room temperature (RT) and then taken out. The obtained $Ni_3[Fe(CN)_6]_2$ film was washed alternately with water and ethanol, and dried at 60 °C for 24 h.

Synthesis of HKUST-1 thin film: Prepare two separate ethanol solutions: Solution A containing 10 mg L^{-1} of $Cu(NO_3)_2 \cdot 2H_2O$, and Solution B containing 5 mg L^{-1} of trimesic acid (H_3BTC). One deposition cycle consists of sequentially immersing the glass substrate with pre-deposited gFe-DOBDC in Solution A for 10 seconds, followed by pure ethanol for 10 seconds, and then in Solution B for 10 seconds. Repeat this cycle for 30 times. The obtained HKUST-1 film was washed three times with ethanol, and dried at 60 °C for 24 h.

Synthesis of Ag[Ag(CN)$_2$] thin film. Prepare two separate aqueous solutions: Solution A containing 10 mg L^{-1} of silver nitrate ($AgNO_3$), and Solution B containing 5 mg L^{-1} of $K[Ag(CN)_2$. One deposition cycle consists of sequentially immersing the substrate in Solution A for 10 seconds, followed by deionized water for 10 seconds, and then in Solution B for 10 seconds. Repeat this cycle for 30 times. The obtained $Ag[Ag(CN)_2]$ film was washed three times with ethanol, and dried at 60 °C for 24 h.

Characterization

The powder X-ray diffraction (XRD) patterns were acquired on a Bruker D8 diffractometer using Cu Kα1 radiation (λ = 1.5406 Å). A Thermo Nicolet Magna 750 FTIR spectrometer was utilized to collect Fourier transform infrared spectra, and all powder specimens were prepared using the standard KBr pressing technique. Raman spectra were acquired with an XPLORA Plus Raman microscope system, employing a 532 nm laser as the excitation source. The structures and morphologies of the samples were analyzed using scanning electron microscopy (SEM, LEO 1530 field emission SEM). Scanning electron microscopy analyses, coupled with energy dispersive X-ray spectrometry (EDX), were carried out using a Brucker QUANTAX detector for mapping the element distribution of gFe-DOBDC film. The atomic force microscope (Bruker Corporation, Multimode, Nanoscope 8) was operated with a J-scanner in a Scanasyst mode. We used Scanasyst-Air cantilevers (Bruker Corporation). The N_2 adsorption-desorption isotherms were obtained by using Quantachrome Autosorb-1 system performed at 77 K. CO_2 adsorption measurements were performed on a BSD-PH instrument at 0 °C up to 30 bar, with the sample degassed at 150 °C for 300 min prior to testing. The thermal stability of gFe-DOBDC was acquired through thermogravimetric analysis (TGA) in a Netzsch TG 209F1 Iris under Argon. The X-ray reflectivity (XRR) measurements were carried out using a PANalytical MPD diffractometer in specular reflection geometry with a X-ray wavelength of 1.5406 Å. The experimental data were analyzed and fitted using the X'Pert Reflectivity software package. Nanoindentation and nanoscratch tests were performed on a Kla iMicro instrument. Differential scanning calorimetry (DSC) was conducted on a TA Discovery DSC2500 instrument. Patterning of the MOF thin film was carried out on a ZEISS Crossbeam 340 system with a Ga^+ ion source.

Total X-ray scattering measurements and PDF analysis

Common experimental conditions

Total X-ray scattering (TXS) measurements for atomic pair distribution function (PDF) analysis were performed at the Powder Diffraction and Total Scattering Beamline P02.1 at PETRA III, Deutsches Elektronen-Synchrotron (DESY), Hamburg, Germany. [1] The X-ray wavelength was 0.207362 Å (59.8 keV). The X-ray beam dimensions were 1.0 mm × 1.0 mm. Measurements were performed in transmission geometry using the rapid-acquisition PDF setup**.** Diffraction images were collected using a Varex XRD 4343CT area detector (pixel size of 150 µm × 150 µm, active area of 2880 × 2880 pixels, CsI scintillator directly deposited on amorphous silicon photodiodes). LaB_6 (NIST SRM 660c) was loaded into a 0.8 mm Special Glass (soda-lime glass) capillary (0.01 mm wall thickness, WJM-Glass Müller GmbH) and measured for 300 s for detector calibration. For each capillary type, an empty capillary was measured as the background. All measurements were acquired as consecutive 60 s sub-exposures. Individual subframes were corrected for detector dark current and averaged into a single diffraction image. Measurements were performed at room temperature, with the capillaries continuously rotating during data acquisition. Pixels shadowed by the beamstop and beamstop arm, dead pixels, hot pixels, and the outer ten pixels were masked prior to azimuthal integration. Polarization and solid-angle corrections

were applied during azimuthal integration. Experimental geometry calibration, detector mask generation, and azimuthal integration were performed using pyFAI.[2,3] TXS data were further processed using the PDFgetX3 algorithm implemented in xPDFsuite, including an *ad hoc* correction for incoherent scattering, to generate PDFs.[4-6] Owing to limited signal-to-noise ratio at high Q, the data were truncated at a Q_{max} of 15.0 Å^{-1} for PDF generation. Beamtime-specific experimental parameters are given below.

Beamtime 1: Crystalline Fe-DOBDC and amorphous Fe-DOBDC

The area detector was positioned with the direct beam incident near the lower-right corner of the detector (viewed downstream from the sample), allowing approximately one quarter of each Debye-Scherrer ring to be collected. Using the LaB_6 calibrant, the sample-to-detector distance was calibrated to 300.230 mm, corresponding to an experimentally accessible Q range of 0.5 Å^{-1} to 27.9 Å^{-1}. Samples were prepared in 0.5 mm borosilicate capillaries (0.01 mm of wall thickness, Hilgenberg GmbH). Samples and the corresponding empty-capillary background were exposed for 900 s.

Beamtime 2: gFe-m-DOBDC, gFe-DOBPDC, and gFe-DONDC

The area detector was positioned with the direct X-ray beam at its center, allowing complete Debye–Scherrer rings to be collected. Using the LaB_6 calibrant, the sample-to-detector distance was calibrated to 230.457 mm, corresponding to an experimentally accessible Q range of 0.55 Å^{-1} to 21.9 Å^{-1} with complete Debye–Scherrer rings. Samples were prepared in 0.7 mm borosilicate capillaries (0.01 mm of wall thickness, Hilgenberg GmbH). Samples and the corresponding empty-capillary background were exposed for 1800 s.

Electrochemical measurements

All the cells were assembled in an argon-filled glove box with H_2O < 1 ppm and O_2 < 1 ppm. For the preparation of Li/Cu coin cells (2032-type), a bare Cu or gBDC-Cu current collector was paired with a Li metal foil and one layer of PP separator, which had been dried at 60 °C under vacuum for 24 h prior to use. The electrolyte was composed of 1 M lithium bis(trifluoromethanesulfonyl)imide (LiTFSI) dissolved in a mixture of 1,3-dioxolane/1,2-dimethoxyethane (DOL/DME, 1:1, v/v) with the addition of 3 wt% lithium nitrate ($LiNO_3$). Anode-free full cells were assembled using a gFe-DOBDC-Cu current collector and a commercial $LiFePO_4$ cathode (with a mass loading of ~16 mg cm^{-2}). Galvanostatic charge/discharge measurements were performed over a voltage range of 2.0–3.8 V at a current density of 17 mA g^{-1} for the initial cycles. All the batteries were tested on a Landian battery testing system.

Molecular dynamics (MD) simulations

The initial molecular configurations were generated using the PACKMOL program.[7] The molar ratio of Fe^{3+}, Cl^-, 2,5-dihydroxyterephthalate (DOBDC), and 1-vinylimidazole was set to 48:96:12:26, with methanol employed as the solvent. The concentration of $FeCl_3$ was fixed at 0.02 mol L^{-1}, and the numbers of DOBDC, 1-vinylimidazole, and methanol molecules were adjusted accordingly to satisfy both the prescribed molar ratios and the target concentration. The resulting

simulation model is shown in **Figure 1C**. Intermolecular interactions were described using the OPLS-AA force field.[8] Prior to molecular dynamics simulations, the system was first energy-minimized using the conjugate gradient algorithm to remove unfavorable atomic contacts. The system was then equilibrated in the NPT ensemble at a temperature of 298 K and a pressure of 1 atm for 2 ns. After reaching thermodynamic equilibrium, production simulations were performed in the NVT ensemble for 100 ns. Long-range electrostatic interactions were treated using the particle–particle particle–mesh (PPPM) method, with a real-space cutoff of 10 Å. A time step of 1 fs was employed throughout. All molecular dynamics simulations were carried out using LAMMPS.[9]

Adsorption energy values for Li bonded onto Cu(100) type cluster using LANL2DZ.[10] For bonding energy between Li and Fe-DOBDC, the spin-restricted method was used based on the Lee-Yang-Parr correlation functional (B3LYP),[11] conjunction with the basis set 6-31G (d).

The Adsorption energy (Eads) between Cu cluster and Li-ions was determined as follows:

$$E\text{ads} = E\text{total} - ES - ELi$$

Where Etotal, ES and ELi represent the total energy of the Li^+–cluster/molecular complex, the energy of single solvent molecules and the energy of single Li^+, respectively.

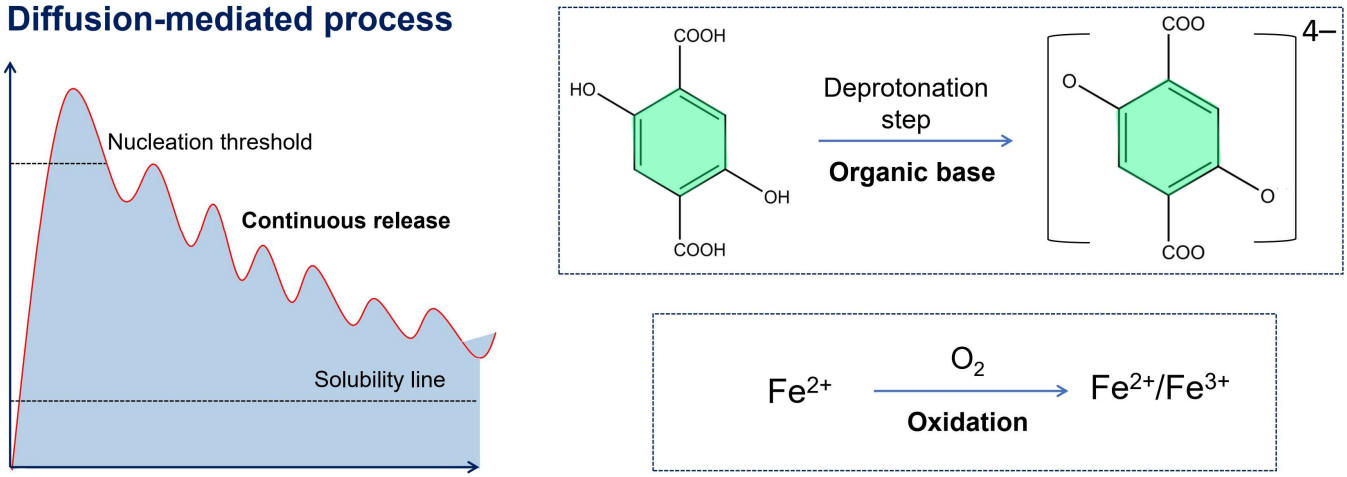


Figure S1. Schematic illustration of the evolution of monomer concentration during diffusion-mediated synthesis. Using 1-vinylimidazole as a deprotonating agent and dissolved O_2 as an oxidant, the diffusion-mediated process provides continuous and controlled release of deprotonated 2,5-dihydroxyterephthalic acid (DOBDC) and iron (III) ions

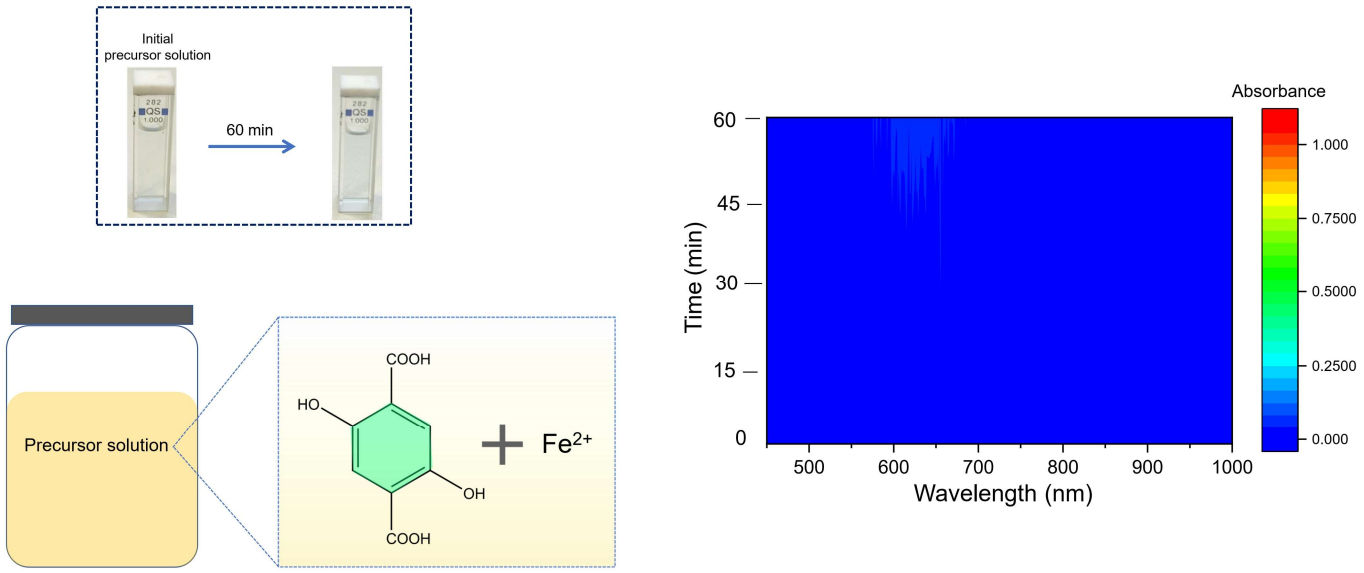


Figure S2. Time-resolved in situ UV-Vis spectra of precursor solution in the absence of 1-vinylimidazole. During the reaction, the absorption showed no change. Thus, all regions appear blue with values close to zero.

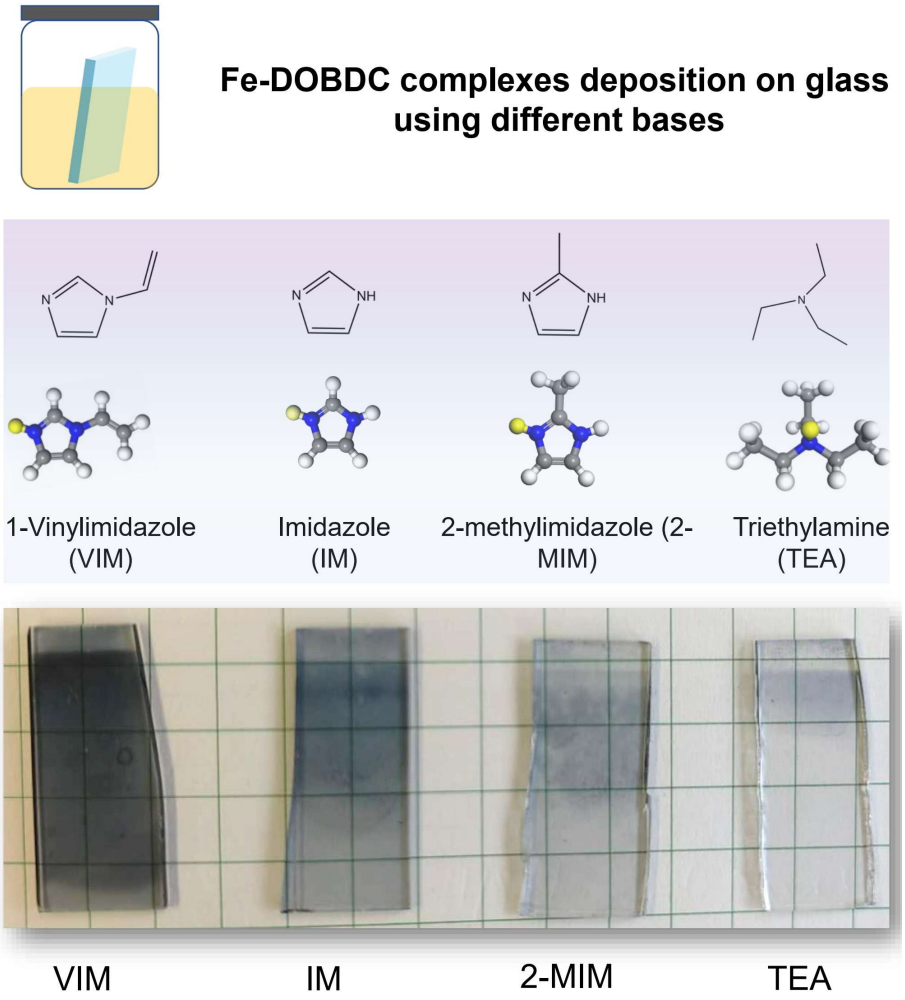


Figure S3. Digital images of Fe-DOBDC complexes deposition on glass in presence of different bases. 1-vinylimidazole exhibits the optimal regulatory effect and enables the most uniform deposition.

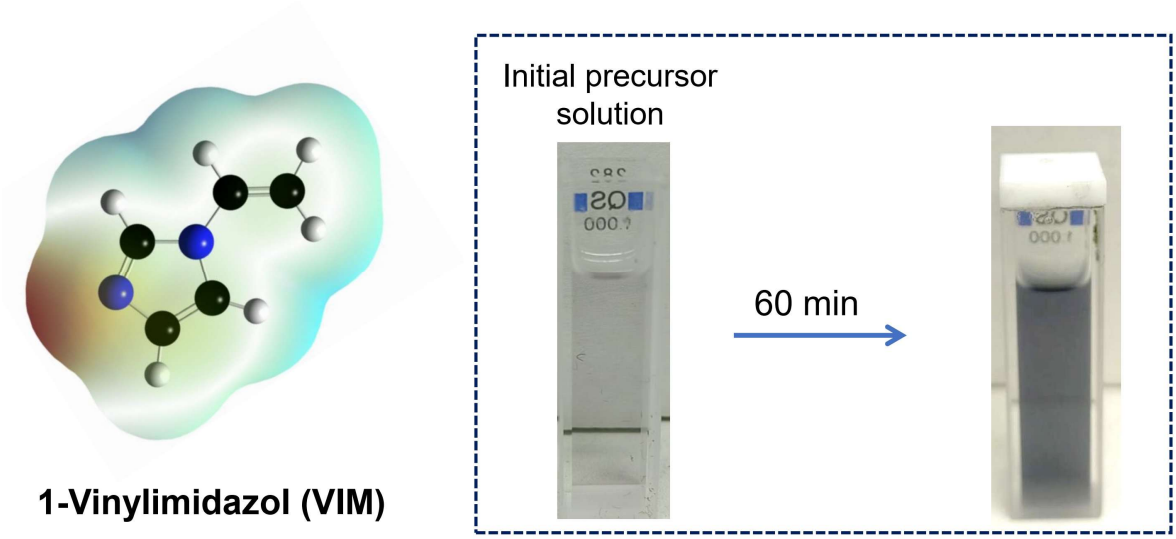


Figure S4. Digital images of initial precursor solution and after 60 min in the presence of 1-vinylimidazole.

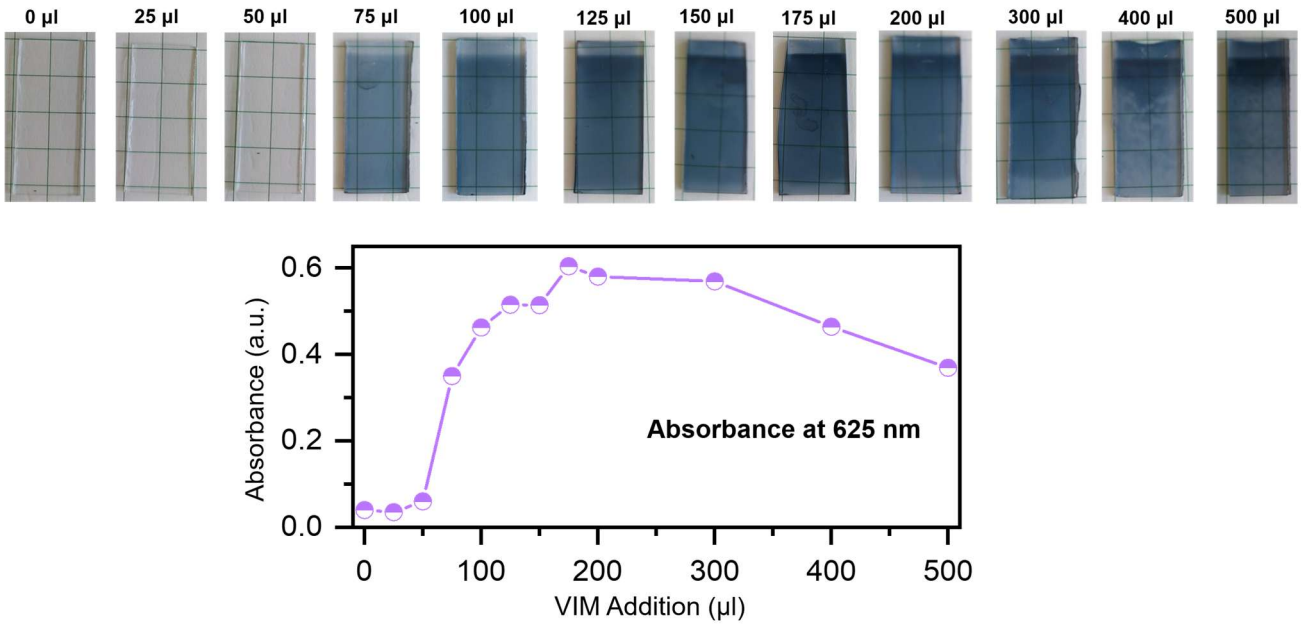


Figure S5. The influence of 1-vinylimidazole usage on the deposition of Fe-DOBDC on glass. The UV-vis absorbance for all samples is consistently located at 625 nm.

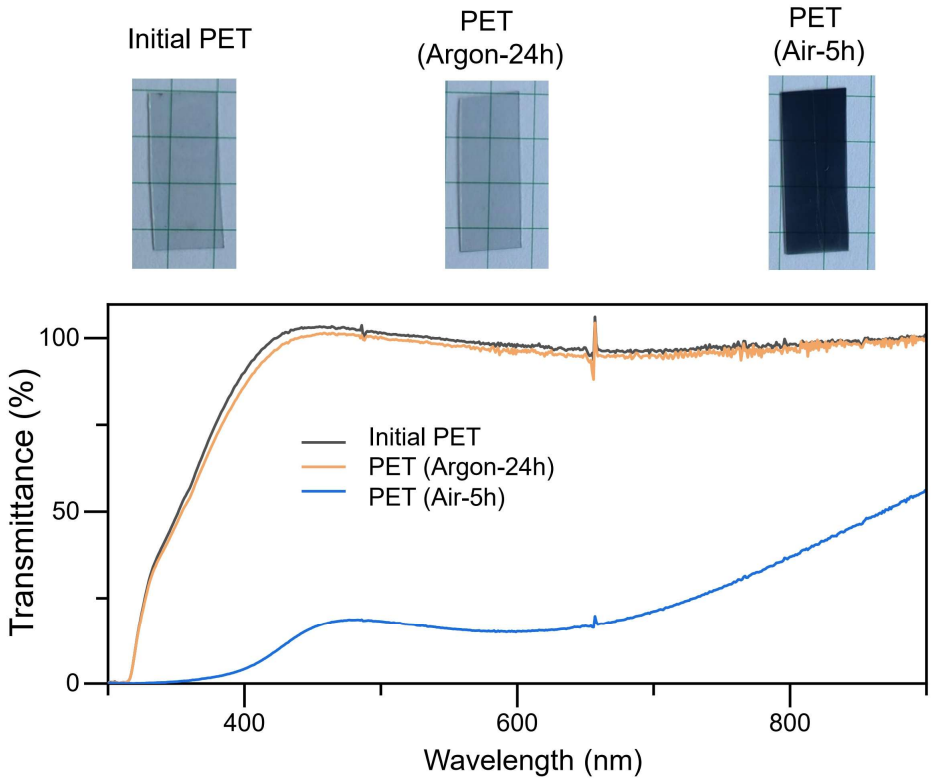


Figure S6. UV-Vis spectra of initial Polyethylene Terephthalate (PET), PET under argon and air. Negligible Fe-DOBDC deposition was observed on PET under argon atmosphere, confirming the regulatory effect of dissolved oxygen.

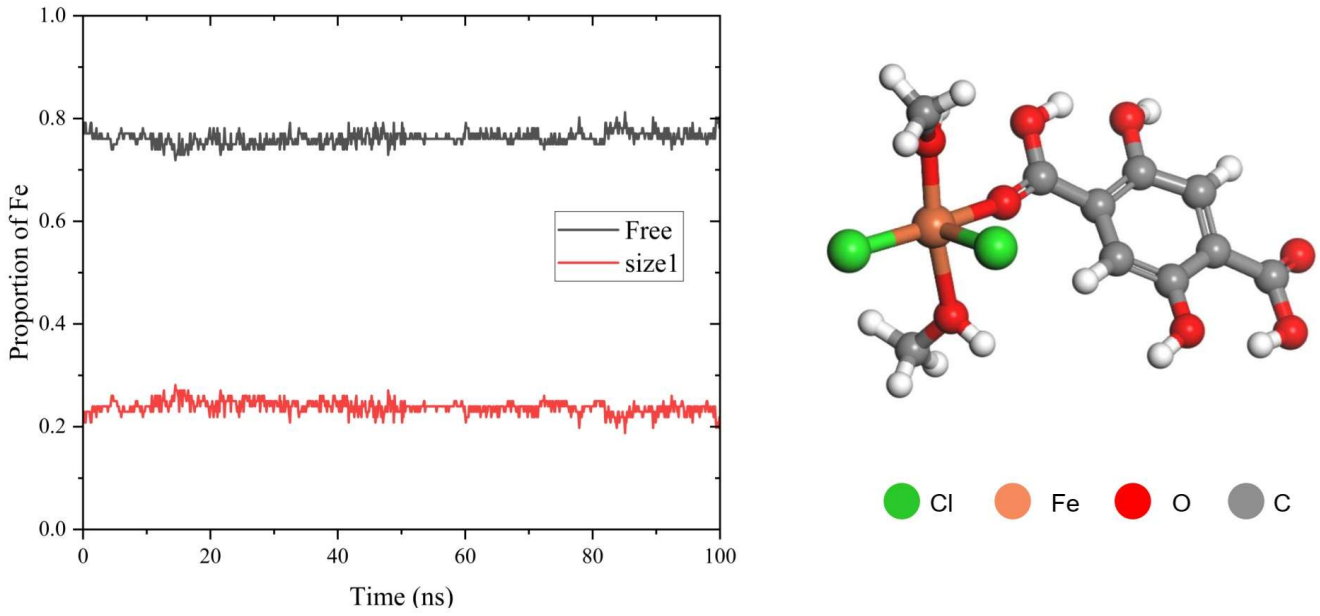


Figure S7. The distribution of Fe(III) ions in different cluster fractions over time. In this simulation, protonated H_4DOBDC was used, with only monodentate structures formed throughout the process.

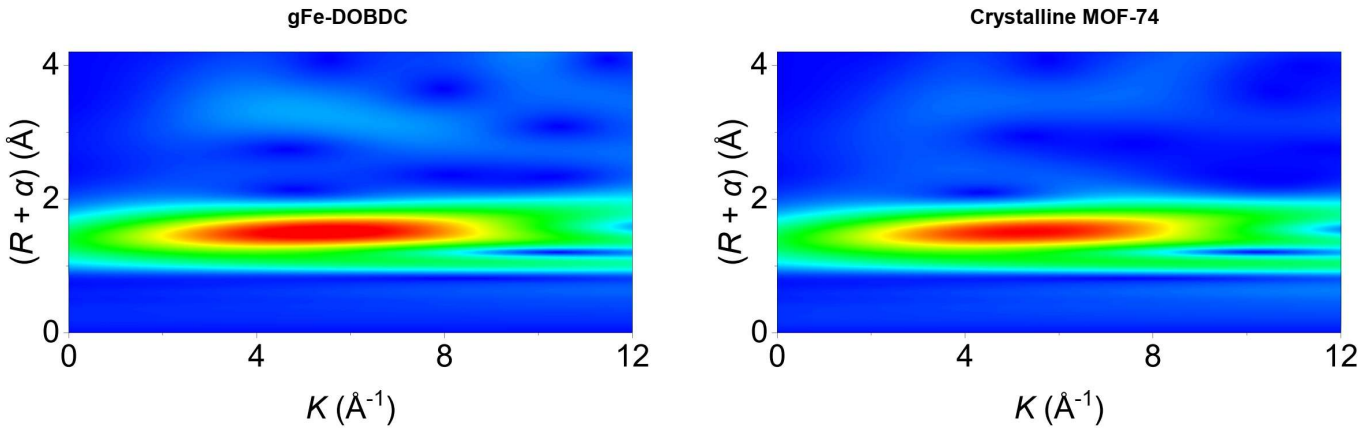


Figure S8. Wavelet transform of the Fe K-edge EXAFS spectra of gFe-DOBDC and crystalline MOF-74.

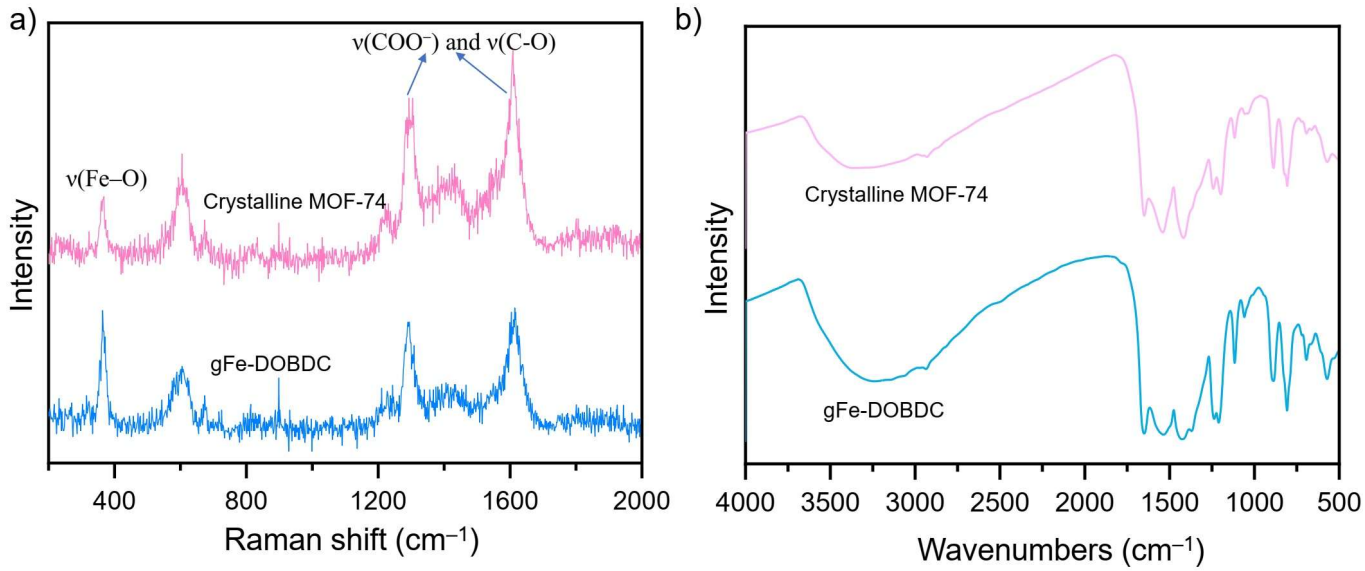


Figure S9. (a) Raman spectra of gFe-DOBDC and crystalline MOF-74. (b) FTIR spectra of gFe-DOBDC and crystalline MOF-74.

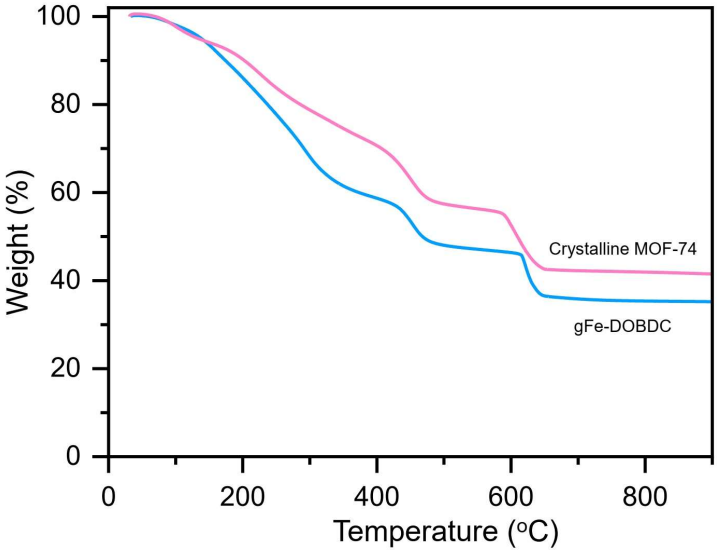


Figure S10. Thermogravimetric analysis (TGA) curves of gFe-DOBDC and crystalline MOF-74 at a heating rate of 10K/min under argon atmosphere.

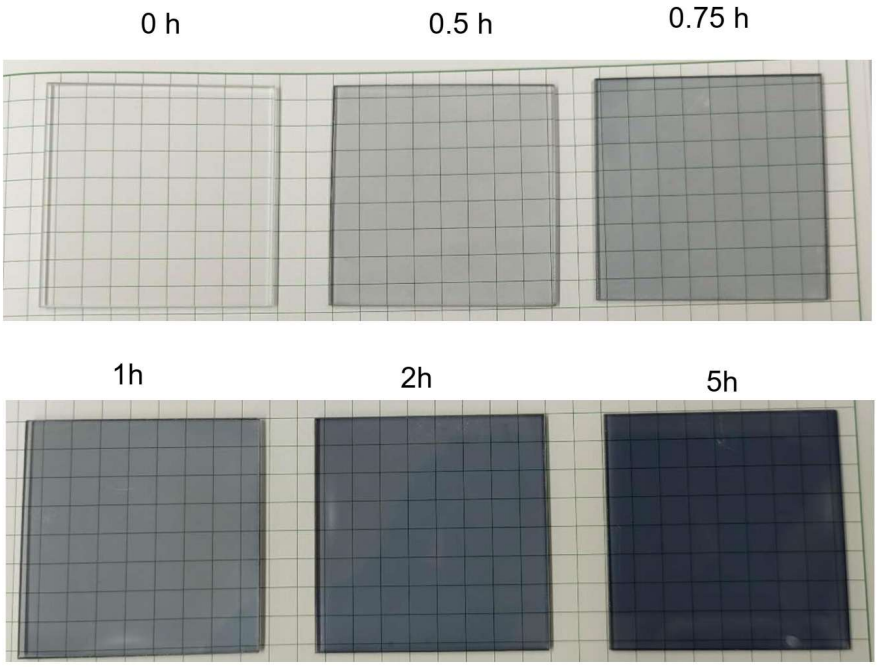


Figure S11. Optical photographs of glass substrates after gFe-DOBDC deposition for 0 h, 0.5 h, 0.75 h, 1 h, 2 h, and 5 h.

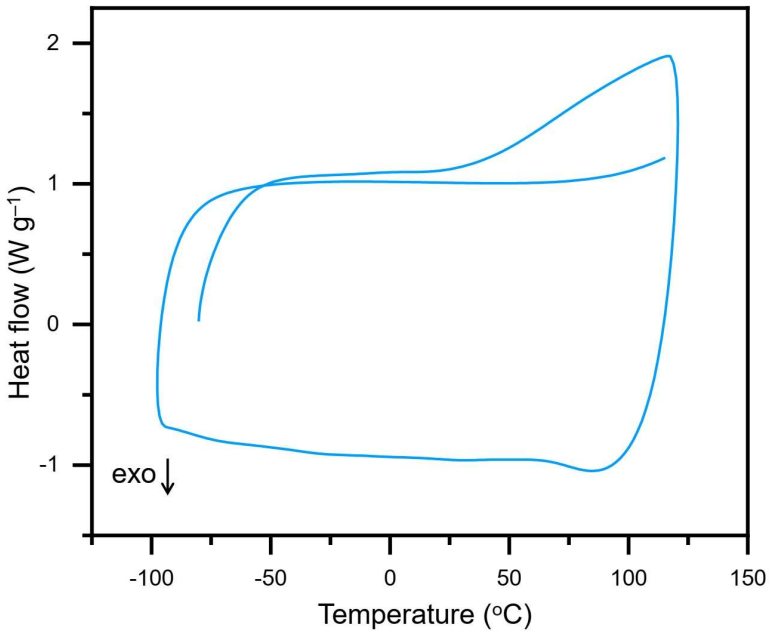


Figure S12. Differential Scanning Calorimetry (DSC) signals of Fe-DOBDC complexes at a heating rate of 10 K/min under N_2 atmosphere.

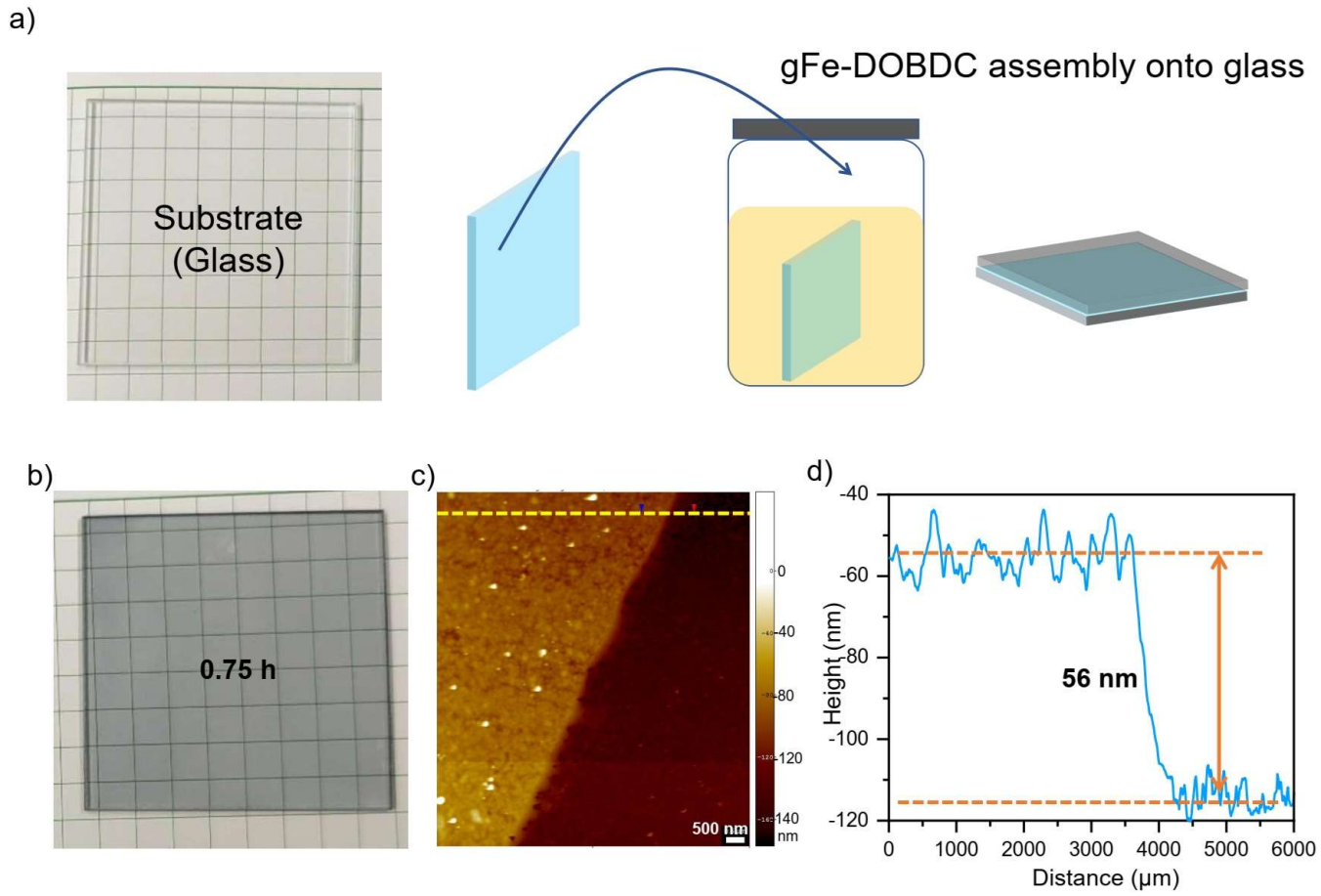


Figure S13. (a) Schematic illustration of the deposition process of gFe-DOBDC thin films on glass. (b) Optical photograph of the glass substrate after film deposition. (c) AFM image of the film with a step used for thickness measurement. (d) Height profile extracted from the AFM image along the step.

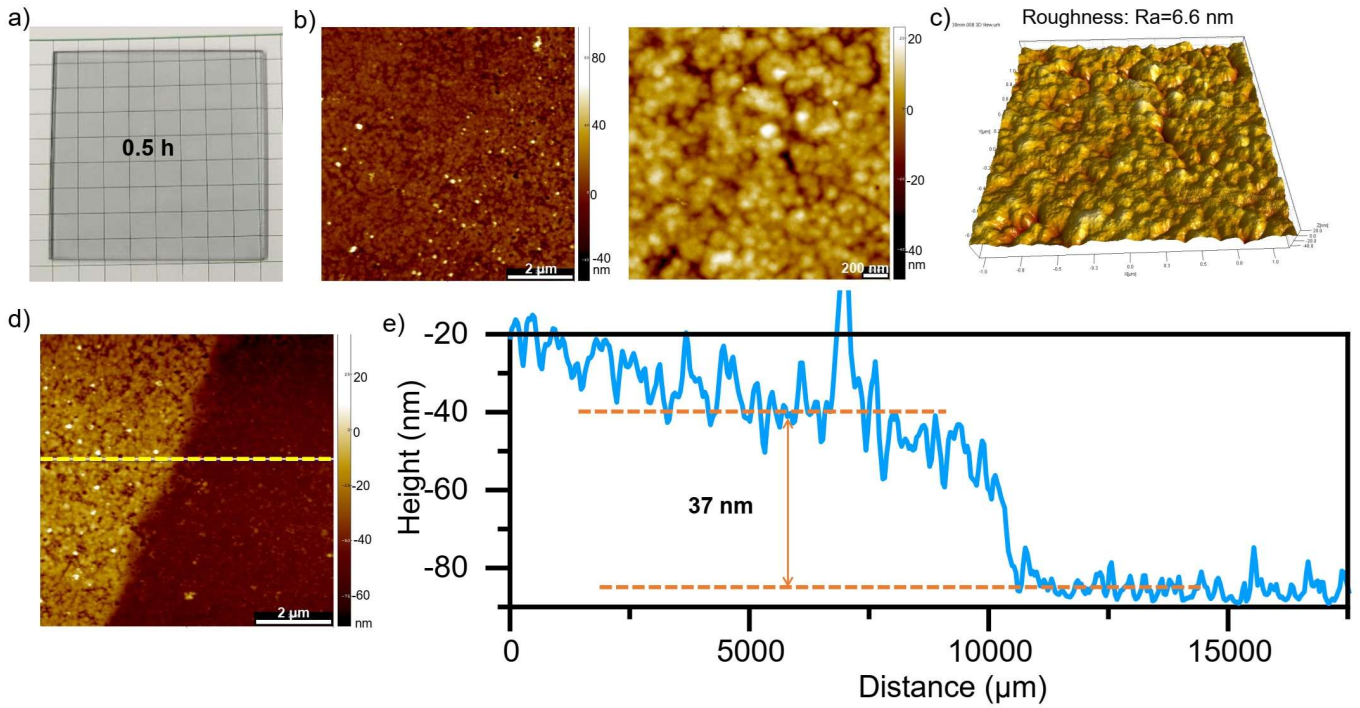


Figure S14. (a) Optical photograph of the glass substrate after film deposition for 0.5 h. (b) AFM image of the film surface. (c) Corresponding 3D AFM image of the film surface. (d) AFM image of the film with a step used for thickness measurement. (e) Height profile extracted from the AFM image along the step.

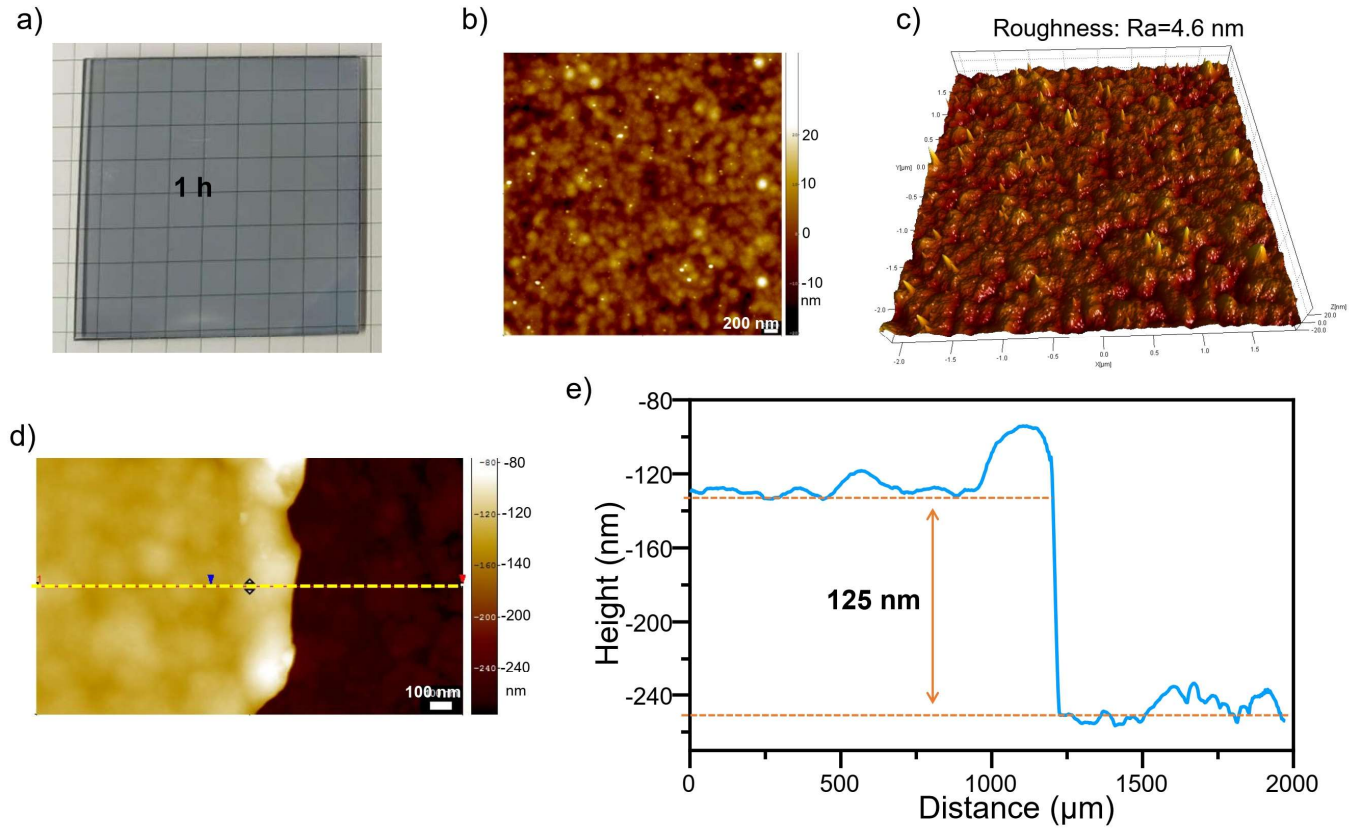


Figure S15. (a) Photograph of the glass substrate after film deposition for 1 h. (b) AFM image of the film surface. (c) Corresponding 3D AFM image of the film surface. (d) AFM image of the film with a step used for thickness measurement. (e) Height profile extracted from the AFM image along the step.

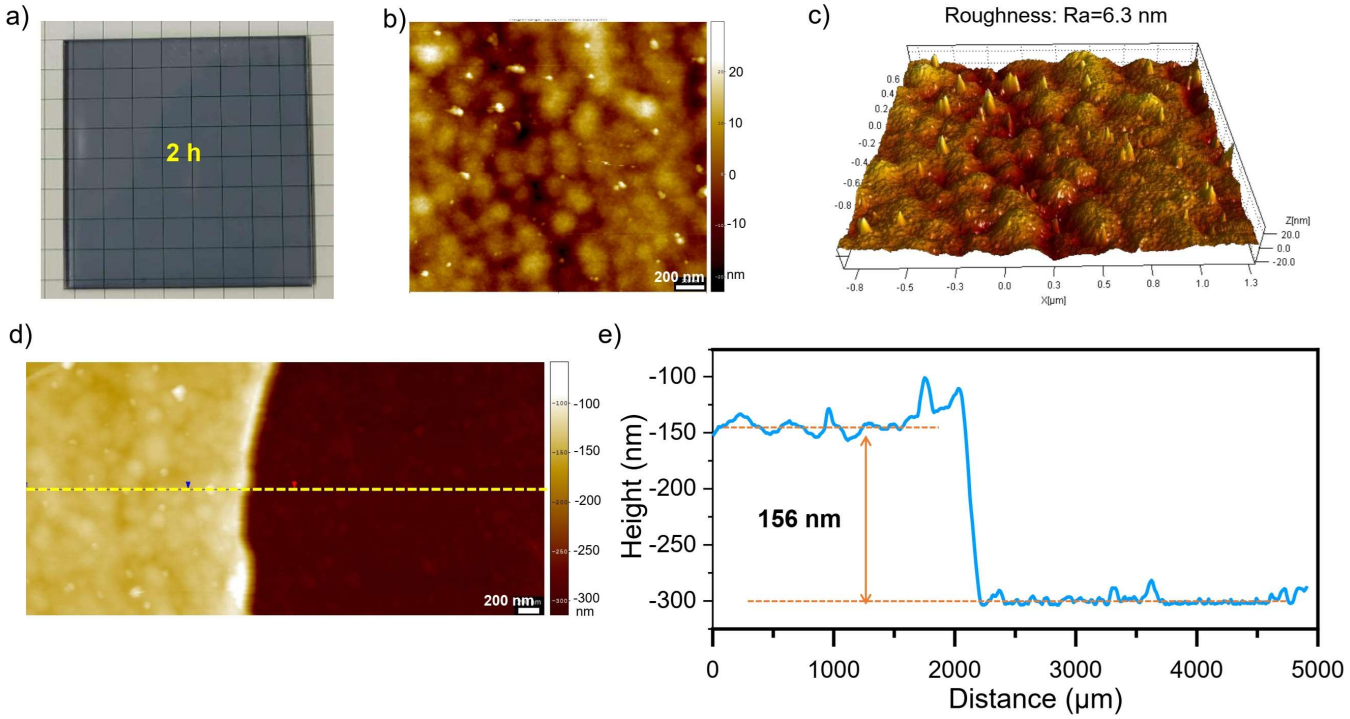


Figure S16. (a) Photograph of the glass substrate after film deposition for 2 h. (b) AFM image of the film surface. (c) Corresponding 3D AFM image of the film surface. (d) AFM image of the film with a step used for thickness measurement. (e) Height profile extracted from the AFM image along the step.

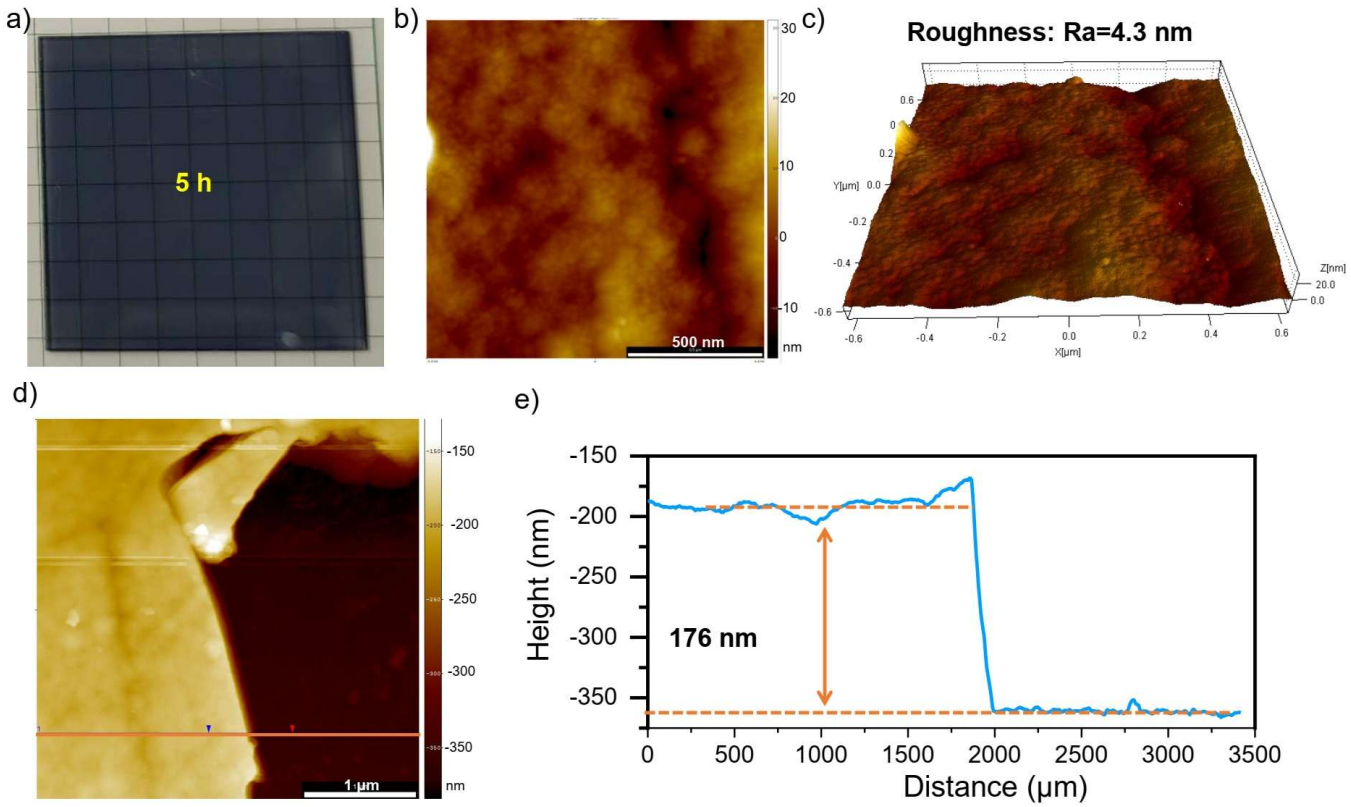


Figure S17. (a) Photograph of the glass substrate after film deposition for 5 h. (b) AFM image of the film surface. (c) Corresponding 3D AFM image of the film surface. (d) AFM image of the film with a step used for thickness measurement. (e) Height profile extracted from the AFM image along the step.

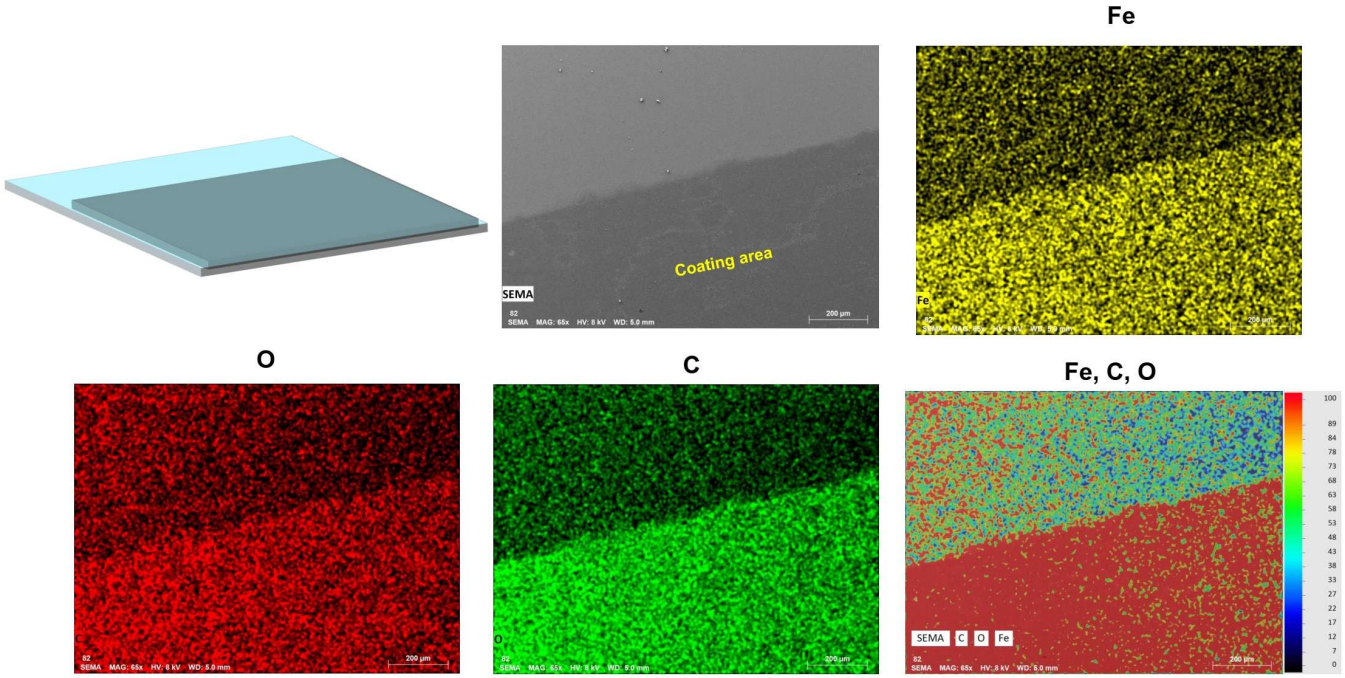


Figure S18. The 3D schematic of, SEM image and corresponding element distribution maps of the film, where a part of the film is masked for comparison.

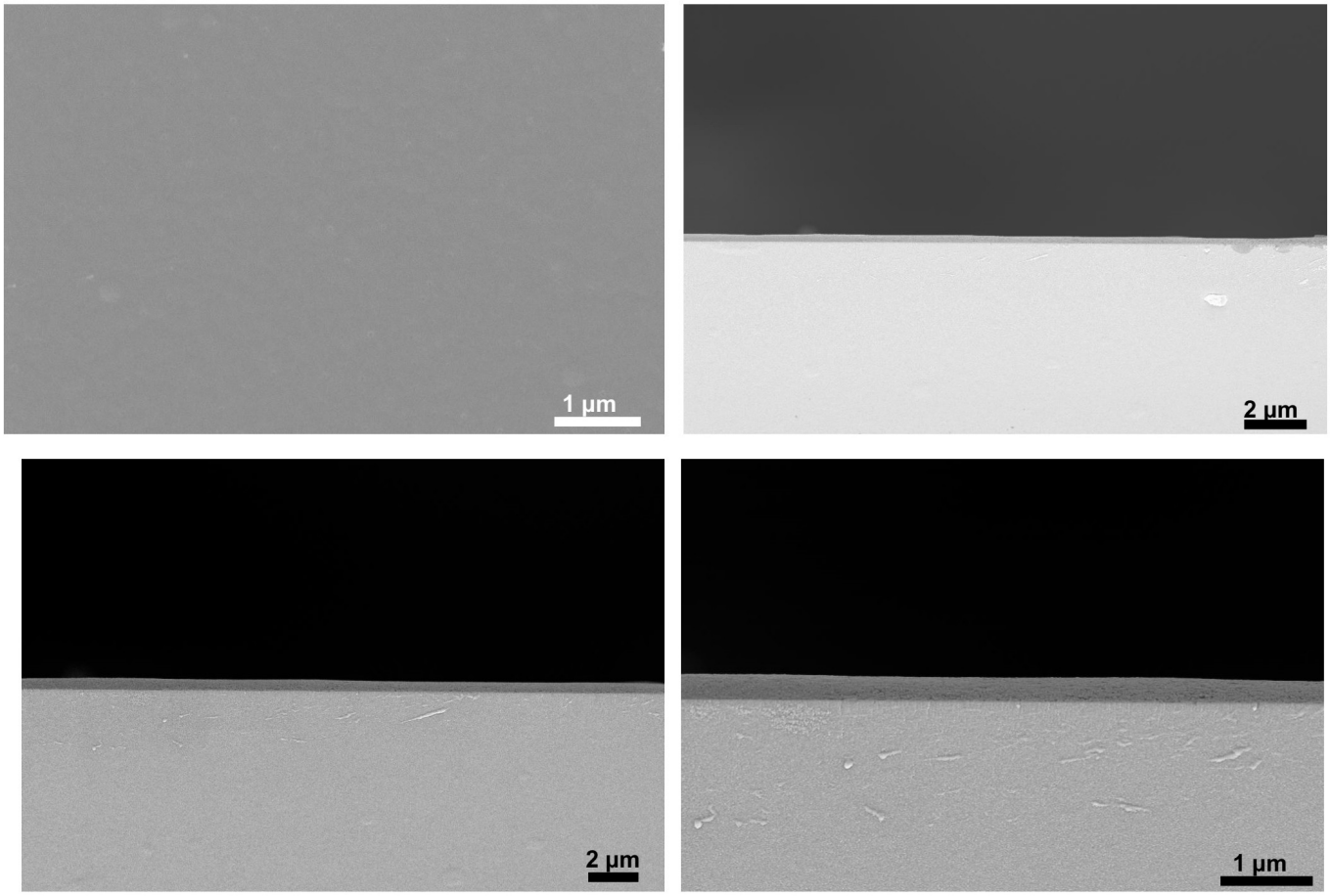


Figure S19. SEM surface and cross-sectional images of the deposited thin film on glass with different magnifications. The SEM images reveal that the thin-film surface is highly flat.

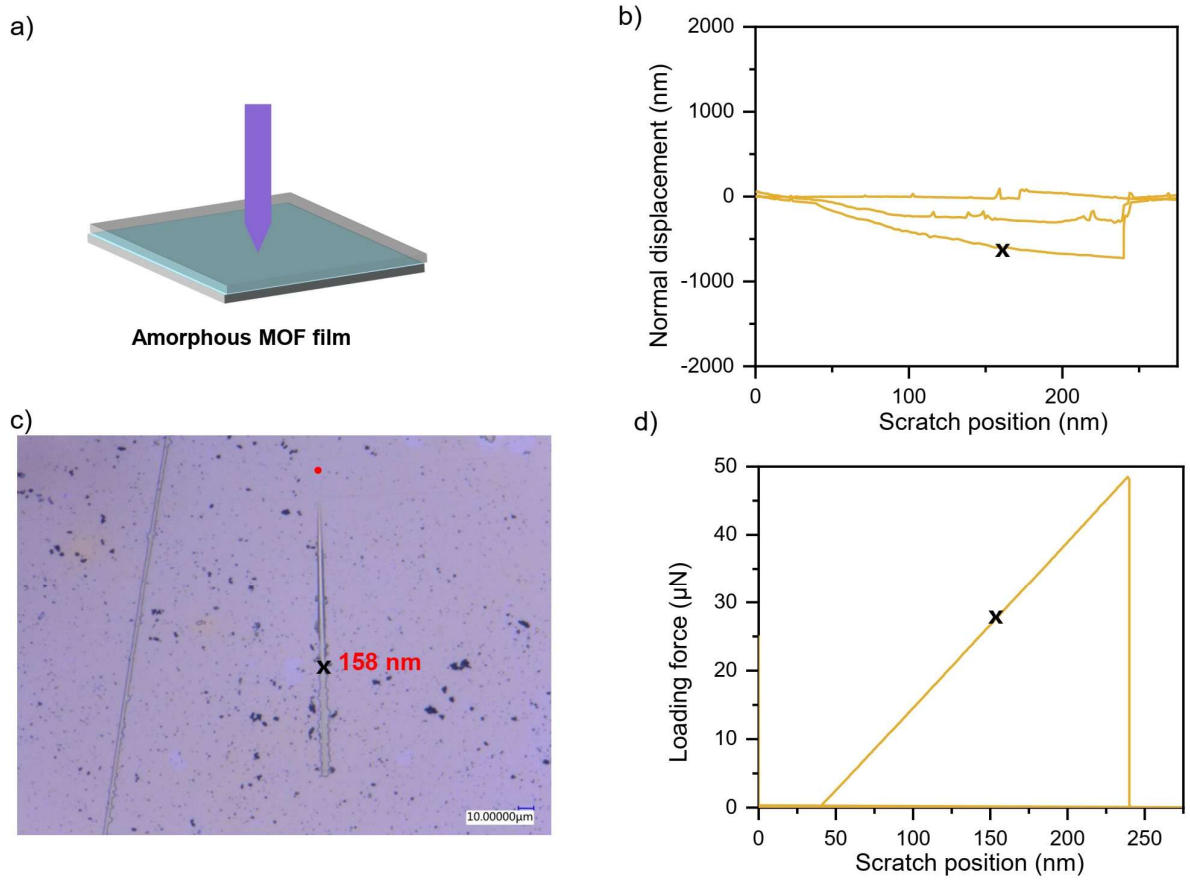


Figure S20. (a) Schematic diagram of the thin film nanoscratch test. (b) Curve of scratch position versus displacement. (c) Photograph of the thin film nanoscratch. (d) Curve of scratch position versus loading force. The cross symbols in the b-d indicate the same position.

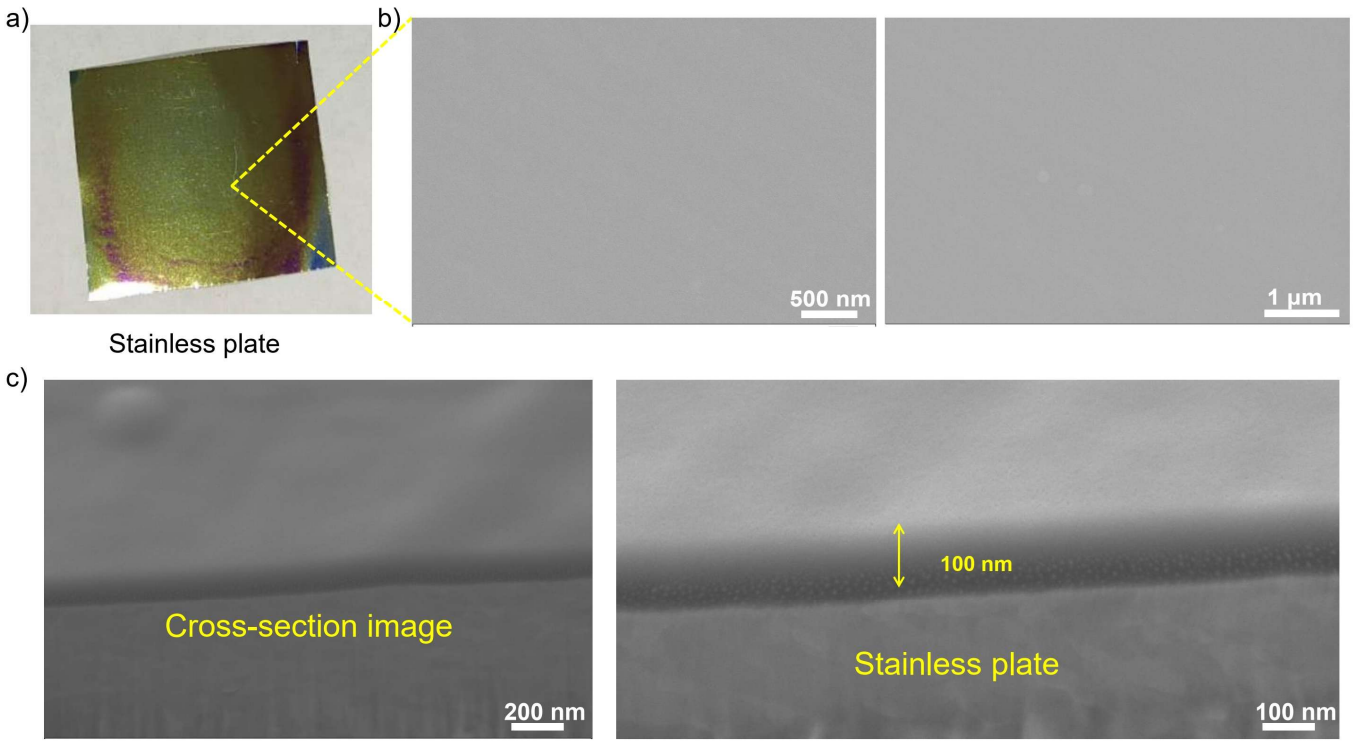


Figure S21. (a) Photograph of the gFe-DOBDC films on stainless steel. (b) SEM surface images of the deposited thin film. (c) cross-sectional images of the deposited thin film with different magnifications. The SEM images reveal that the thin-film surface is flat.

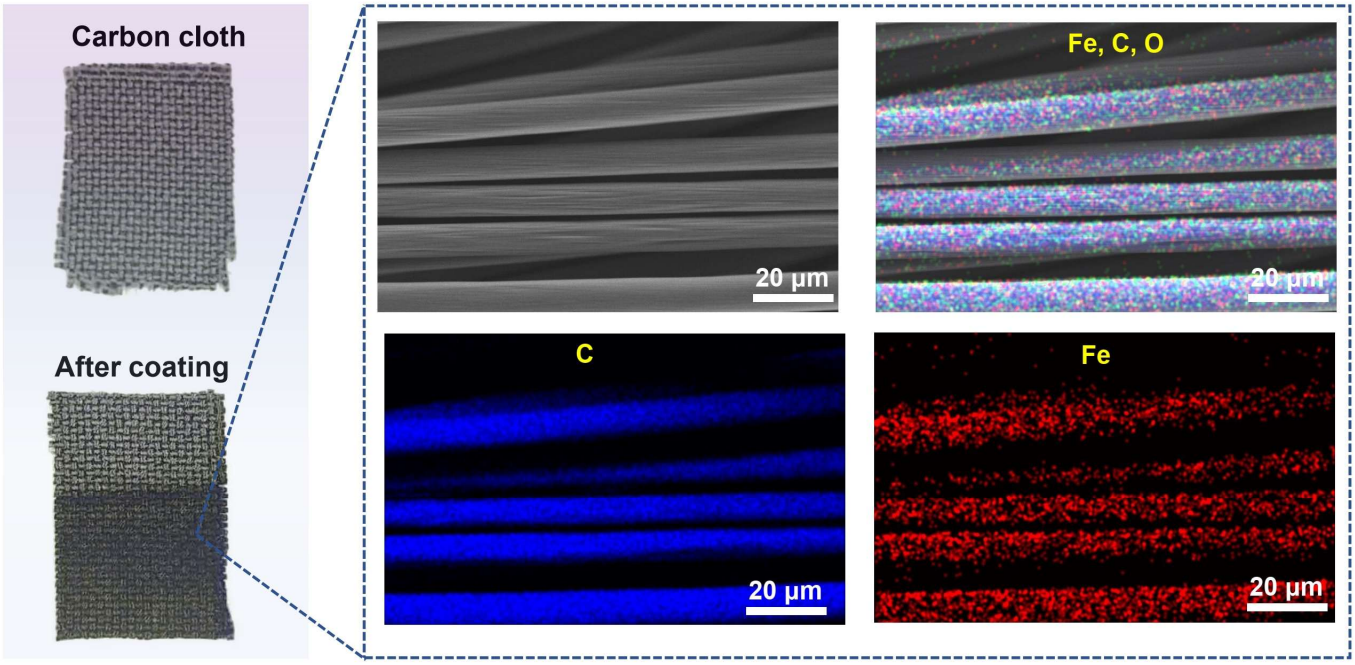


Figure S22. SEM image and corresponding element distribution maps of the gFe-DOBDC films on carbon cloth. The left side shows the photograph of pristine carbon cloth and the carbon cloth after coating.

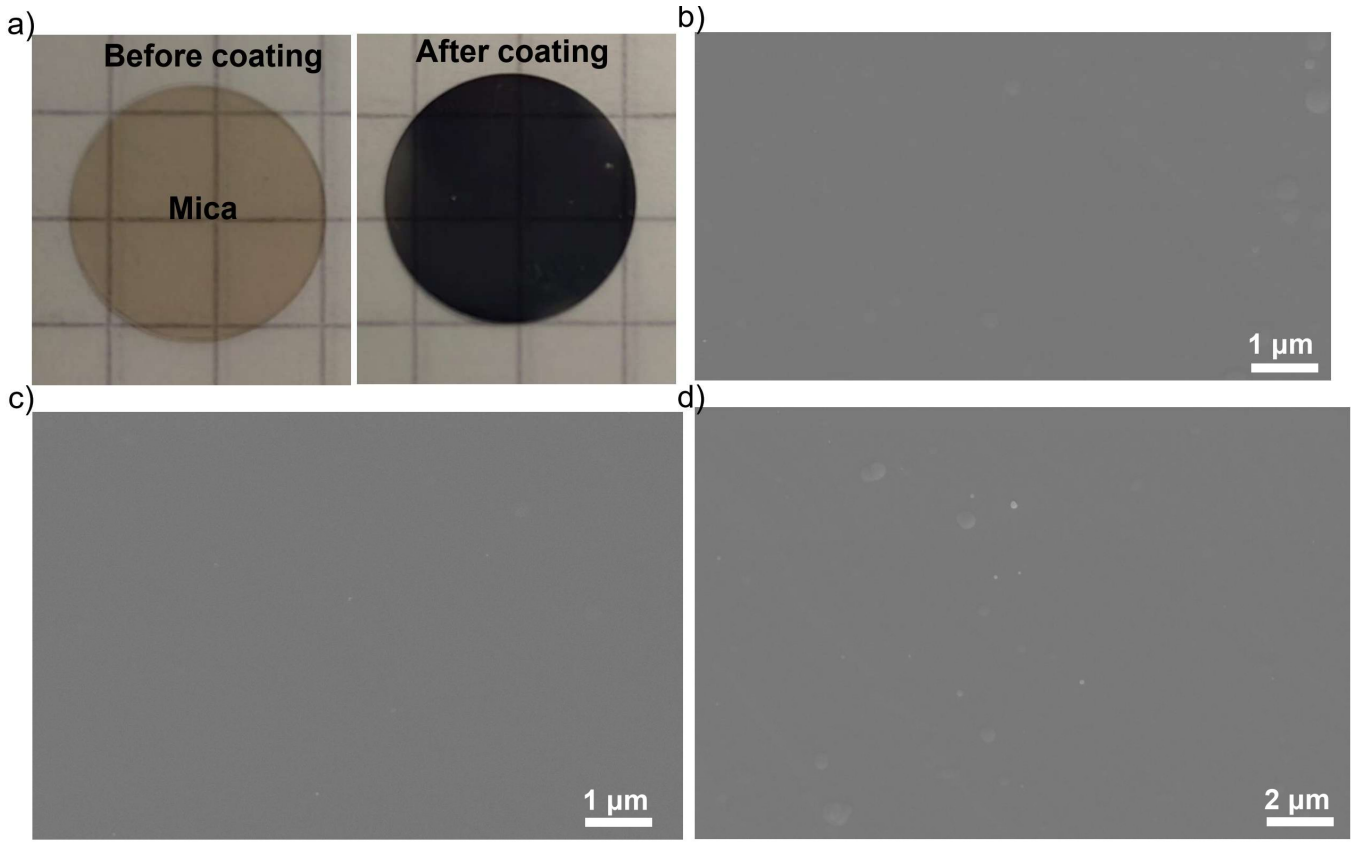


Figure S23. (a) Photograph of the mica before and after gFe-ODBDC deposition. (b-d) SEM images of the film surface at different magnifications. The SEM images reveal that the thin-film surface is flat.

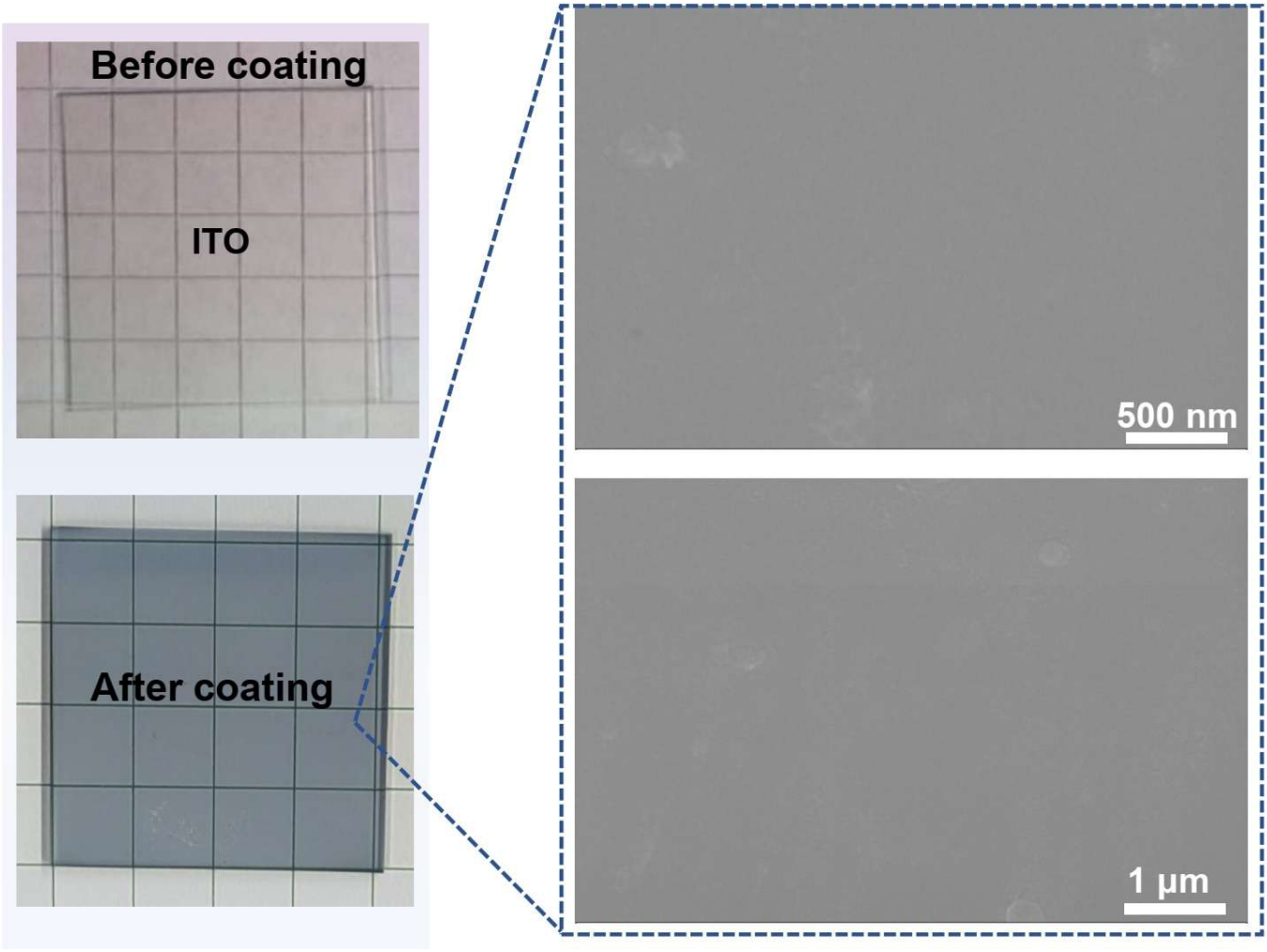


Figure S24. Photograph of the ITO before and after gFe-ODBDC deposition and the SEM images of the film surface with different magnifications.

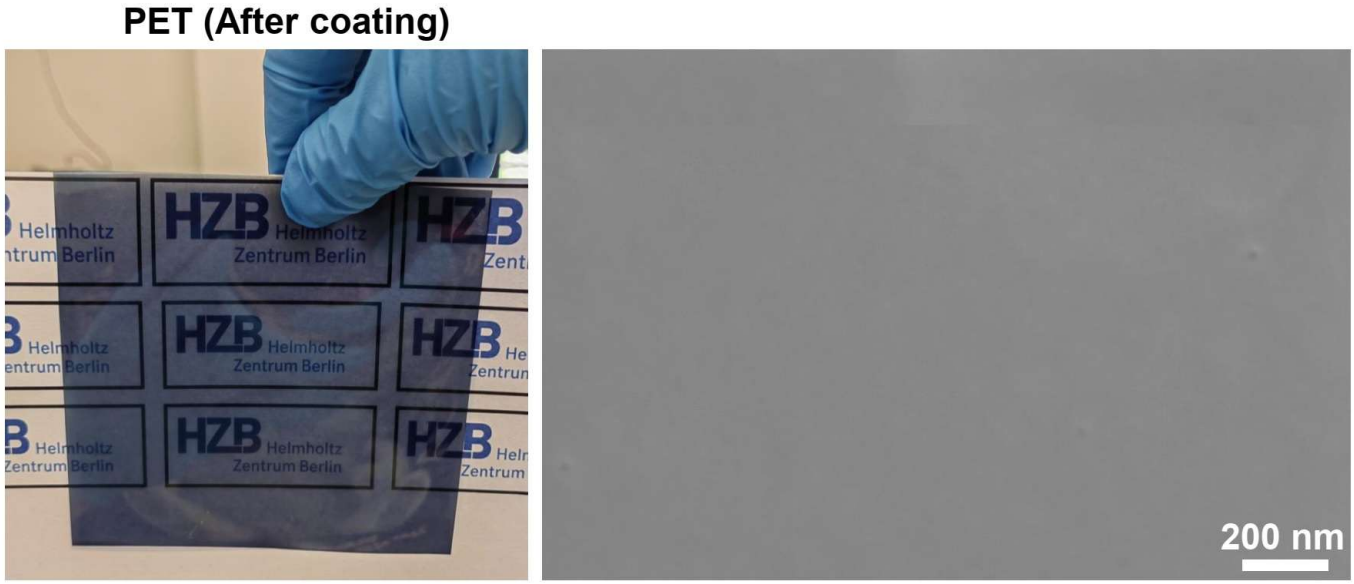


Figure S25. Photograph of the PET after gFe-ODBDC deposition and the SEM images of the film surface.

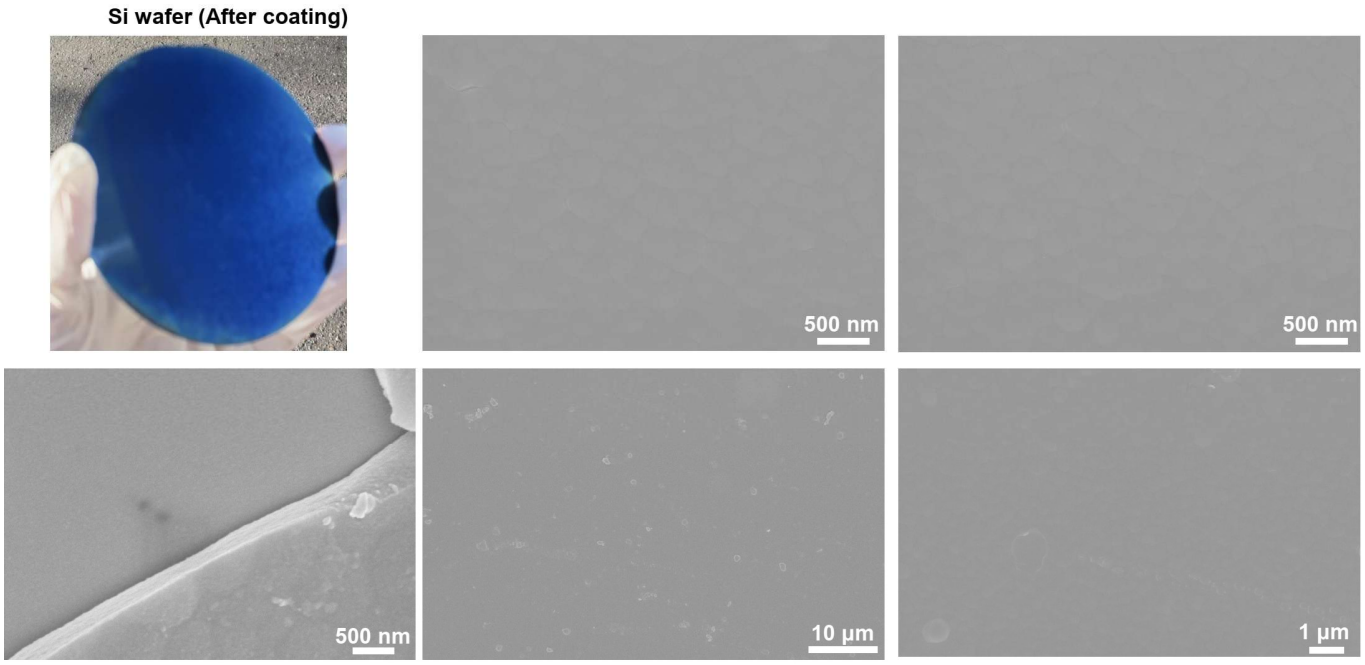


Figure S26. Photograph of the gFe-ODBDC films on silicon wafer and the SEM images of the film surface at different magnifications.

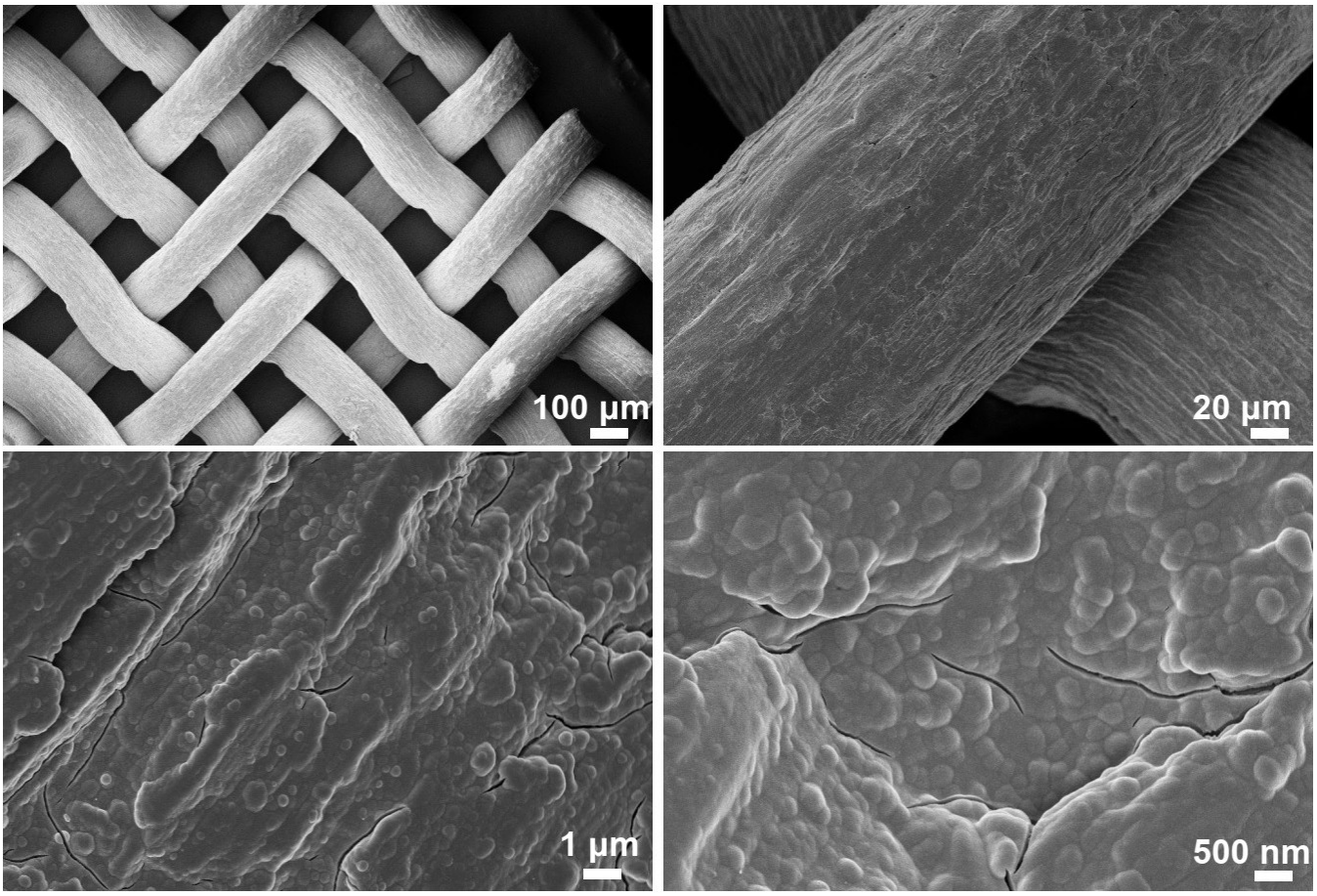


Figure S27. The SEM images of gFe-ODBDC films on Ti mesh at different magnifications.

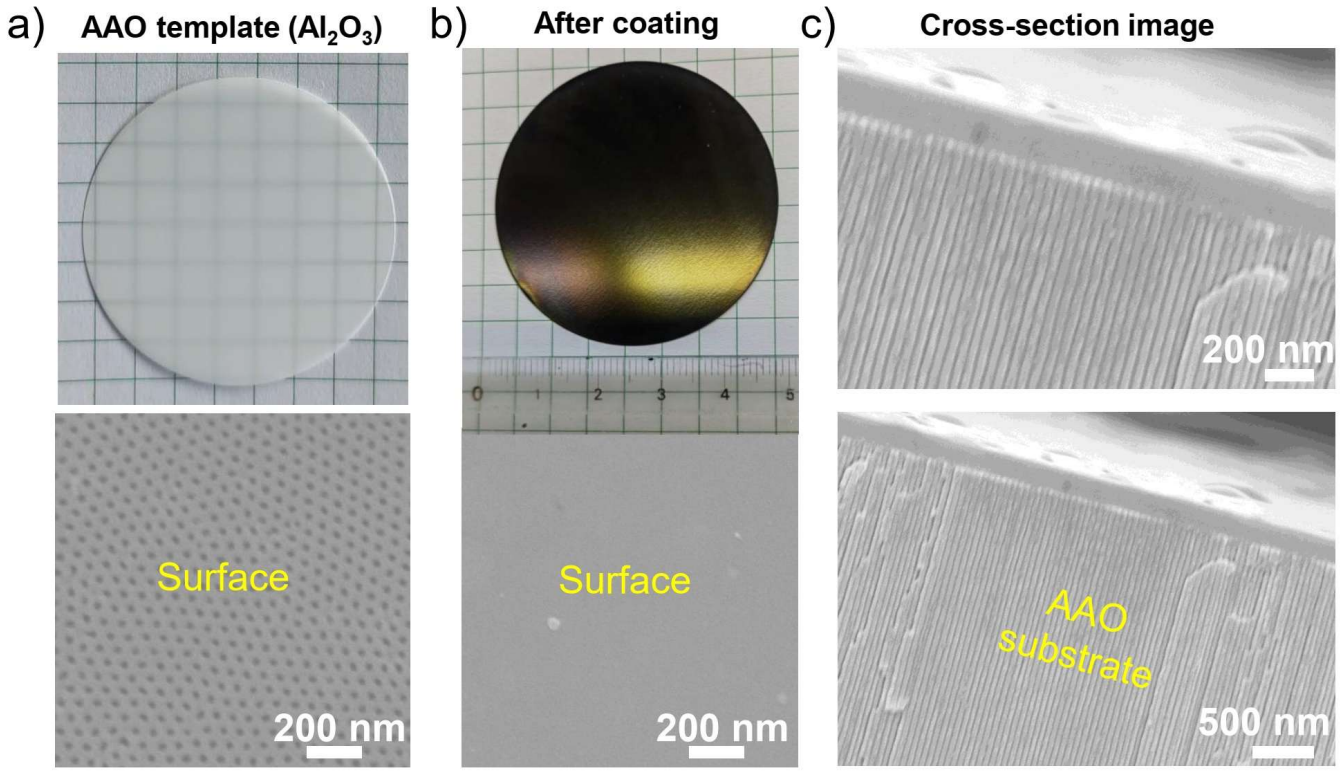


Figure S28. (a) Photograph and SEM image of the initial AAO membrane. (b) Photograph and SEM image of the AAO membrane after deposition of g-Fe-DOBDC. (c) Cross-sectional images of the deposited thin film on AAO.

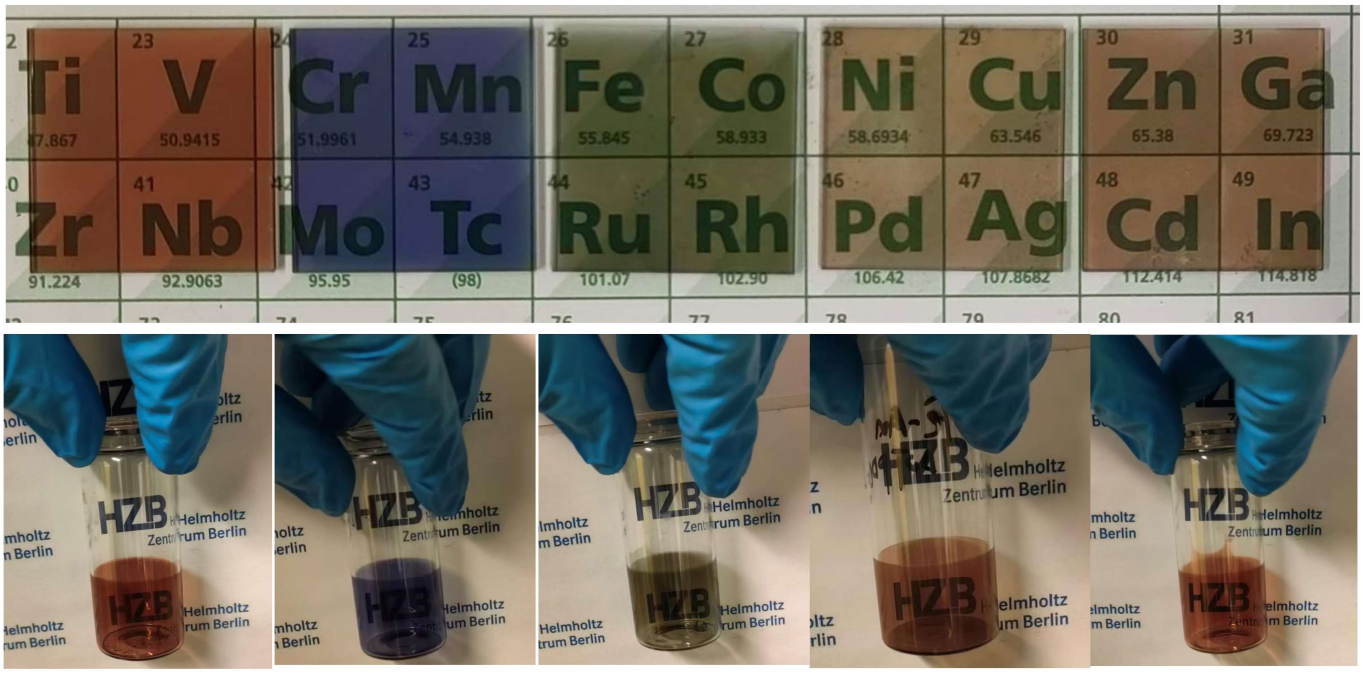


Figure S29. (a) Photograph images of other hydroxycarboxylate ligand-based thin film on ITO and vial. The same films are arranged in vertical correspondence with different substrates employed used. From left to right, the hydroxycarboxylate ligand are m-H_4DOBDC, H_4DOBPDC, H_4DONDC, H_4DOTPDC, and H_4An-DOBDC, respectively. The elements under the transparent film are purely illustrative to visualize its high transparency and have no scientific implication.

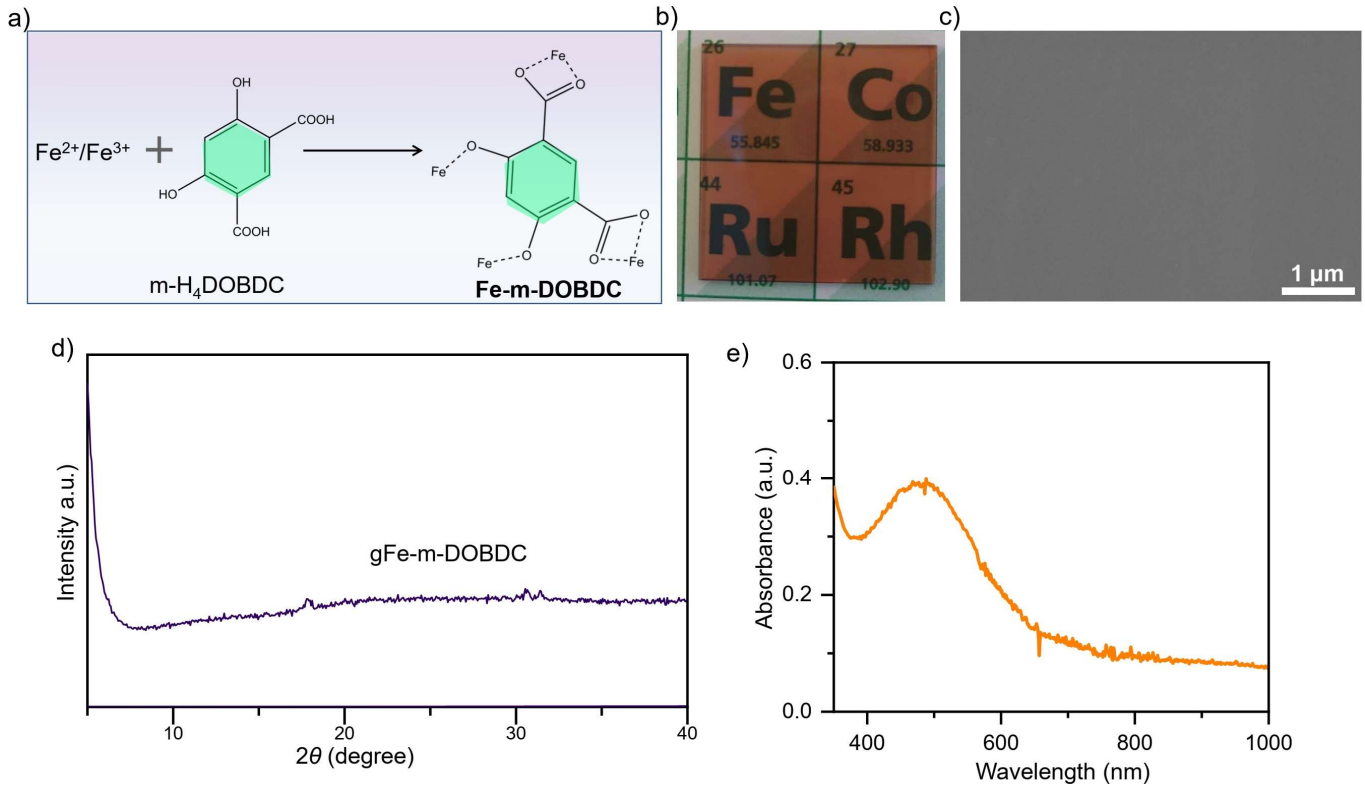


Figure S30. (a) Schematic illustration of the preparation of gFe-m-DOBDC. (b) Photograph of the gFe-m-DOBDC thin film. (c) SEM image of gFe-m-DOBDC. (d) PXRD patterns of gFe-m-DOBDC. (e) UV-vis absorption spectra of gFe-m-DOBDC.

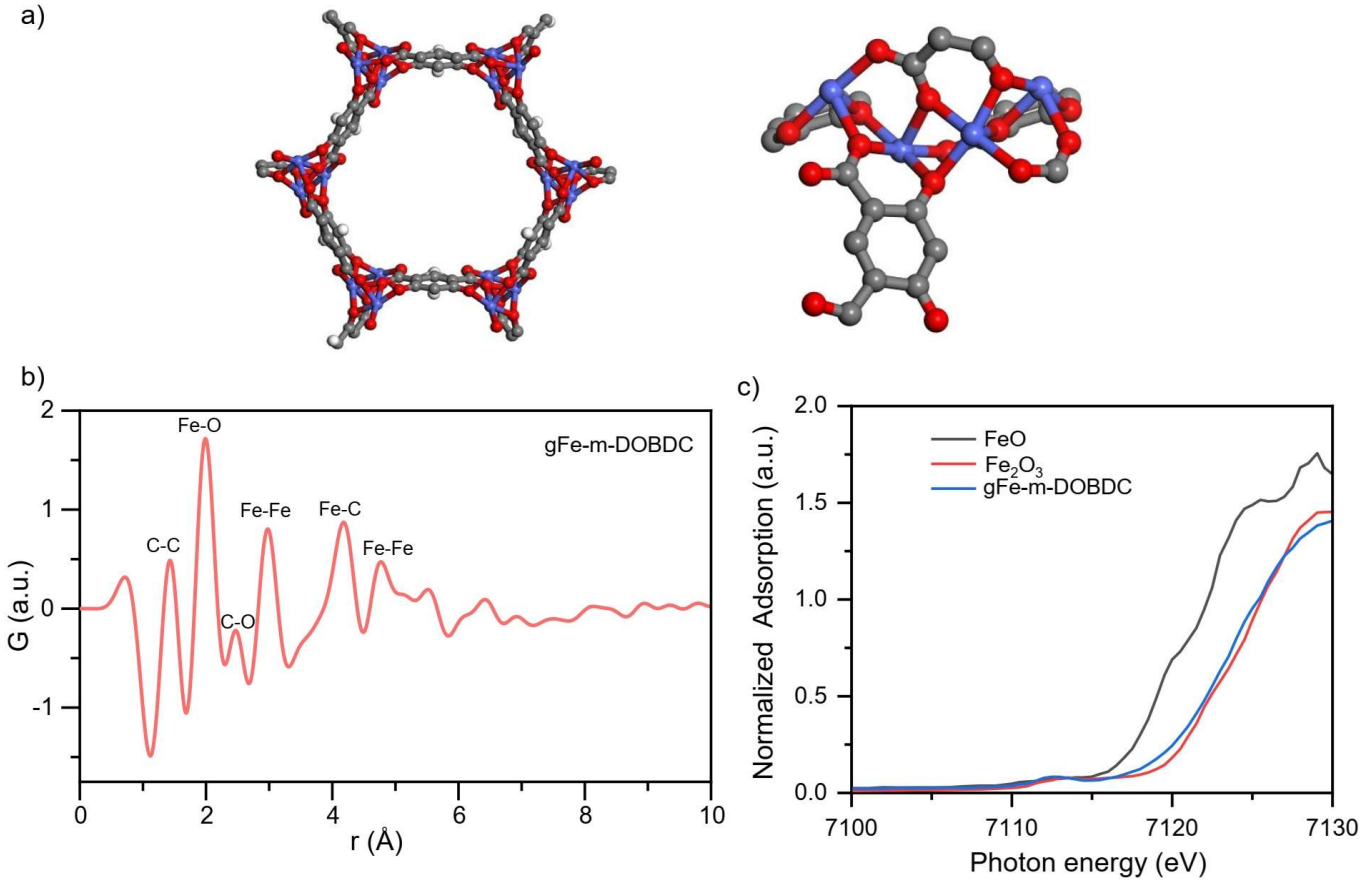


Figure S31. (a) The molecular models of the gFe-m-DOBDC. (b) Experimental pair distribution functions of the gFe-m-DOBDC. (c) Normalized XANES spectra of gFe-m-DOBDC. The curves of FeO and Fe_2O_3 are used as comparisons, representing the valences of Fe^{2+} and Fe^{3+}, respectively.

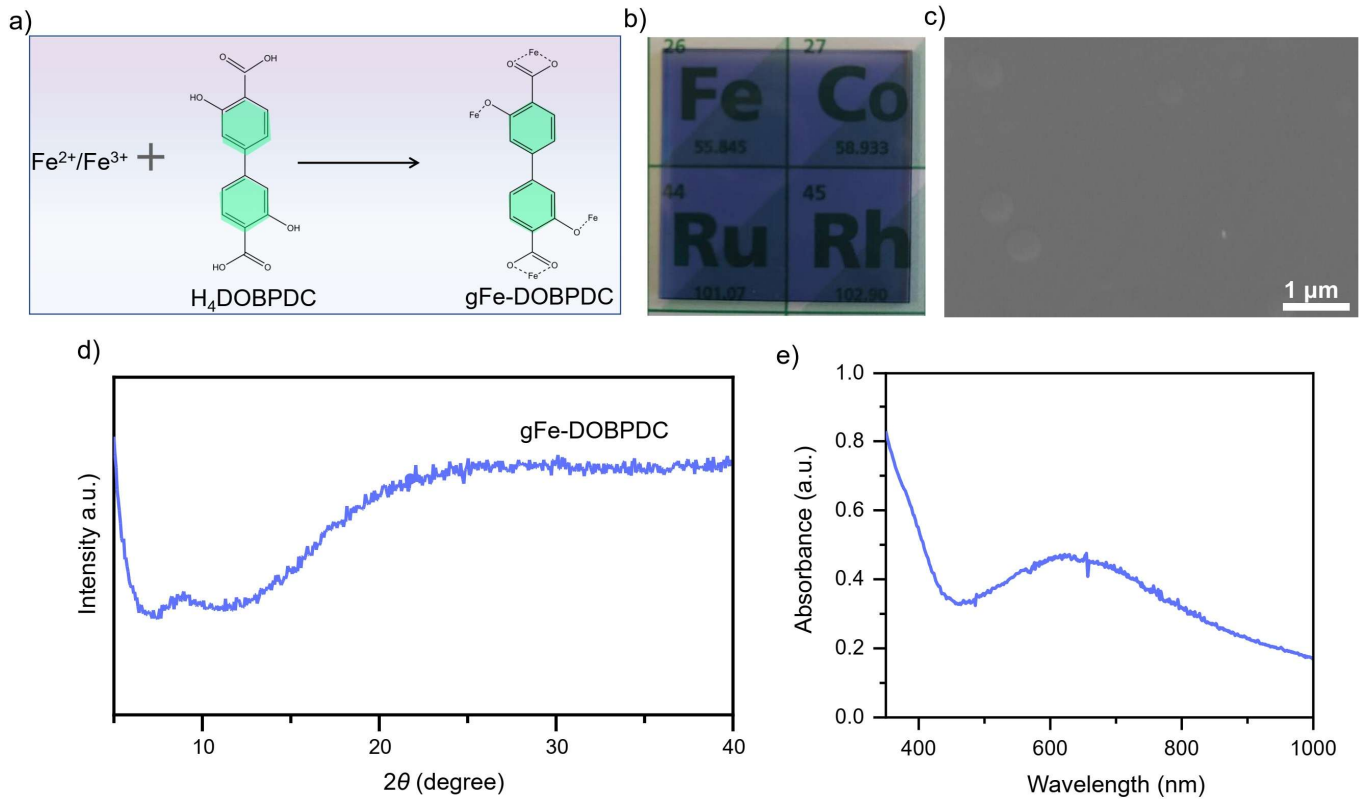


Figure S32. (a) Schematic illustration of the preparation of gFe-DOBPDC. (b) Photograph of the gFe-DOBPDC thin film. (c) SEM image of gFe-DOBPDC. (d) PXRD patterns of gFe-DOBPDC. (e) UV-vis absorption spectra of gFe-DOBPDC.

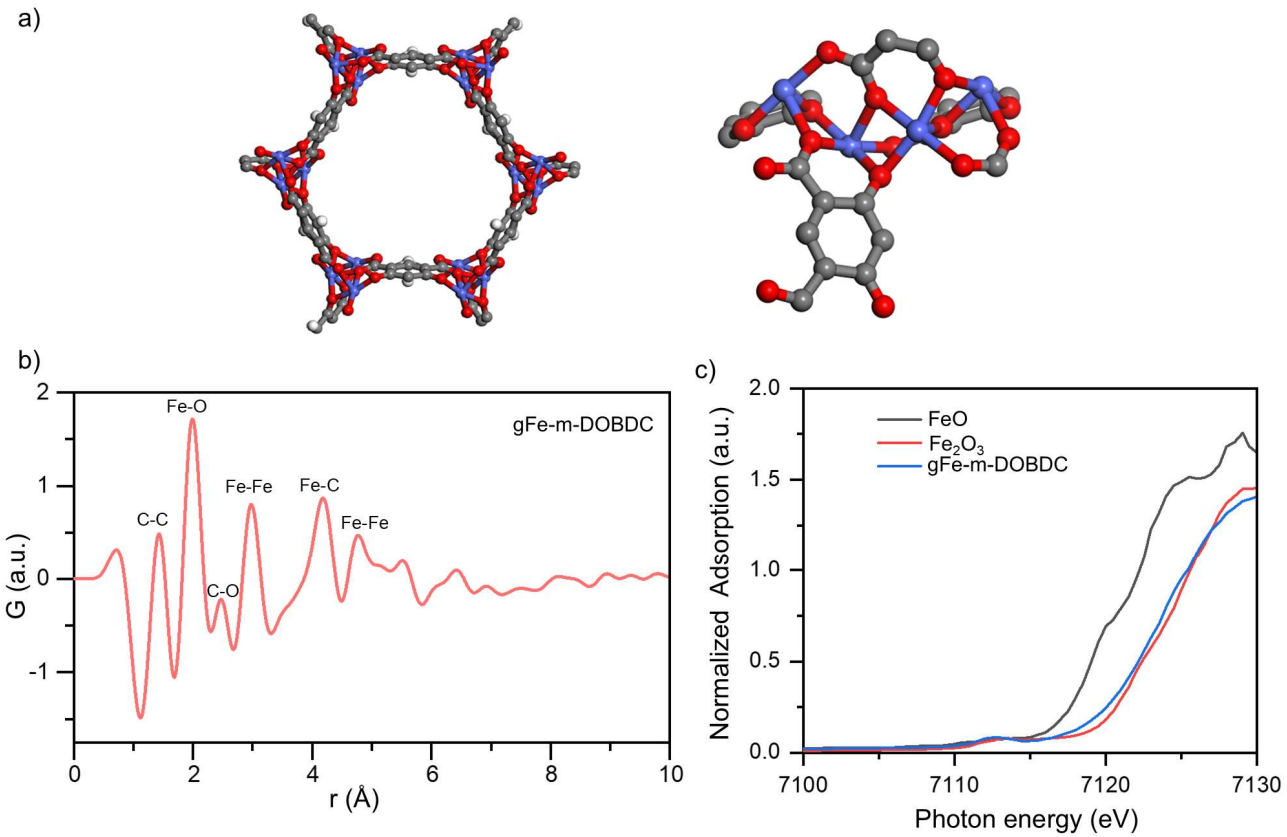


Figure S33. (a) The molecular models of the gFe-DOBPDC. (b) Experimental pair distribution functions of the gFe-DOBPDC. (c) Normalized XANES spectra of gFe-DOBPDC. The curves of FeO and Fe_2O_3 are used as comparisons, representing the valences of Fe^{2+} and Fe^{3+}, respectively.

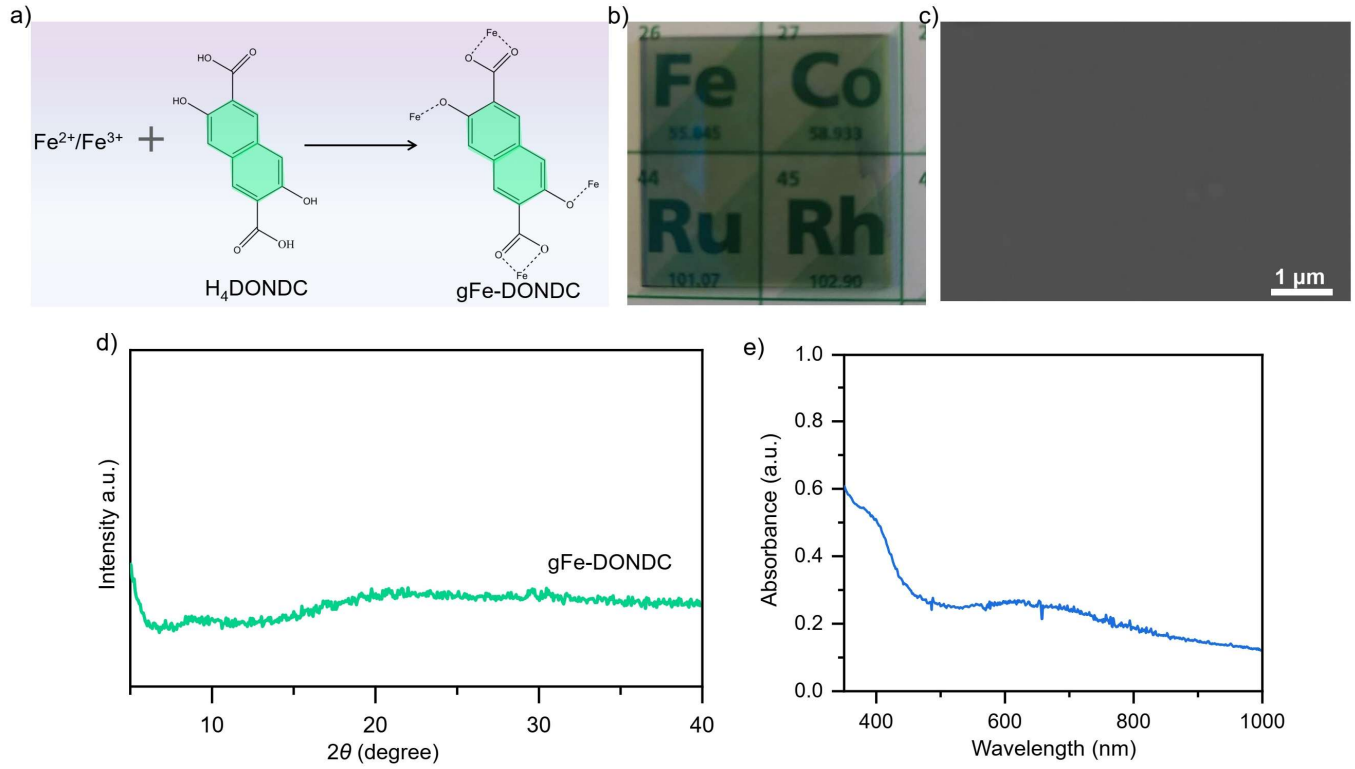


Figure S34. (a) Schematic illustration of the preparation of gFe-DONDC. (b) Photograph of the gFe-DONDC thin film. (c) SEM image of gFe-DONDC. (d) PXRD pattern of gFe-DONDC. (e) UV-vis absorption spectra of gFe-DONDC.

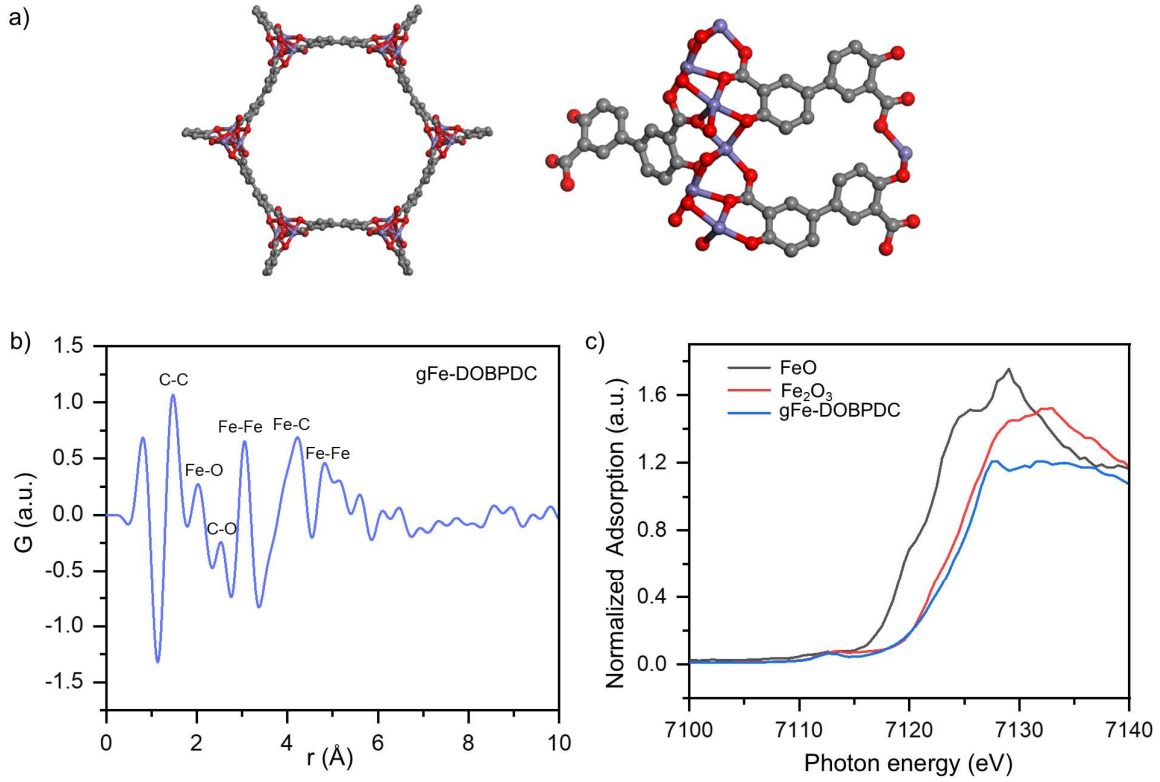


Figure S35. (a) The molecular models of the gFe-DONDC. (b) Experimental pair distribution functions of the gFe-DONDC. (c) Normalized XANES spectra of gFe-DONDC. The curves of FeO and Fe_2O_3 are used as comparisons, representing the valences of Fe^{2+} and Fe^{3+}, respectively.

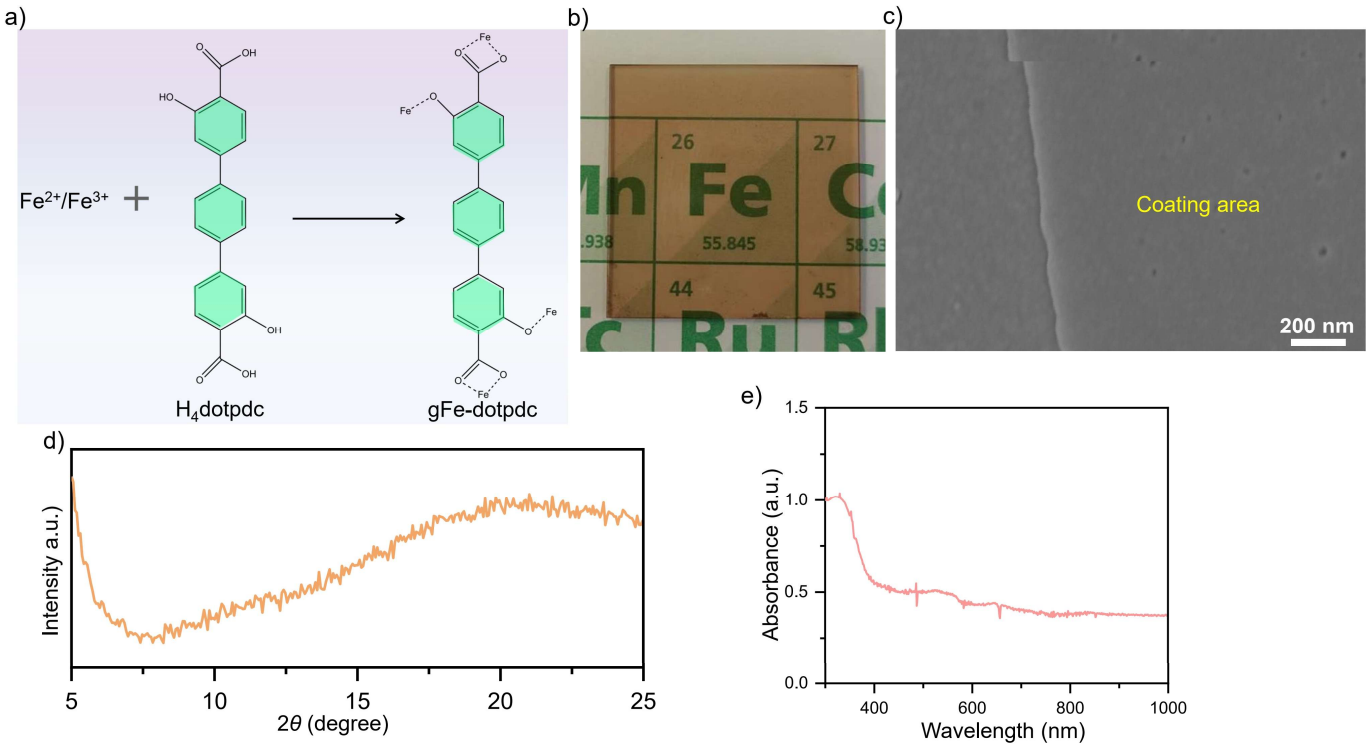


Figure S36. (a) Schematic illustration of the preparation of gFe-DOTPDC. (b) Photograph of the gFe-DOTPDC thin film. (c) SEM image of gFe-DOTPDC. (d) PXRD pattern of gFe-DOTPDC. (e) UV-vis absorption spectra of gFe-DOTPDC.

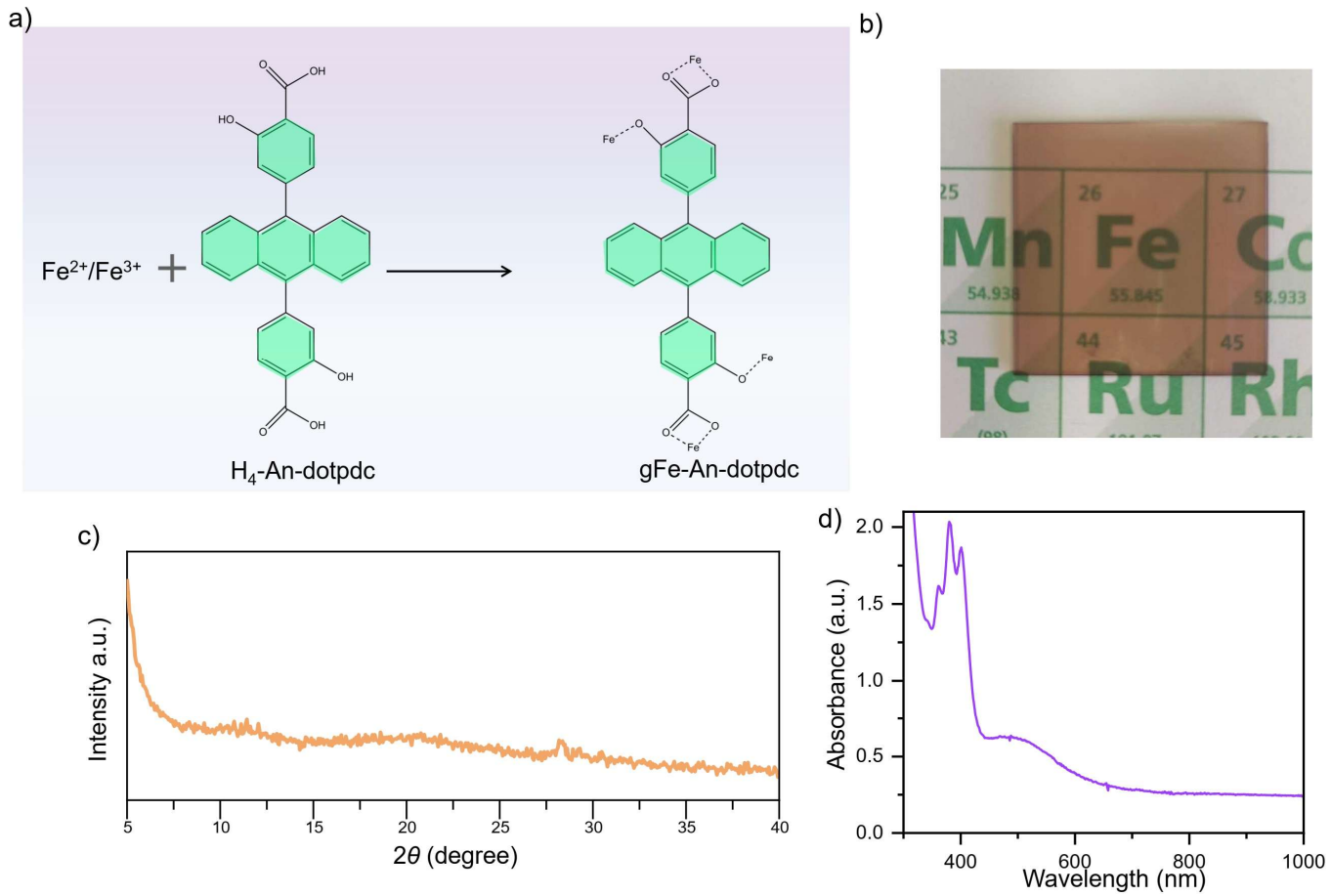


Figure S37. (a) Schematic illustration of the preparation of gFe-An-DOTPDC. (b) Photograph of the gFe-An-DOTPDC. (c) PXRD pattern of gFe-An-DOTPDC. (d) UV-vis absorption spectra of gFe-An-DOTPDC

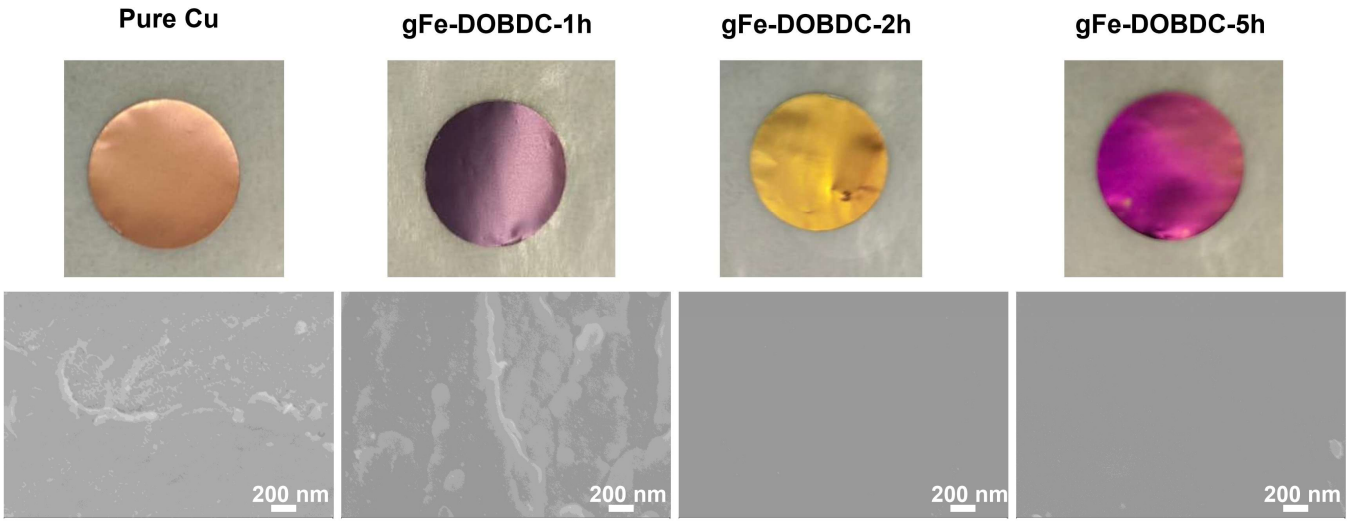


Figure S38. Photographs and corresponding SEM surface images of initial Cu, Cu deposited with gFe-DOBDC for 1 h, 2 h, and 5 h.

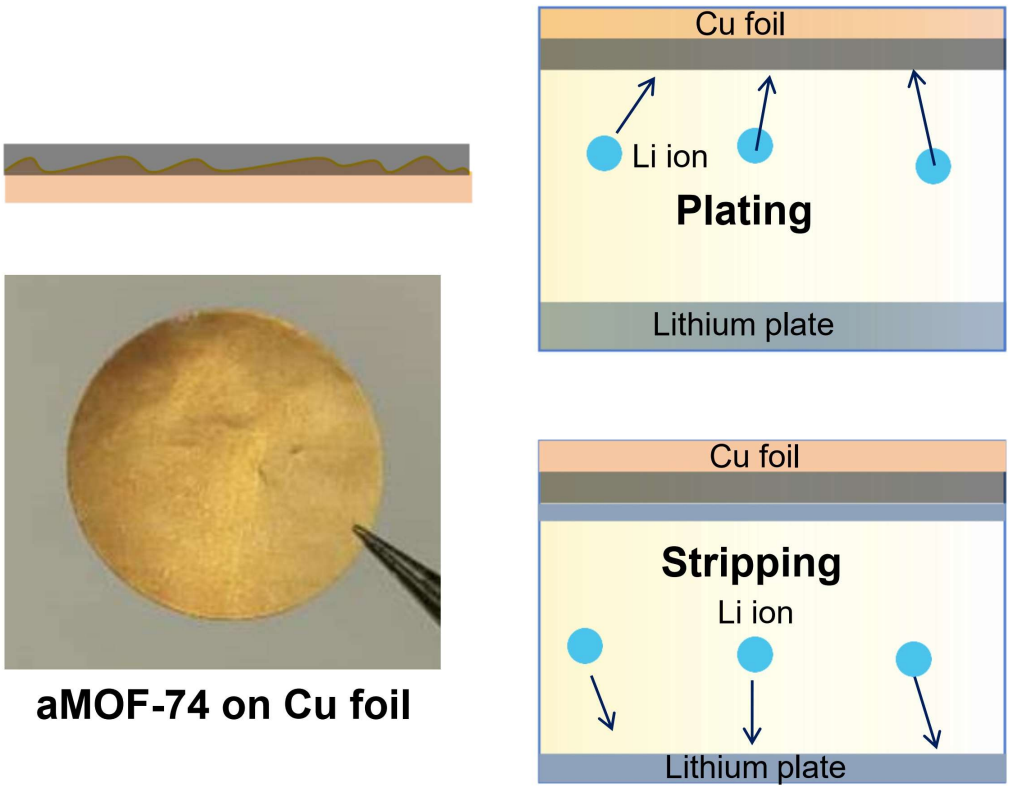


Figure S39. Photograph of gFe-DOBDC film on Cu foil and the schematic illustration of Li stripping and deposition on gFe-DOBDC films on Cu.

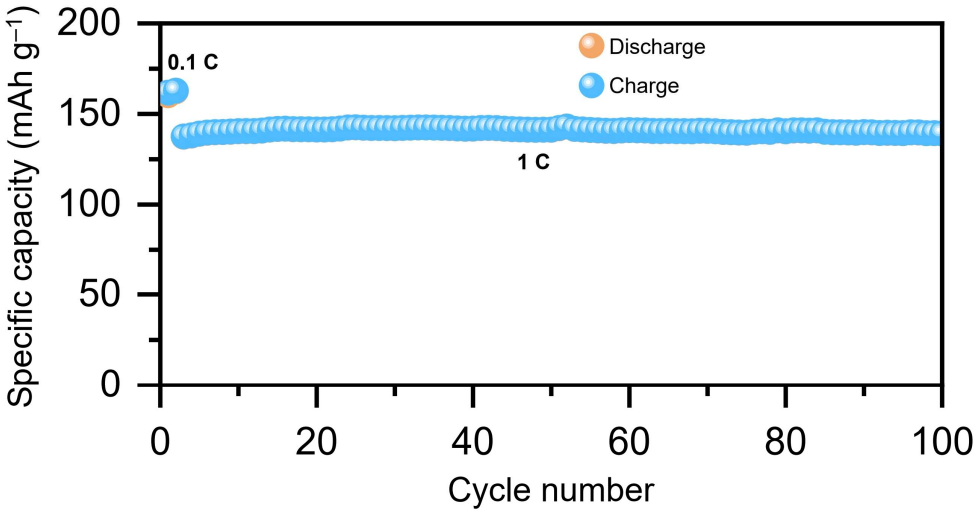


Figure S40. Cycling performance of gFe-DOBDC-Cu/$LiFePO_4$ anode-free batteries at 1C.

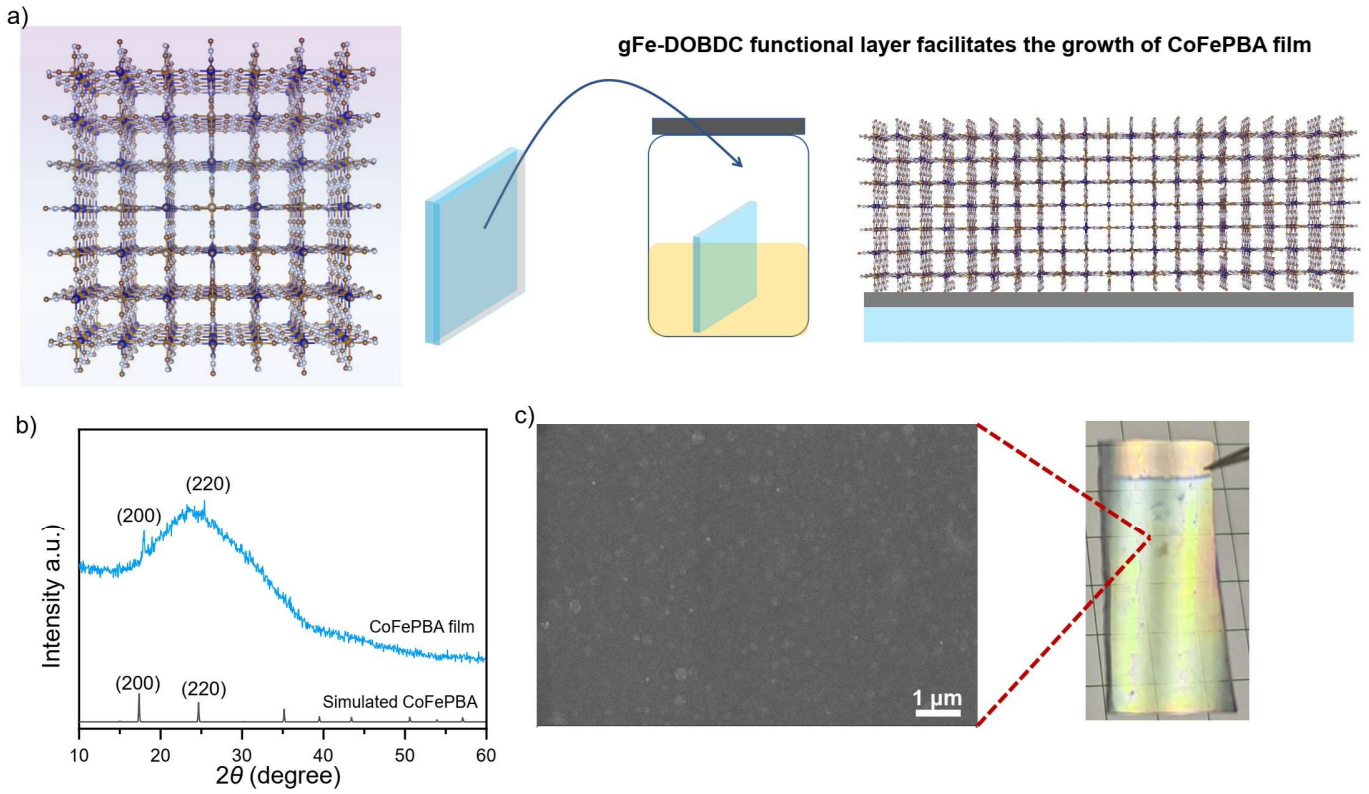


Figure S41. (a) Schematic diagram of the synthesis of CoFePBA films, where the gFe-DOBDC modification layer can assist the growth of CoFePBA. (b) PXRD pattern of the film. (c) SEM image and Photograph of the film.

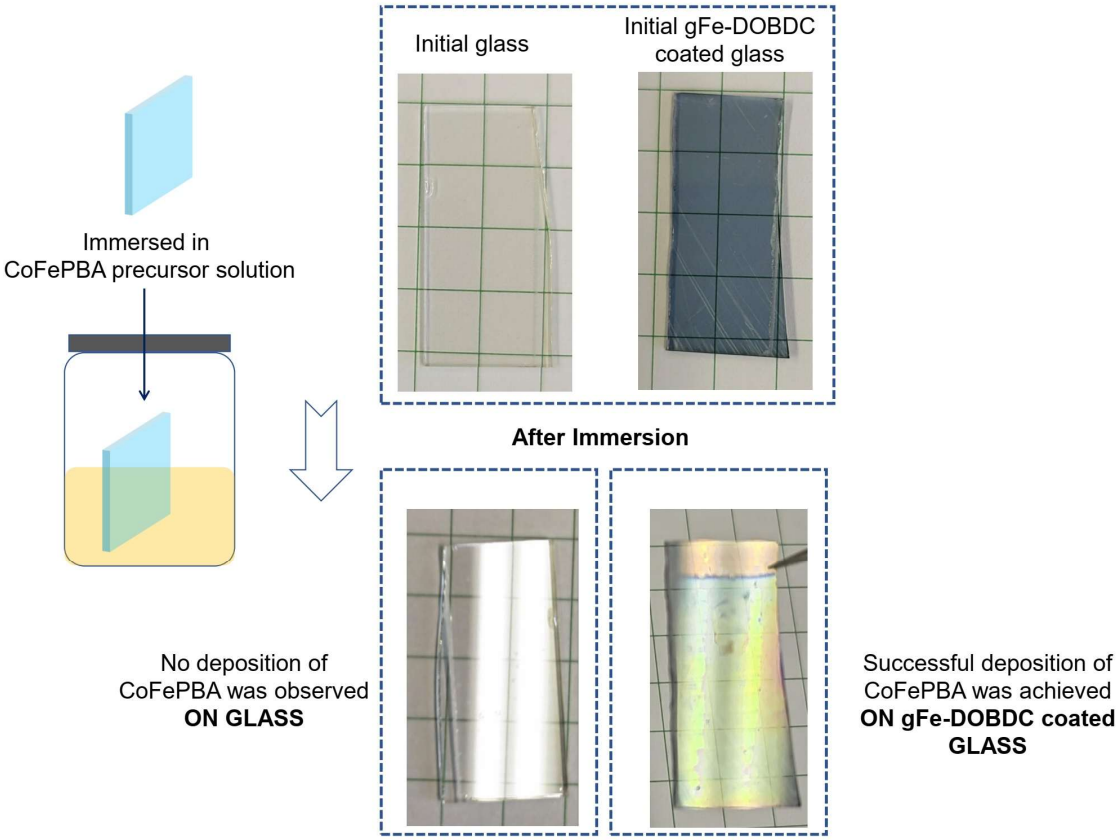


Figure S42. Comparison of CoFePBA growth on glass substrates with and without gFe-DOBDC modification layer. It is shown that CoFePBA films are successfully grown only on the substrates with gFe-DOBDC modification layer, while no CoFePBA deposition is observed on the pure glass without any modification.

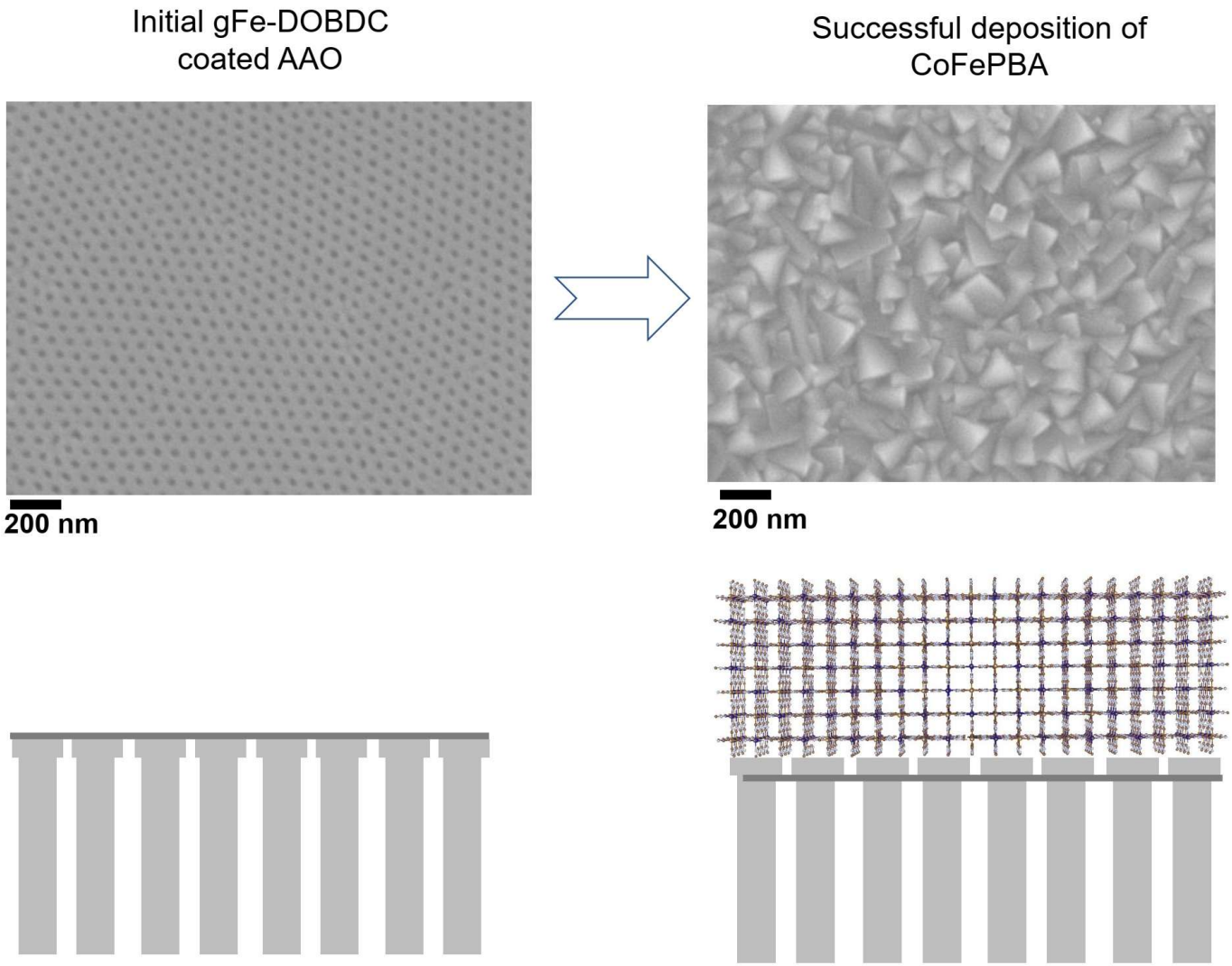


Figure S43. Schematic illustration of the synthesis of CoFePBA film on AAO, and the corresponding SEM image the film.

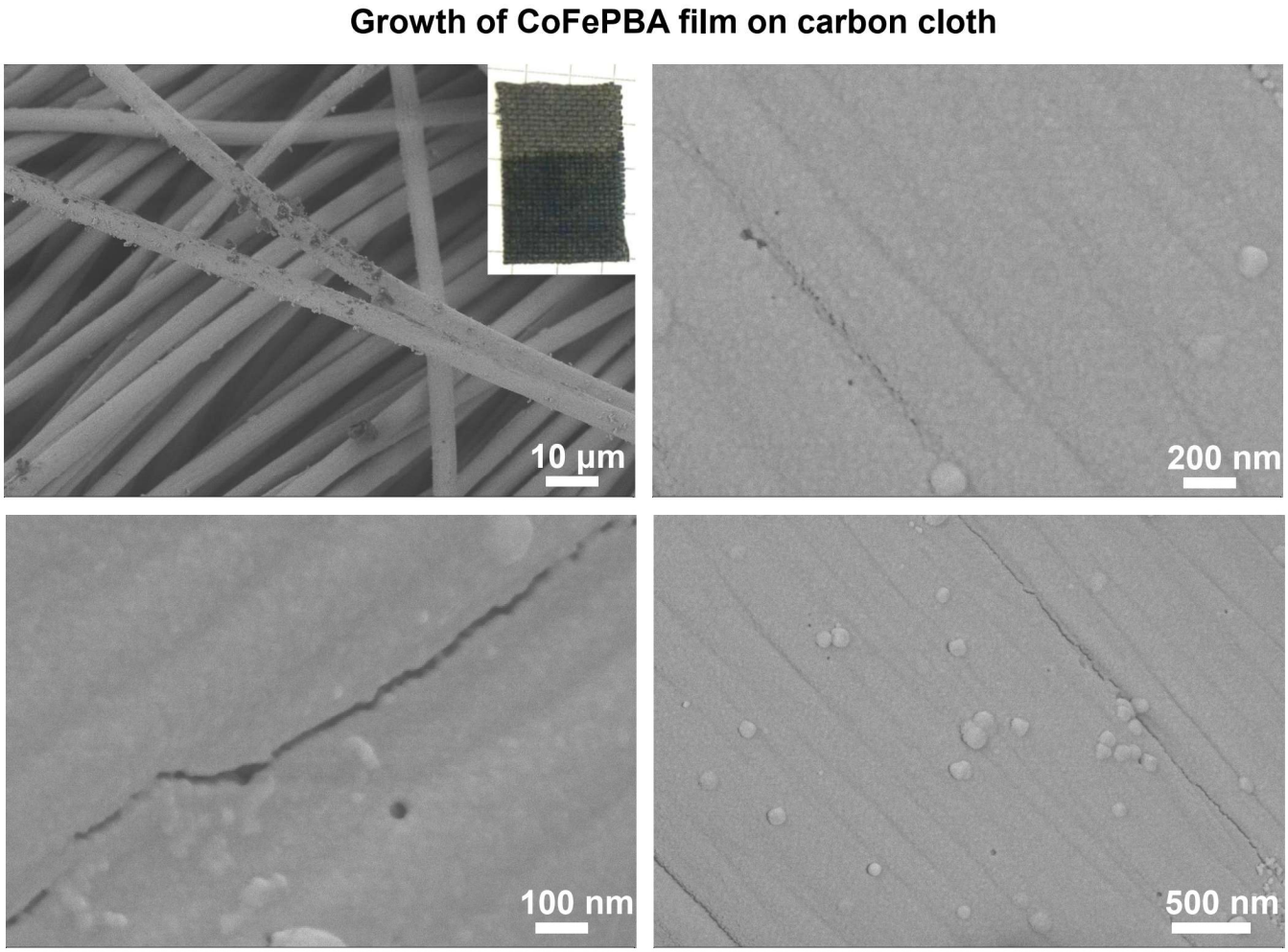


Figure S44. The Photograph of the CoFePBA film on carbon cloth and the SEM images of the film surface at different magnifications.

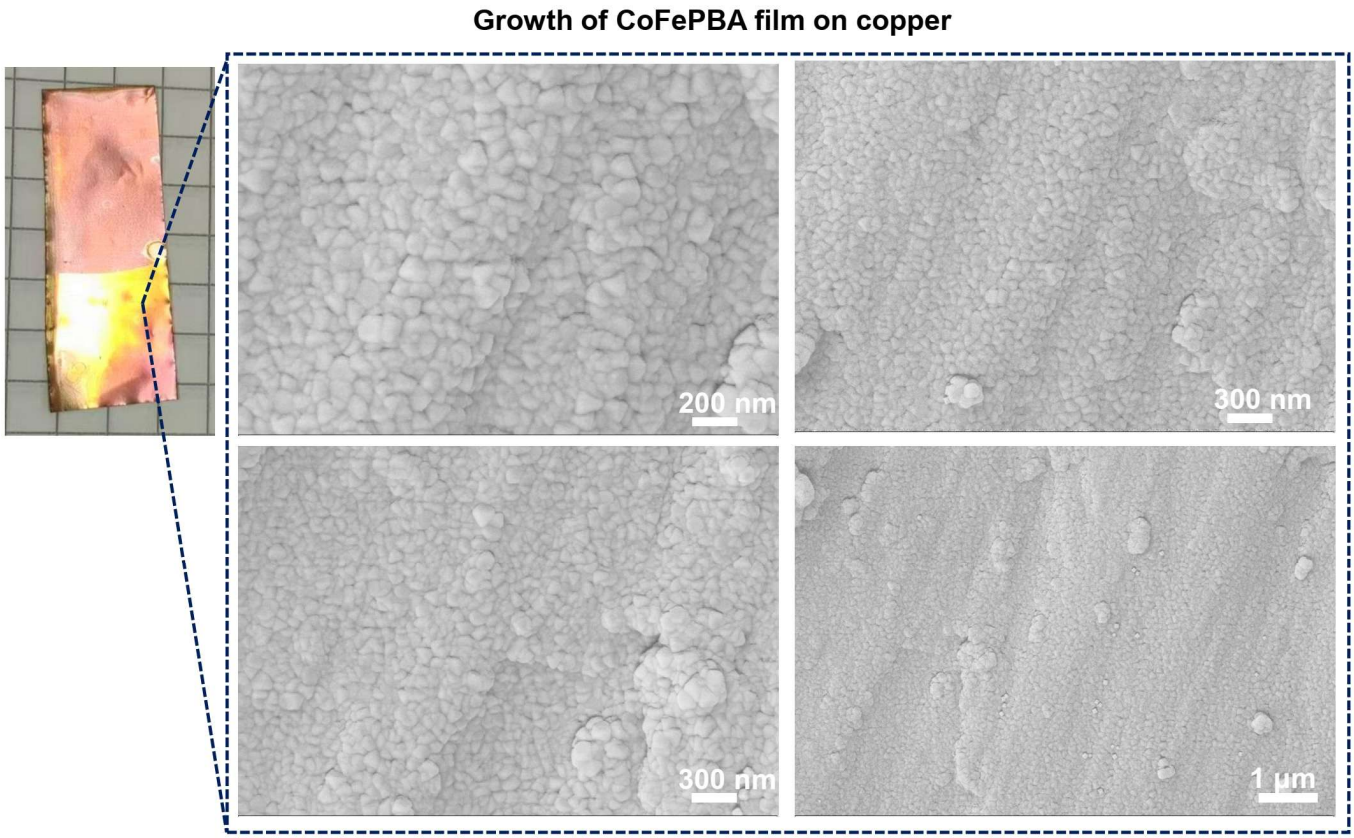


Figure S45. The Photograph of the CoFePBA film on copper foil and the SEM images of the film surface at different magnifications.

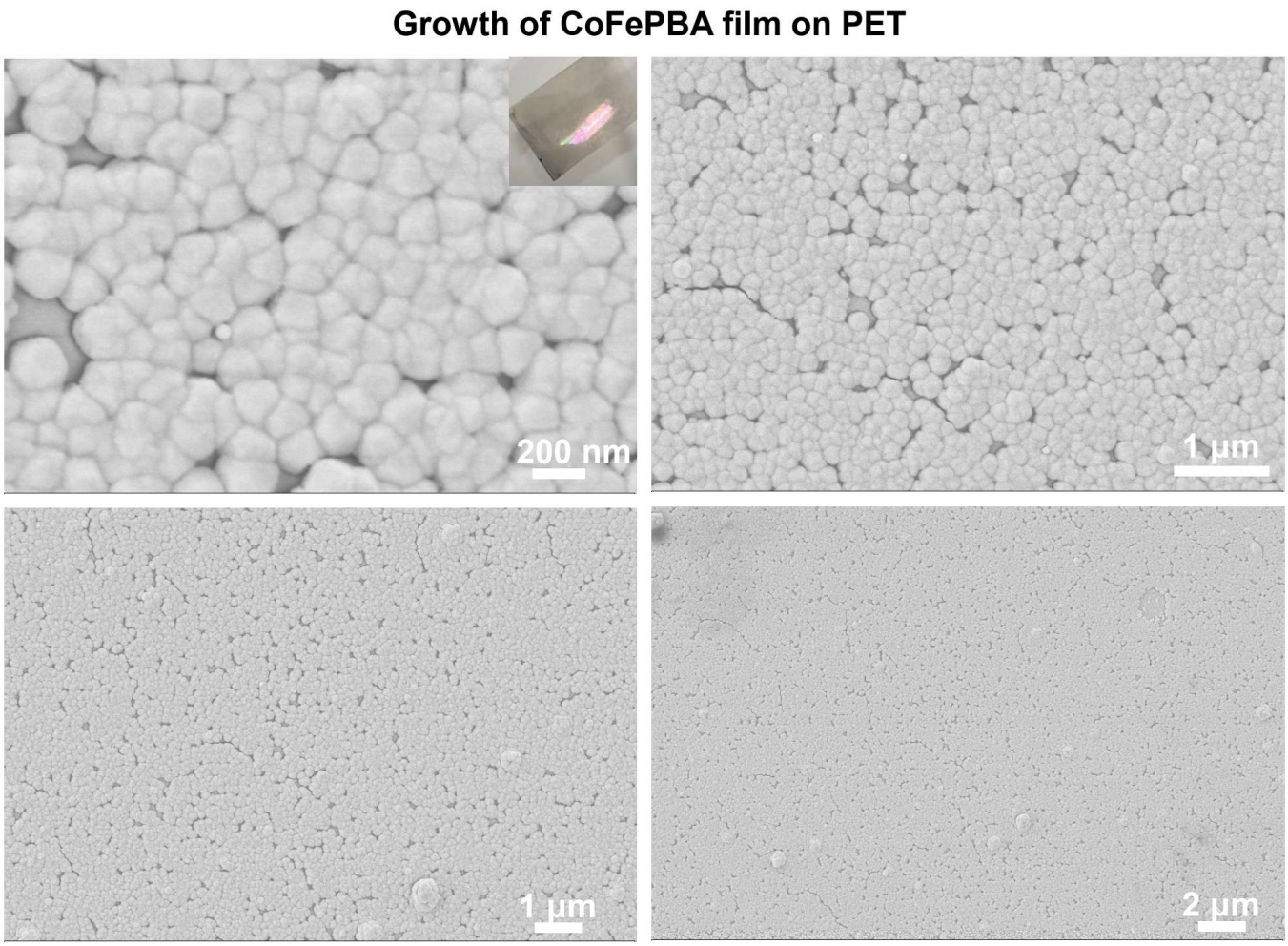


Figure S46. The Photograph of CoFePBA film on PET and the SEM images of the film surface at different magnifications.

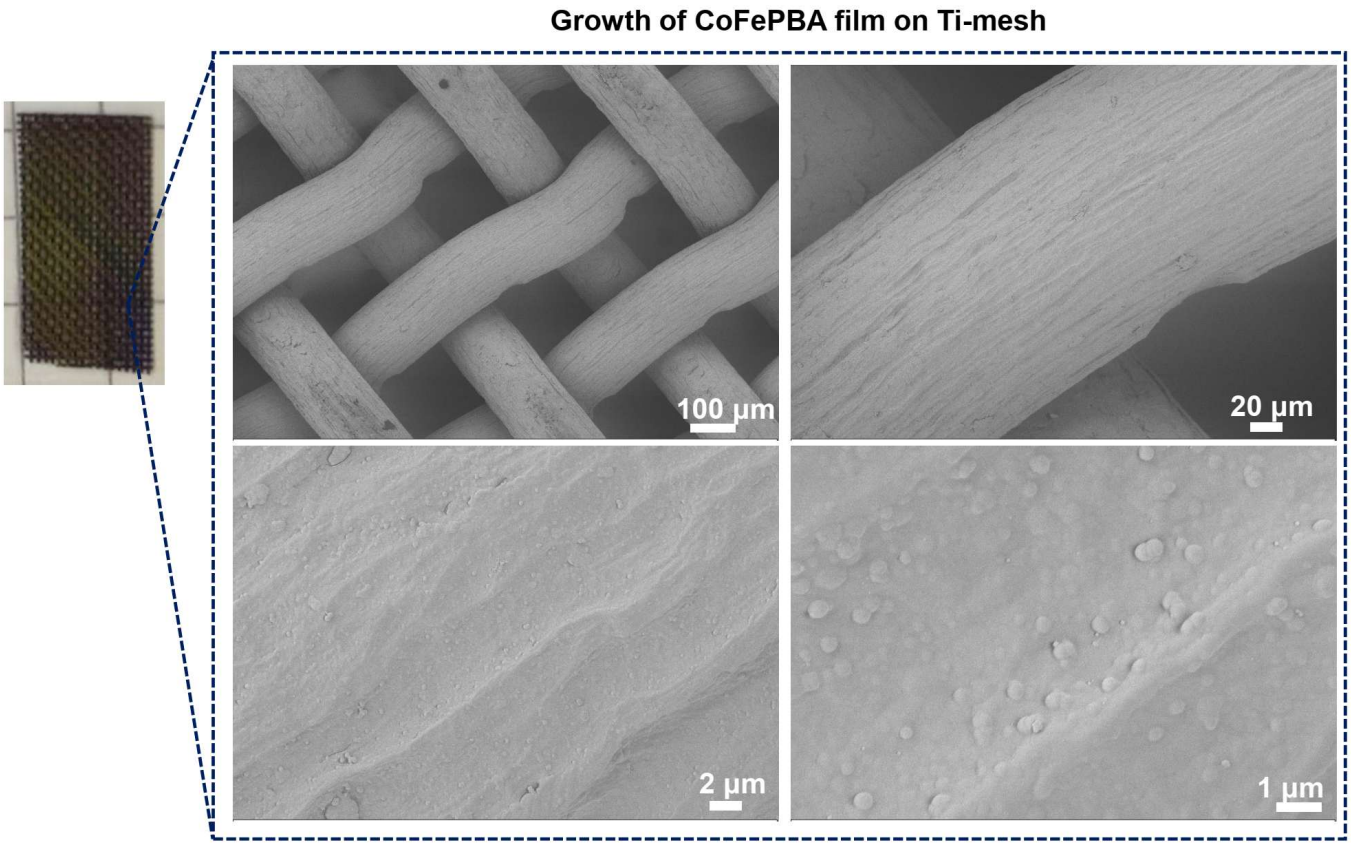


Figure S47. Photograph of the CoFePBA film on Ti-mesh and the SEM images of the film surface at different magnifications.

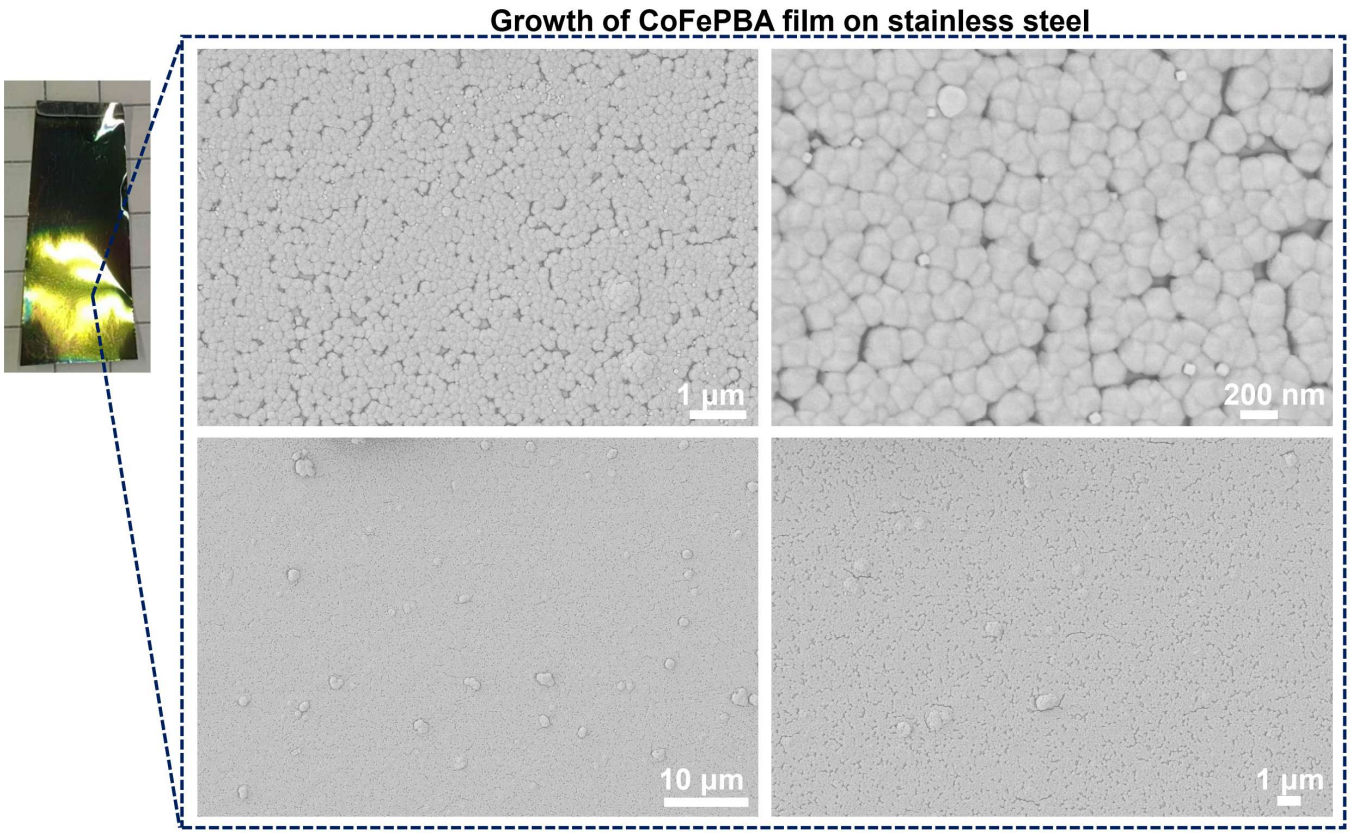


Figure S48. Photograph of the CoFePBA film on stainless steel plate and the SEM images of the film surface at different magnifications.

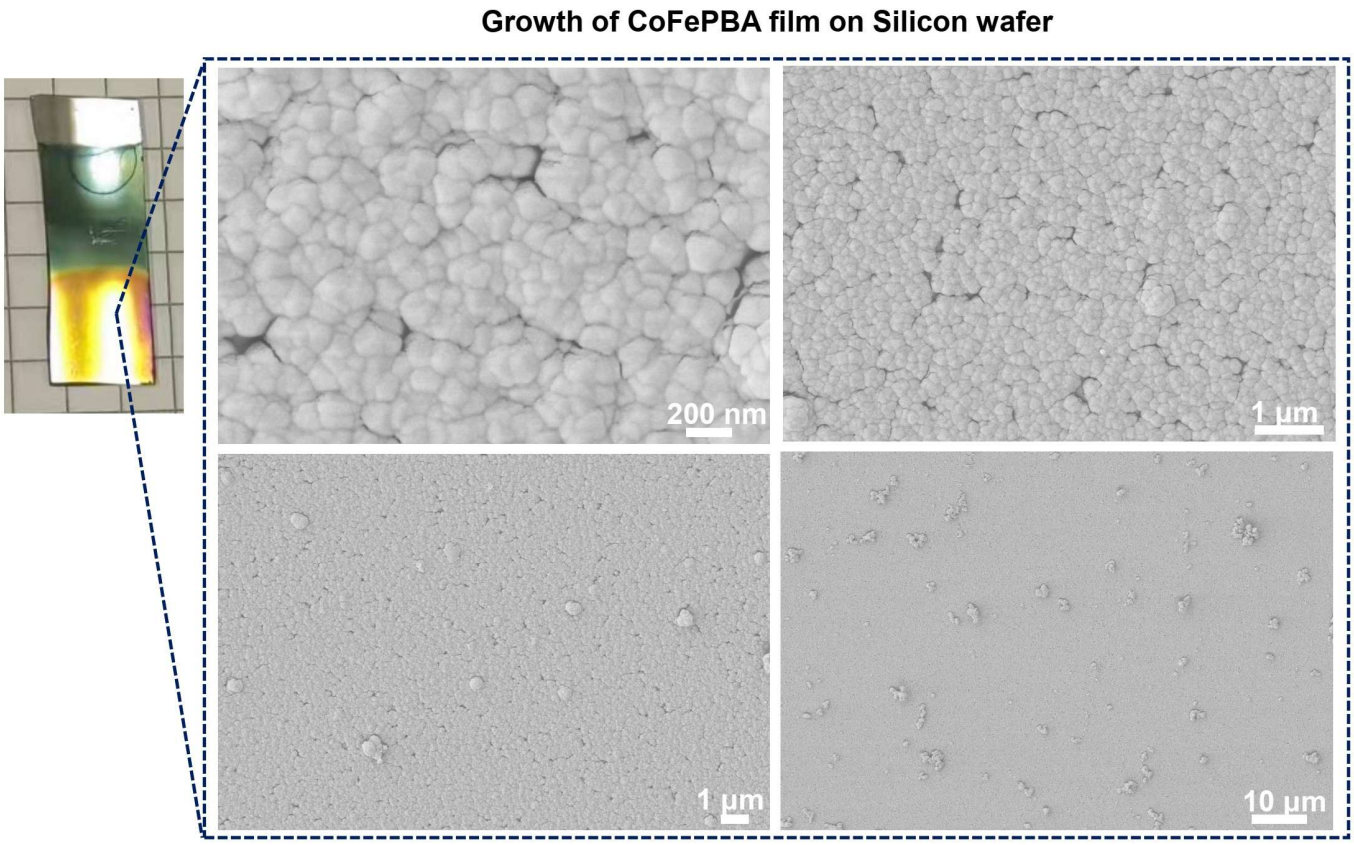


Figure S49. Photograph of the CoFePBA film on silicon wafer and the SEM images of the film surface at different magnifications.

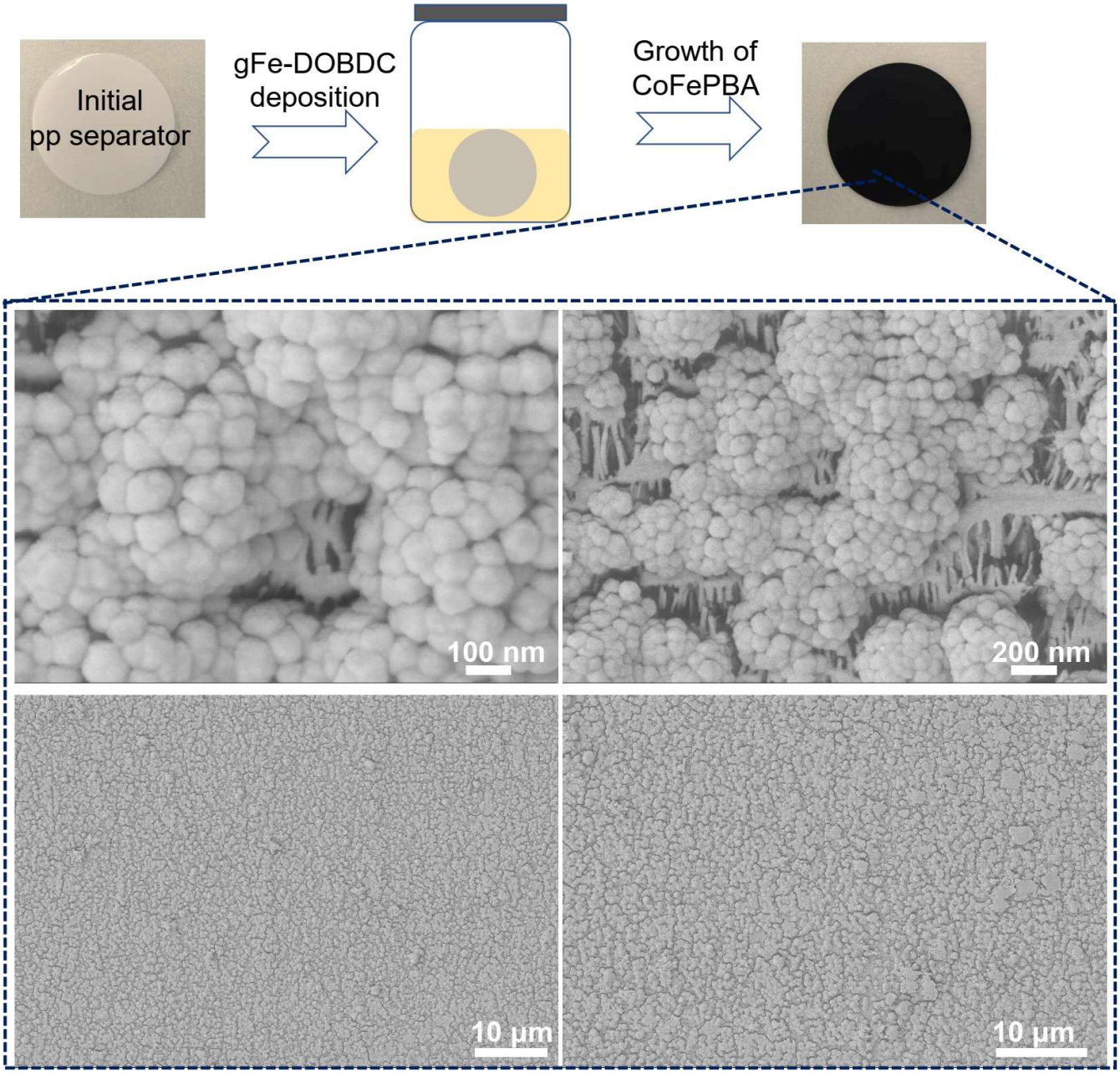


Figure S50. The schematic illustration of preparation of CoFePBA film on pp separator and the SEM images of the film surface at different magnifications.

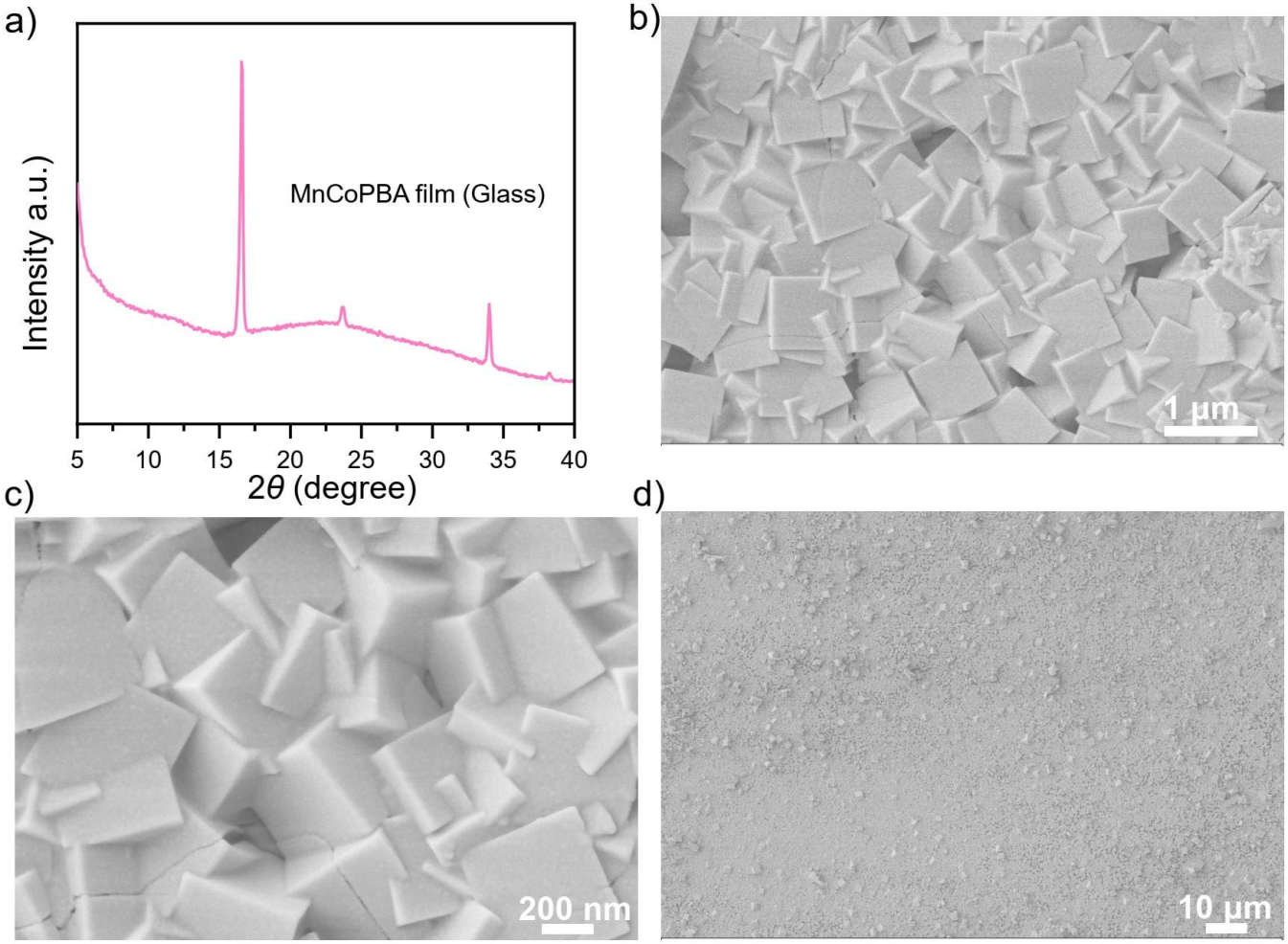


Figure S51. (a) The PXRD pattern of $Mn_3[Co(CN)_6]_2$ film on glass. (b-d) the SEM images of $Mn_3[Co(CN)_6]_2$ film at different magnifications.

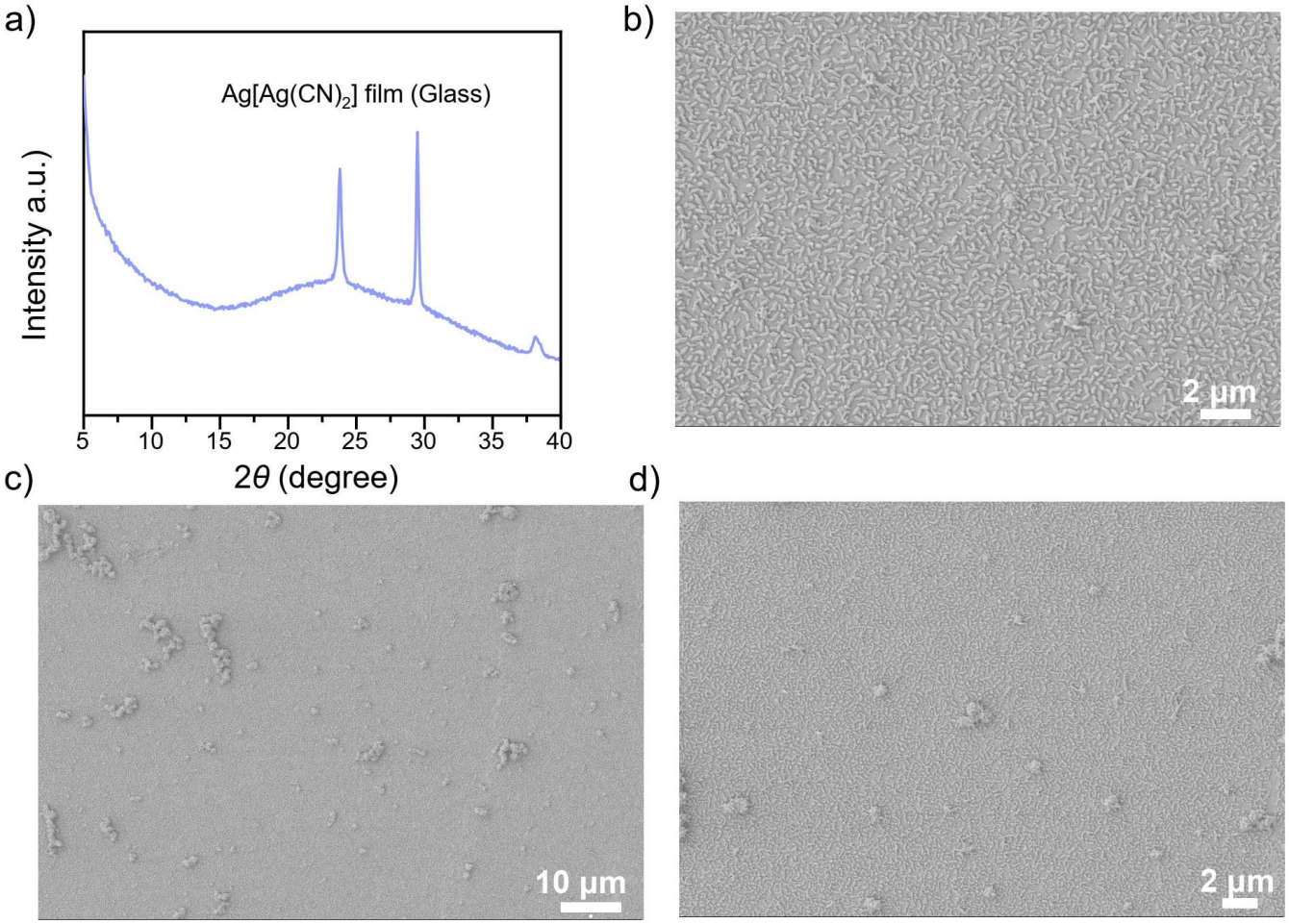


Figure S52. (a) The PXRD pattern of $Ag[Ag(CN)_2]$ film on glass. (b-d) the SEM images of $Ag[Ag(CN)_2]$ film at different magnifications.

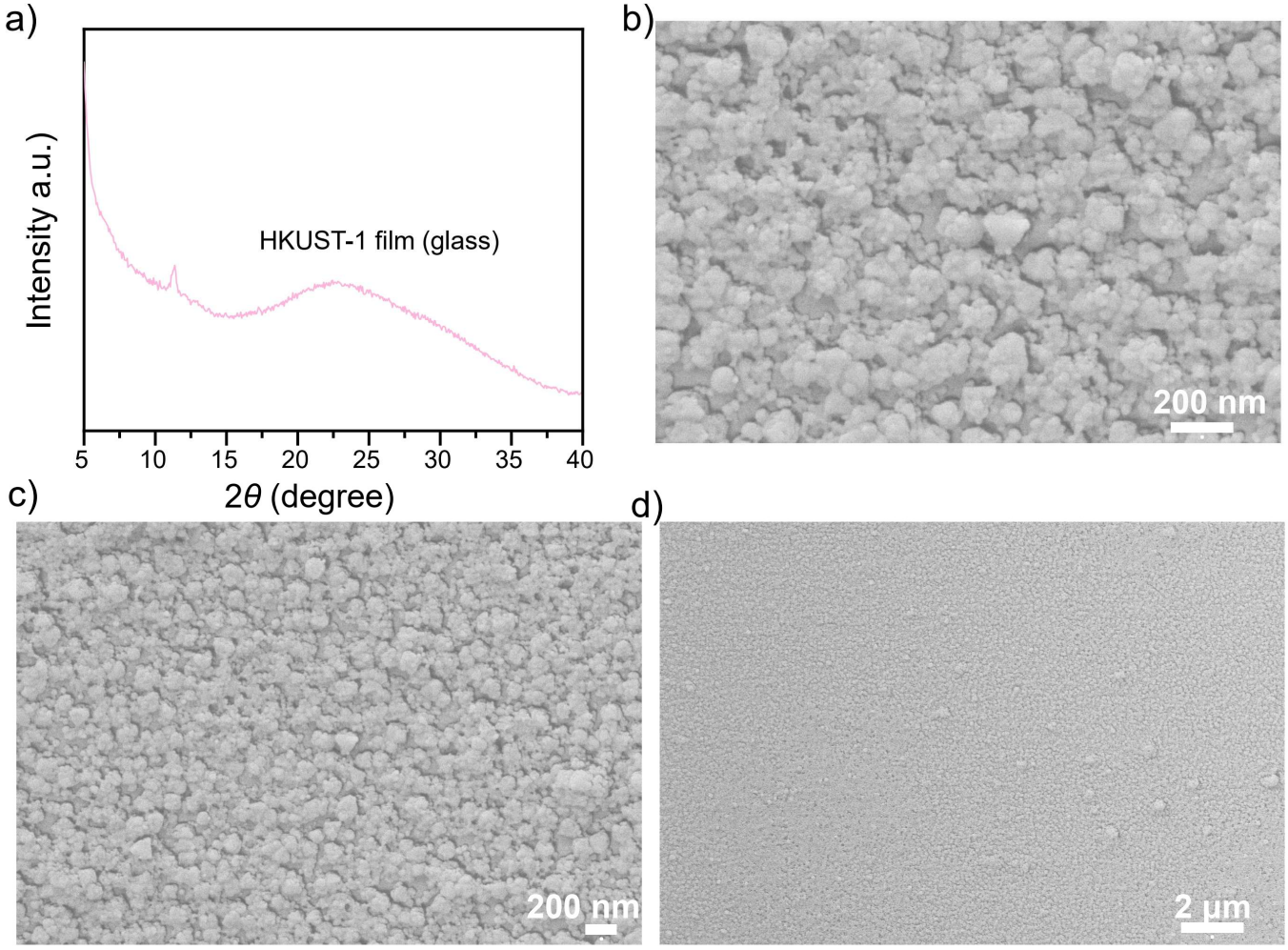


Figure S53. (a) The PXRD pattern of HKUST-1 film on glass. (b-d) the SEM images of HKUST-1 film at different magnifications.

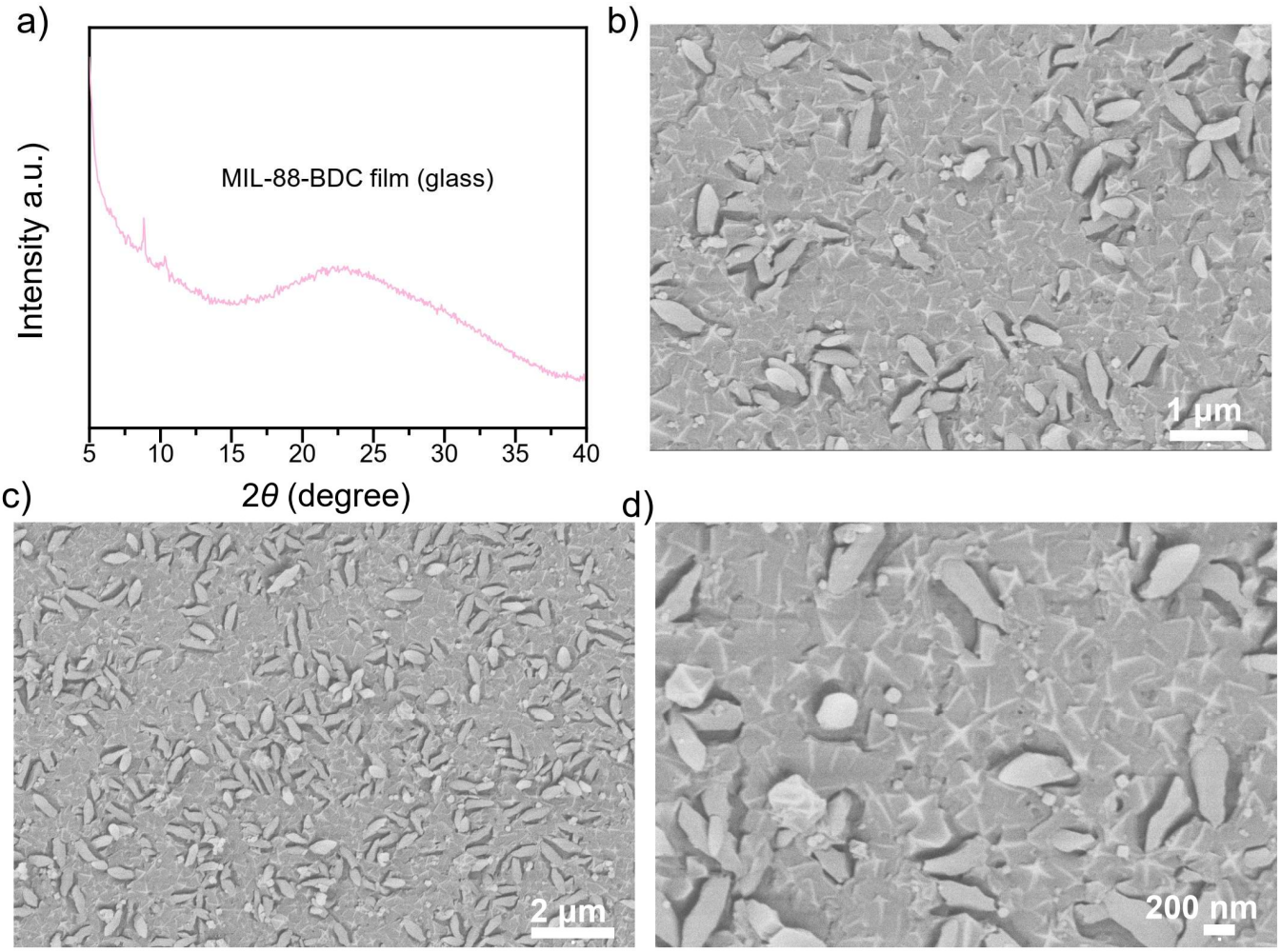


Figure S54. (a) The PXRD pattern of MIL-88b film on glass. (b-d) the SEM images of MIL-88b film at different magnifications. MIL-88b with two different morphologies are grown on the substrate.

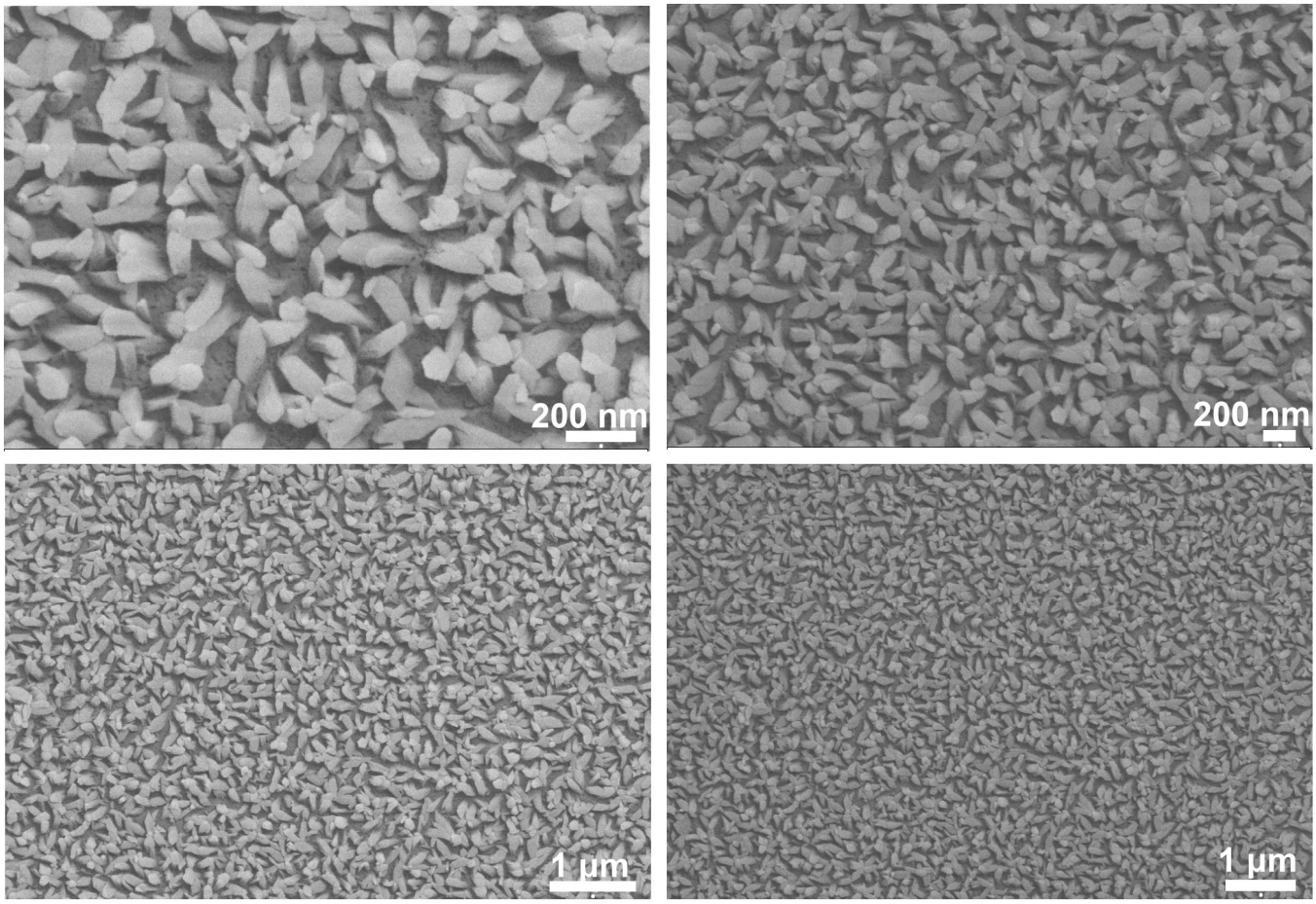


Figure S55. The SEM images of MIL-88c-NDC film at different magnifications.

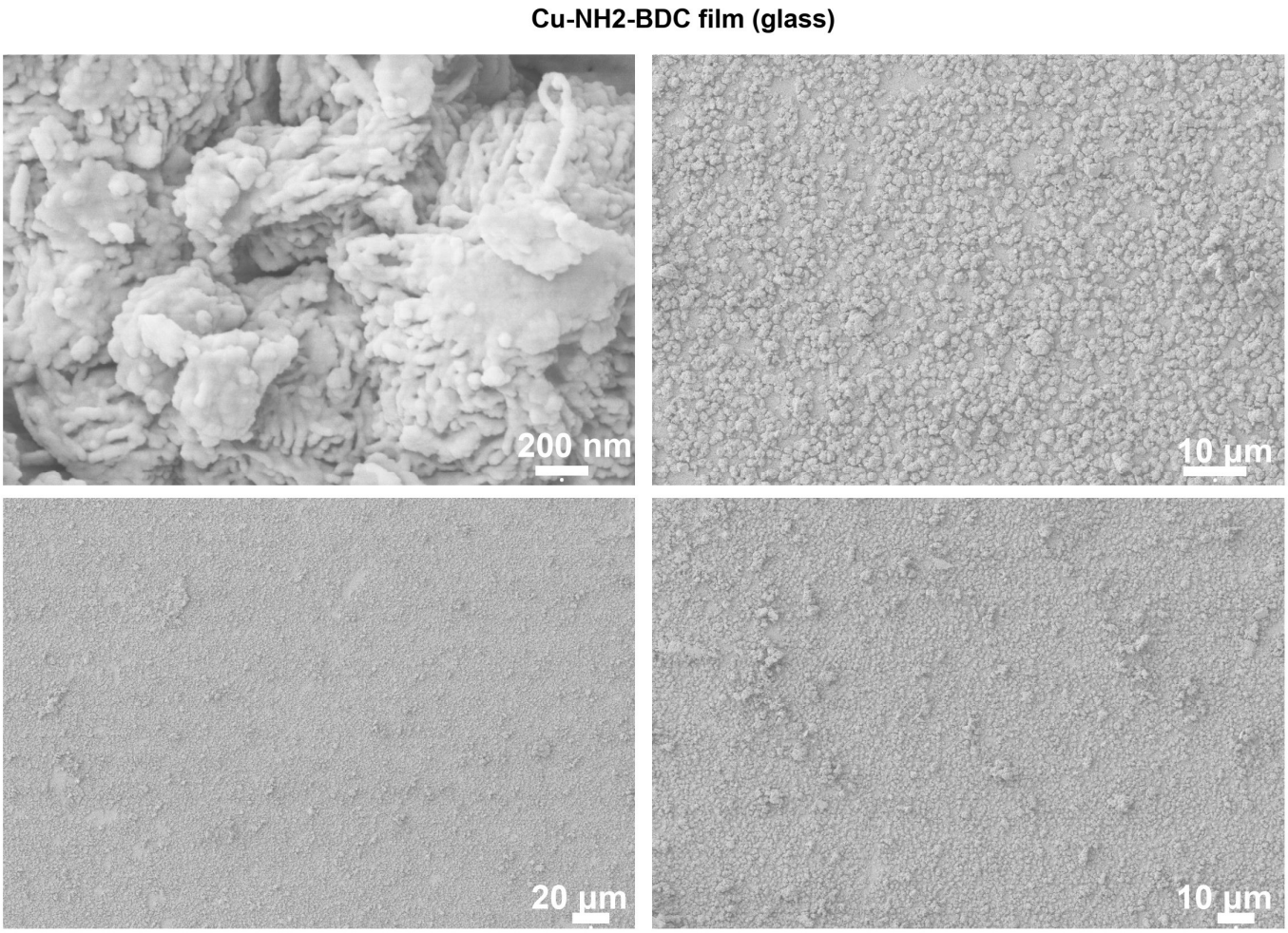


Figure S56. The SEM images of Cu-BDC-NH_2 film at different magnifications.

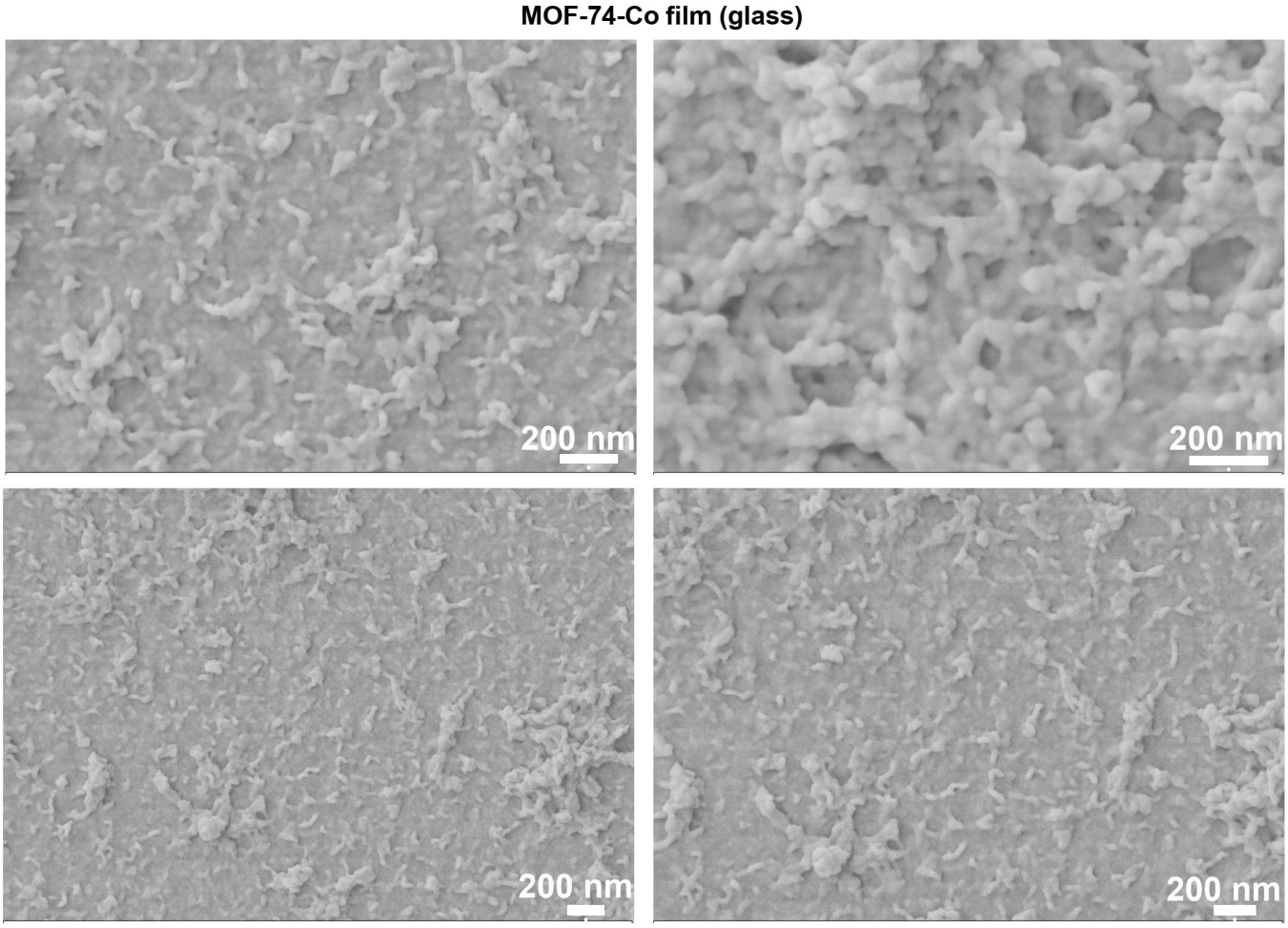


Figure S57. The SEM images of MOF-74(Co) film at different magnifications.

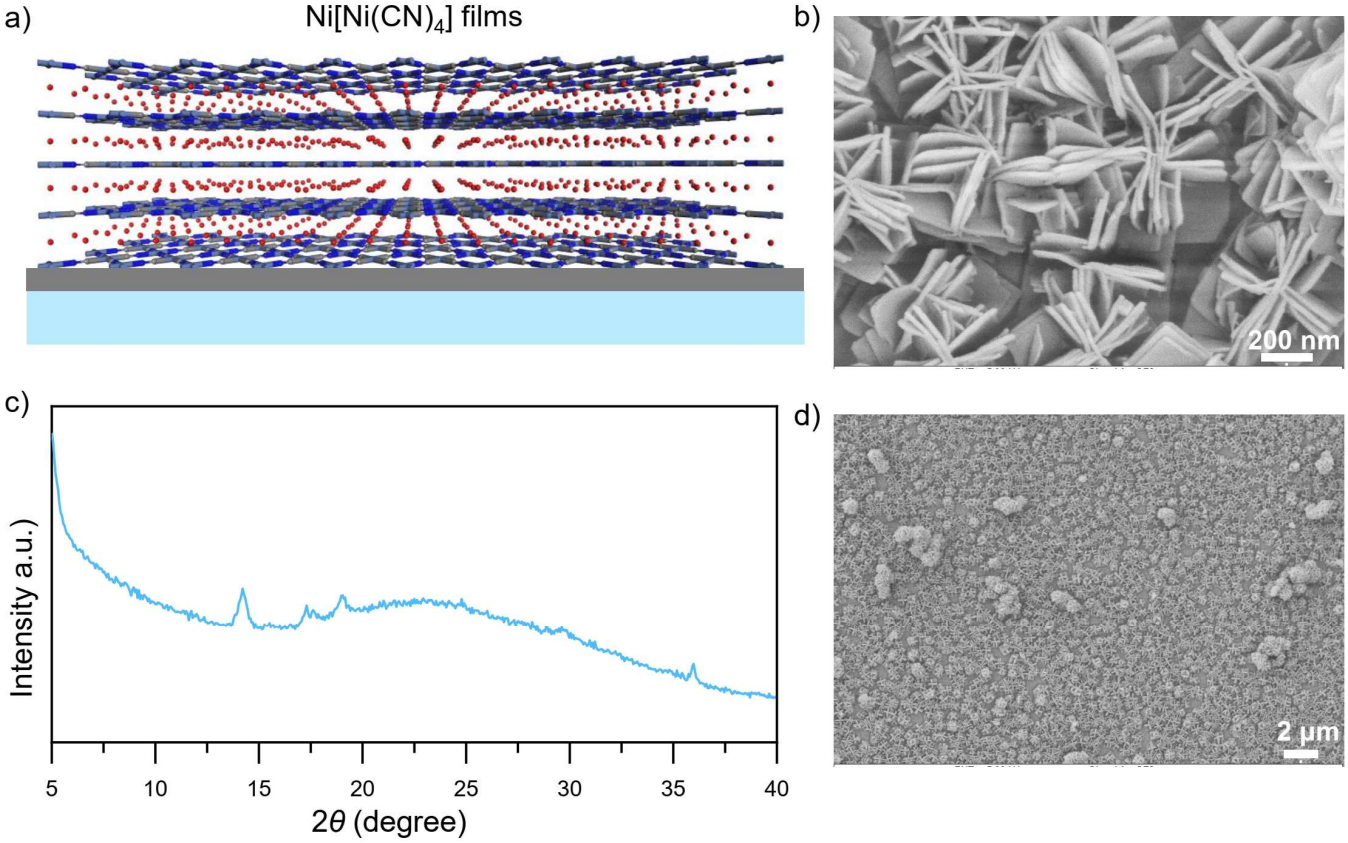


Figure S58. (a) The schematic illustration of $Ni[Ni(CN)_4]$ film on glass. (b, d) the SEM images of the film surface at different magnifications. (c) PXRD pattern of $Ni[Ni(CN)_4]$ film on glass.

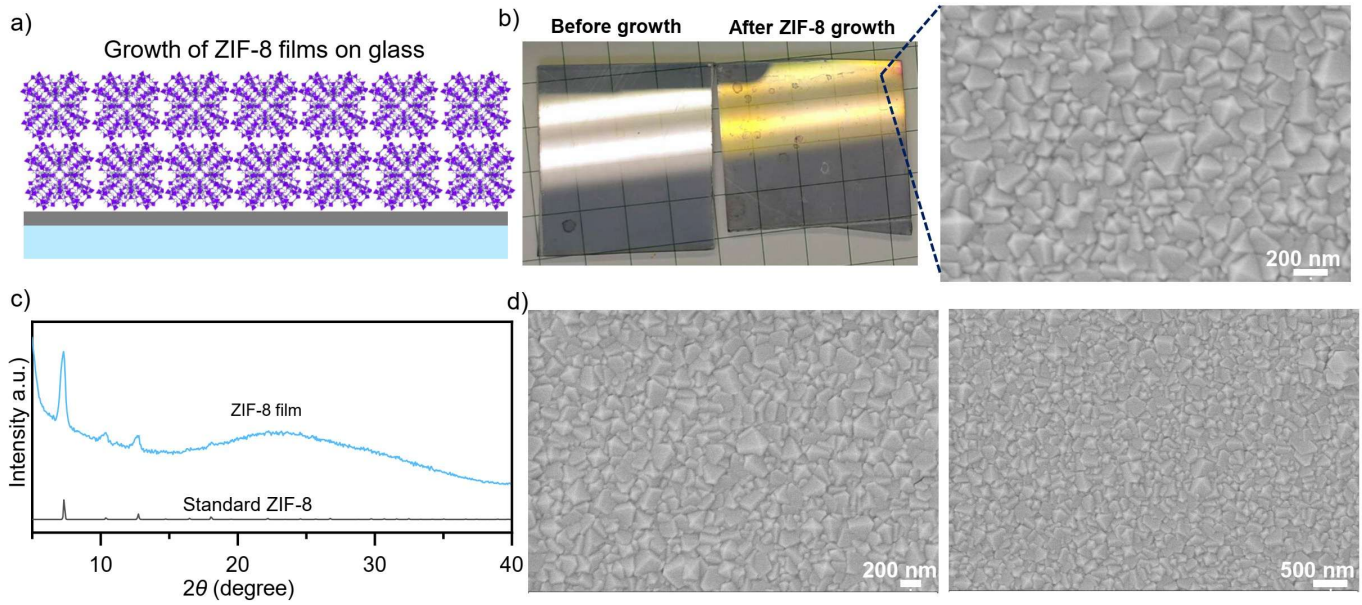


Figure S59. (a) The schematic illustration of ZIF-8 film on glass. (b, d) the SEM images of the film surface at different magnifications. (c) PXRD pattern of ZIF-8 film on glass.

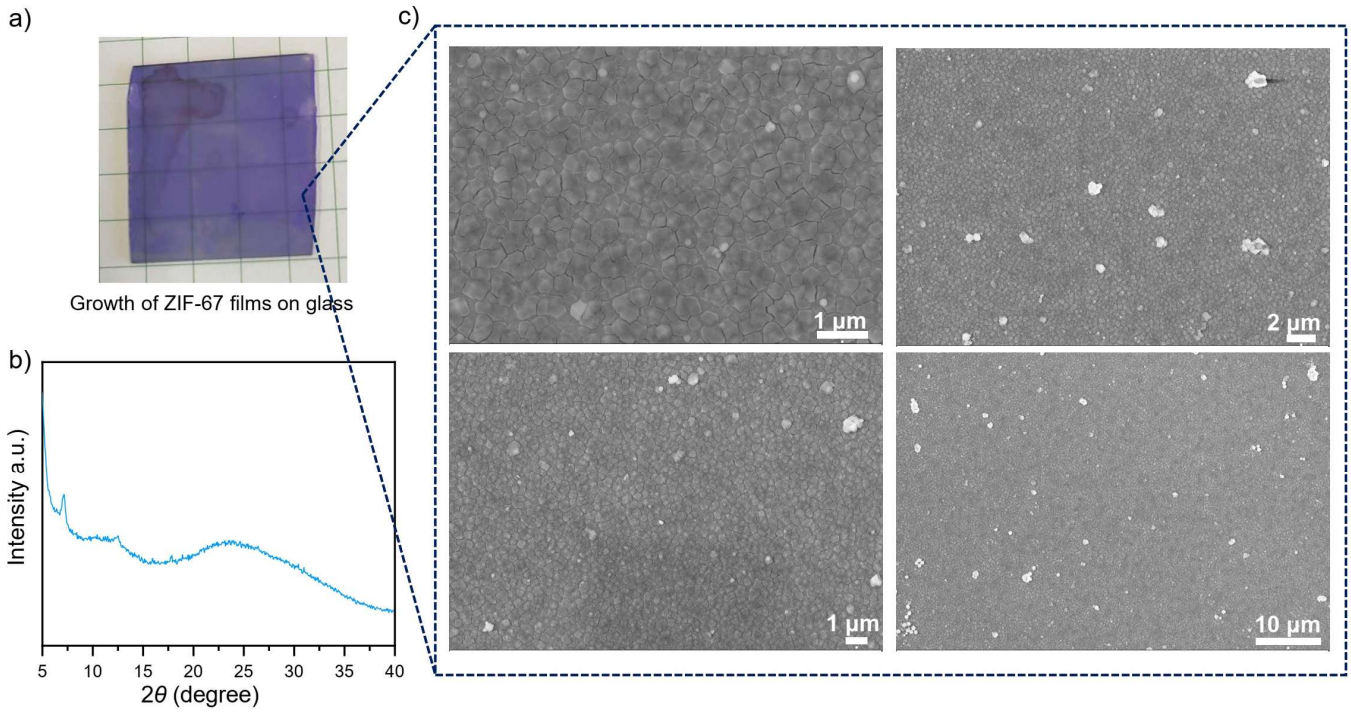


Figure S60. (a) The Photograph of the ZIF-67 film. (b) PXRD pattern of ZIF-67 film on glass. (c) the SEM images of the film surface at different magnifications.

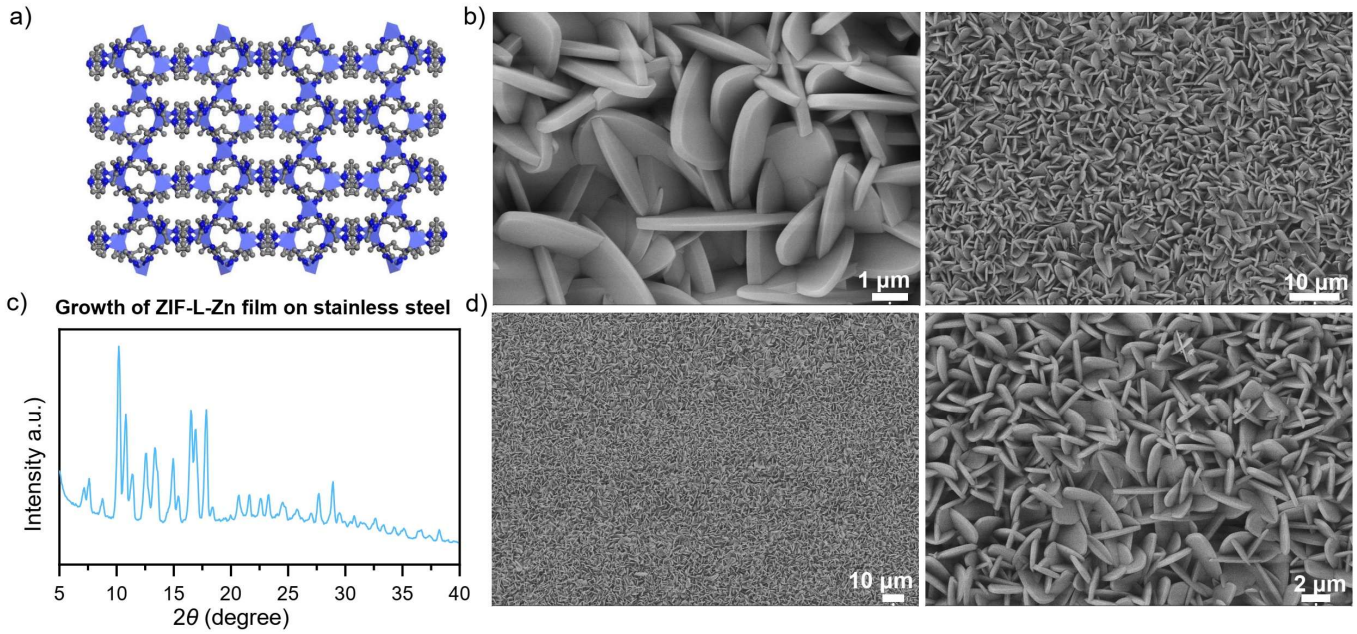


Figure S61. (a) The schematic illustration of ZIF-L-Zn film on glass. (b, d) the SEM images of the film surface at different magnifications. (c) PXRD pattern of ZIF-L-Zn film on glass.

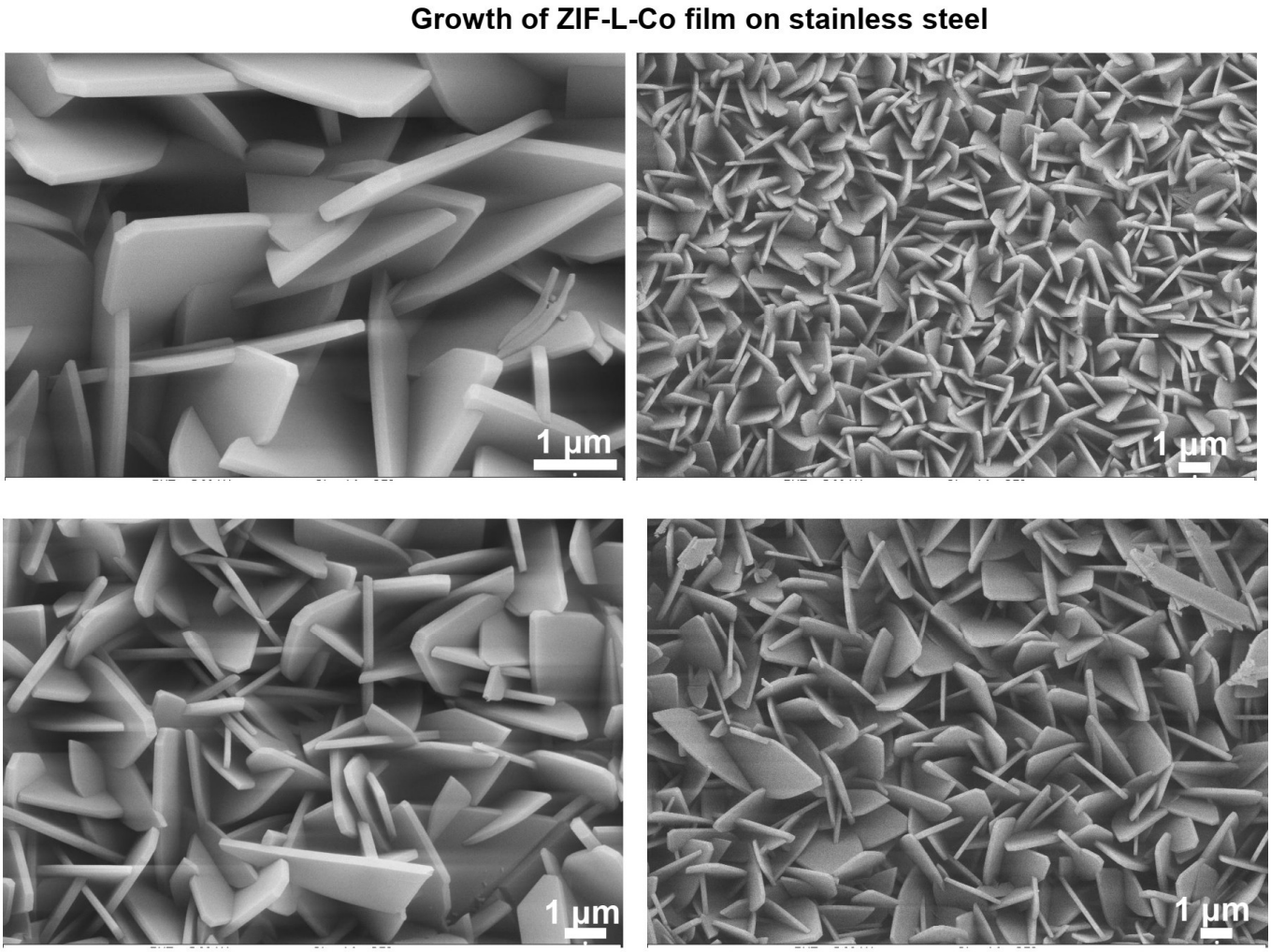


Figure S62. The SEM images of ZIF-L-Co film surface at different magnifications.

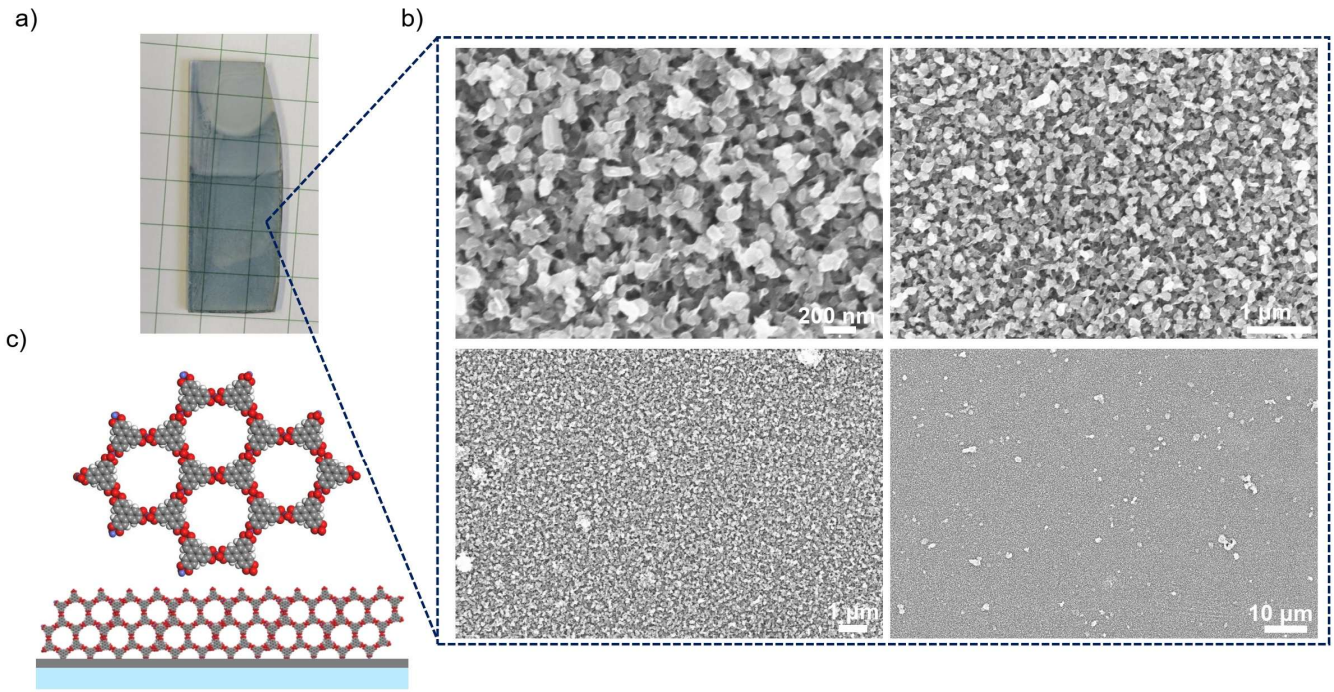


Figure S63. (a) The Photograph of Cu-HHTP film on glass. (b) The SEM images of the film surface at different magnifications. (c) The schematic illustration of Cu-HHTP film.

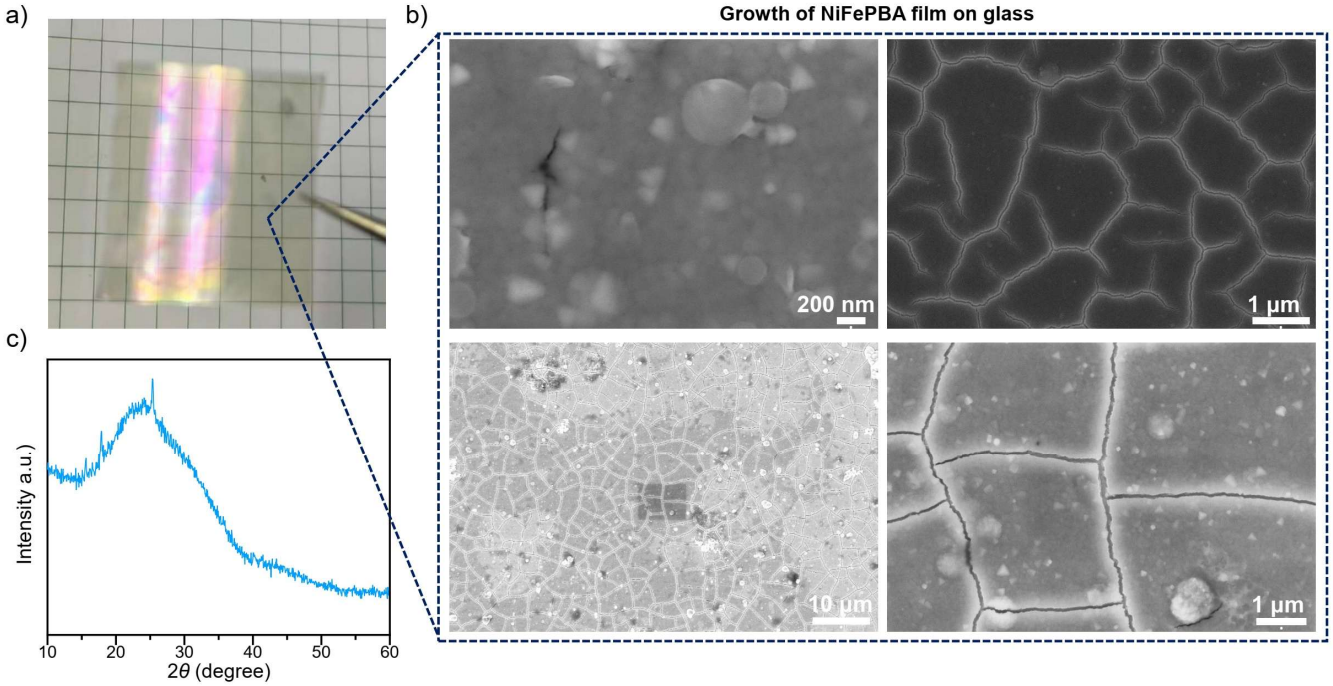


Figure S64. (a) The Photograph of $Ni_3[Fe(CN)_6]_2$ film on glass. (b) The SEM images of the film surface at different magnifications. (c) The PXRD pattern of $Ni_3[Fe(CN)_6]_2$ film.

References:

1. Dippel, A. C., Liermann, H. P., Delitz, J. T., Walter, P., Schulte-Schrepping, H., Seeck, O. H., & Franz, H. Beamline P02. 1 at PETRA III for high-resolution and high-energy powder diffraction. *Synchrotron Radiation*, 2015, 22, 675-687.
2. Ashiotis, G., Deschildre, A., Nawaz, Z., Wright, J. P., Karkoulis, D., Picca, F. E., & Kieffer, J. The fast azimuthal integration Python library: pyFAI. *Applied Crystallography*, 2015, 48, 510-519.
3. Kieffer, J., Valls, V., Blanc, N., & Hennig, C. (2020). New tools for calibrating diffraction setups. *Synchrotron Radiation*, 2020, 27, 558-566.
4. Juhás, P., Davis, T., Farrow, C. L., & Billinge, S. J. (2013). PDFgetX3: a rapid and highly automatable program for processing powder diffraction data into total scattering pair distribution functions. *Applied Crystallography*, 2013, *46*, 560-566.
5. Yang, X., Juhas, P., Farrow, C. L., & Billinge, S. J. (2014). xPDFsuite: an end-to-end software solution for high throughput pair distribution function transformation, visualization and analysis. *arXiv preprint arXiv:*1402.3163.
6. Billinge, S. J., & Farrow, C. L. Towards a robust ad hoc data correction approach that yields reliable atomic pair distribution functions from powder diffraction data. *Journal of Physics: Condensed Matter*, 2013, *25*, 454202.
7. L. Martínez, R. Andrade, E. G. Birgin, J. M. Martínez. Packmol: A package for building initial configurations for molecular dynamics simulations. *Journal of Computational Chemistry*, 2009, 30, 2157-2164.
8. Jorgensen, W. L., & Tirado-Rives, J. Potential energy functions for atomic-level simulations of water and organic and biomolecular systems. *Proceedings of the National Academy of Sciences*, 2005, 102, 6665-6670.
9. Thompson, A. P., Aktulga, H. M., Berger, R., Bolintineanu, D. S., Brown, W. M., Crozier, P. S., ... & Plimpton, S. J. LAMMPS-a flexible simulation tool for particle-based materials modeling at the atomic, meso, and continuum scales. *Computer physics communications*, 2022, 271, 108171.
10. Hay, P. J., & Wadt, W. R. Ab initio effective core potentials for molecular calculations. Potentials for the transition metal atoms Sc to Hg. *The Journal of chemical physics*, 1985, 82, 270-283.
11. Becke, A. D. Density-functional thermochemistry. III. The role of exact exchange. *The Journal of chemical physics*, 1993, 98, 5648-5652.